CHAPTER 1

INTRODUCTION

1.1 Background of organic solar cell and major function of buffer layer in the device.

The extending requirement in renewable energy technology is the main reason of focusing on solar cell which seems to be the best choice for convenient device since it do not require chemical reactions and does not contain any mechanical generator or moving equipment that involves maintenance and fuels for power refill in order to produce electricity.

Solar cell device consists of three main components namely anode, semiconductor material and cathode. The fundamental concept of solar cell device is based on the photovoltaic effect which occurs when the light strikes to the device. The photon energy from the sunlight is responsible in providing the excitation motion of electrons and holes in semiconductor device hence producing electricity when both free charge carriers flow out to the external circuit.

Inorganic semiconductor material such as silicon is used widely in the commercial solar cell. The basic working principle of conventional inorganic solar cell is that the generating of electrons and holes are in the bulk of silicon or other inorganic semiconductor material. Although electrons and holes in inorganic material are not bonding together, they need to be separated by a built-in electric field because the photoinduced chemical potential gradient in the inorganic material tends to drive them in the same directions. The built in-

electric field will create a potential gradient that may transfer them to their respective electrode before producing electric power at the external circuit (Gregg & Hann, 2003).

The wide interest in using organic material in solar cell started with the findings in 1839 where a photocurrent had been observed with the lighting in an aqueous solution when platinum electrodes coated with silver bromide or silver chloride (Williams,1960). Consequently, the research on organic material for photovoltaic application was widely spread with an athracene was used as the first organic substance (Spanggaard & Krebs, 2004).

The interesting part of using organic material lies on the behavior of their charge carriers of hole and electrons which were attached to each other and namely as excitons. In specific, the separation of excitons for organic heterojunction devices is happened at the interface between two active layers in the device which consists of donor and acceptor materials. Both layers creates heterojunctions interface which are different in their energy level. The difference in energy level or work function of the organic interface layer results in the existence of built-in electric field (Peumans & Forrest, 2004). The electric field offers driving force to dissociate the excitons to electrons and holes in the active layer of the device. In contrast to the inorganic material which mostly rely on the built-in electric field to diffuse them to different directions, the charge carriers of electrons and holes in organic material are exist primarily in their own path way which automatically drives them to opposite direction by the force of photoinduced chemical potential that is naturally applied to these charge carriers (Benanti & Venkataraman, 2006).

Hence based on the working principle in organic solar cell, upon dissociation process at the active layer component, the free charge carriers of electrons and holes must

move to the respective electrodes, namely anode and cathode to generate electricity. During transportation, material defects or interface states may cause these free charge carriers to recombine, hence decreasing the photocurrent effect in the device. A higher internal electrical field allows the photo-generated carriers to smoothly move to the electrodes, results in reducing the probability of recombination process (Tsai et al., 2011).

The details on the wide spread research activities on organic solar cell are summarized on Table 1.1. The summary shows the apparent interesting highest efficiency of organic solar cell has been achieved to 10.7% in 2012 (Blair & Venkataraman, 2013).

Table 1.1: Timeline of research on organic solar cell

YEAR	INVENTORS	CREATIONS
1839	Alexandre E. Becquerel	Observed a photocurrent between two electrodes submerged in solution
1873	Willough by Smith	Observed a photoconductivity in Selenium
1883	Charles Fritts	Builds Selenium Solar Cell
1888	Aleksandra Stoletov	Build the first photoelectric cell based on photoelectric effect
1954	Bell Laboratories	Developed the first inorganic solar cell based on silicon
1974	P.H.Fang	Use Ohmic contacts in organic photovoltaic device
1978	Ghosh & Feng	Develop a theoretical model **with efficiency 7%** in merocyanine organic solar cell
1978	Researchers of Exxon Mobil	Reported on OPV device with 1% efficiency using semi-transparent aluminum electrodes
1986	C.W.Tang	Creates the first two-layer organic PV cells, efficiency 0.95% reported

Table 1.1 continued: Timeline of research on organic solar cell

YEAR	INVENTORS	CREATIONS
1991	Gratzel	Reports the successful of dye sensitized TiO_2 solar cell
1991	Scientist from Osaka Uni.	Developed the first dye/dye bulk heterojunction PV by co-sublimation
1993	Sariciftci	Report the photoinduced electron transfer from MEH-PPV to C60
1994	Scientist from UC Santa Barbara	Reported the solar cell based on MEH-PPV and C60
1995	Heeger& Groups	Indepedently reported all exploration on polymer active layer
2000	A.Hagfeldt &Gratzel	Proposed TiO_2 nanoparticle fil structure for ultrafast charge separation and increased efficiency
2000	Scienctist from Eindhoven	Reports the use of oligomer-carbon dyads/triads as active material in PV cell
2001	L.Schmidt-Mende	Report a self-organised liquid crystalline solar cell with **efficiency 1.95%** at 495nm
2001	C.J. Brabec et al	Used plastic and buckminster fullerene in solar cells,with **efficiency achieved up to 3%**
2002	Paul Alivisatos et al	Reported the hybrid nanorod polymer solar cells with P3HT-CdSe with **efficiency 1.7%**
2005	G.Li et al	Develop **5% power conversion efficiency** polymer PV using polymer blend of P3HT & methanofullerene
2009	Holcombe et al	Synthesize an all-polymer solar cell to form Grignard Metathesis polymerization
2010	Lu Ping Yu, et al	Report the development of prototype polymer organic PV cells with PtB7 with **efficiency achieved ~7.4%**
2011	Mitsubishi Chemical company	Announce the production of **9.2% PCE** organic PV cell
2012	Van der Poll et al	Produced high-**efficiency 7%** with small molecule organic PV

Table 1.1 continued: Timeline of research on organic solar cell

YEAR	INVENTORS	CREATIONS
2012	Heliatek et al	Produce the prototype **10.7% PCE** organic PV
2012	Ramuz et al	Develop the first all-carbon solar cell
2012	Snaith, et al	Use organometal halide pervoskites results in **efficiency of 10.9%**
2013	Heliatek, et al	Announced the development of organic solar cell with small molecules and **efficiency achieved ~12%**
2013	Yang Yang et al	Report a **10.2% PCE** in tandem organic PV cell with two identical subunits
2013	Marks, et al	Produced high-efficiency with **80% of FF** in organic PV

An efficient organic solar cell device is measured by its ability to prevent recombination process in the carriers dissociation stage which results in increasing its photocurrent. The recombination process mostly occurs at the interface between the electrode and the semiconductor active layers which reduce the transportation rate of free charge carrier (Halls et al., 1999). A common solution is to introduce a thin interlayer called buffer layer between electrode and active layer which may adjusts the electronic behavior of the adjacent materials (Johnev et al., 2005).

The main roles of buffer layer are to diminish recombination of free charge carriers and to increase the rate of holes collection to anode. Moreover, in addition of these major functions, an efficient buffer layer will also contribute to the modification of the unstable anode/active layer interface by the superior injection/collection properties between the buffer layer and active layer interface (Yin et al., 2010).

The common material used as buffer layer is poly (3,4-ethylene dioxythiophene): poly (styrenesulfonate) (PEDOT:PSS) which deposited by spin coating onto indium tin oxide (ITO) film prior to organic deposition. This additional layer is very efficient since it produces surface defects passivation and smoothen the ITO surface (Dahou et al., 2010). PEDOT:PSS also available in modifying the work function between the electrode and the active layer by reducing or increasing the work functions of the cathode and anode (Brown et al., 1999). Moreover, PEDOT:PSS is able to improve the cohesion between difference layer and thus decrease the interfacial series resistance (Park et a;., 2011).

PEDOT:PSS is strongly suggested as an excellent buffer layer due to its better performance in the organic solar cell which supported by the consistent usage and existence of PEDOT:PSS as buffer layer in most of the fabricated organic solar cell to date. Thus it seems that the buffer layer is an important component, which then became permanent material in organic solar cell (Po et al., 2011). Moreover, an effective interfacial property between the buffer layer and the active layer need to be consider as well in order to enhance the efficiency of the organic solar cell device (Kim et al., 2011). Inspite of acting as anode buffer layer in optoelectronic devices, the commercialized polymer PEDOT:PSS also utilized as transistor circuits (Sirringhaus et al., 2000) and photodetector (Gong et al., 2009).

The combination of PEDOT with PSS was purposed to reduce the insoluble issue in PEDOT. However, the insulator behavior of PSS particles leads to the limitation in PEDOT electrical properties, specifically in terms of electrical conductivity (Po et al., 2011). The raise in transparency of PEDOT:PSS leads to the decreasing in its electrical properties which shows the inbalance and unstable behavior in PEDOT:PSS in two most important

characteristics applied in organic solar cell. This issue seems to be the major disadvantage in the use of PEDOT:PSS in optoelectronic devices.

In order to improve this obstacle, many options taken were by modifying PEDOT:PSS structure with the doped of organic solvent such as dimethyl sulfoxide (DMSO), ethylene glycol (EG), glycerol and sorbitol. These organic solvents are able to enhance the conductivity of PEDOT:PSS by reducing the insulator PSS layer on the PEDOT:PSS surface, results in the larger exposed surface of PEDOT conductive thin film that increased the electrical conductivity of PEDOT:PSS thin film (Han & Okuzaki, 2009).

Huang et al also convince that the modification in PEDOT:PSS is needed to improve the electrical properties of PEDOT:PSS thin film and the organic solvent group which possessed superior conductivity are the best candidates to enhance the conductivity of PEDOT:PSS thin film. Their work on sorbitol, DMSO and glycerol doped PEDOT:PSS show tremendous increment in the conductivity of PEDOT:PSS compared to the undoped PEDOT:PSS thin film (Huang et al., 2013).

The existence of organic solvent in PEDOT:PSS thin film also provides great support in enhancing the connectivity between the interface of PEDOT:PSS thin film as hole transport layer (HTL) with the active heterojunction layer of P3HT and PCBM in organic solar cell which results in better performance in the device compared to by using undoped PEDOT:PSS thin film as HTL (Mauger et al., 2012).

Thus, despite its structural stability, high optical transparency and process ability, the modification of PEDOT:PSS is essential in order to enhance its electrical properties to become the efficient buffer layer in optoelectronic device.

1.2 History and background of thermoelectric device.

In the consequent of the extensive research on finding convenient device in renewable energy technology, the highly desired to fully use the tremendous wasted heat which released from the manufacturer processes, industrial activities and automotive exhaust has motivated the work on transforming the wasted heat to electricity through specific instrument namely thermoelectric device (Hochbaum, 2007).

The thermoelectric (TE) generator is a solid state heat engines with special materials properties enable them to convert waste heat into electricity. The efficiency of this device is closely related to the semiconductor's material properties and is determined by its figure of merit, ZT, which is a dimensionless unit depending on the Seebeck coefficient (S), absolute temperature (T), electrical conductivity (σ) and thermal conductivity (κ):

$$ZT = S^2\sigma\frac{T}{\kappa} \qquad 1.1$$

However, the thermoelectric efficiency which consists of electric power produced over waste heat-inis currently only about 1/6 of the maximum Carnot efficiency. Although it is unexpected that thermoelectric device can act as part of the large scale energy production, this device indeed contributes in the recent technologies. Their exclusive solid state properties offer several benefits with respect to other established technologies. One of the attractive performances of thermoelectric device which found similar to the solar cell is that their ability to produce electricity without moving parts. Thus, this device is capable in the convenient aspects as noise free and low in maintenance, operation and instrument cost which permit their usage in a harsh or remote surroundings (Bell, 2008).

The major advantage in thermoelectric devices is their scalability where their efficiencies are maintained regardless of the magnitude of power level although for

example at milliwatt level. As a results, the thermoelectric devices seem to be more efficient and the increase in ZT will only improve the range of applications where thermoelectric are more efficient (Vining, 2009). Table 1.2 tabulates the research summary on thermoelectric performance from 1980 to 2010s while Figure 1.1 demonstrates the thermoelectric performances, ZT on several thermoelectric materials that have been studied (Tritt & Subramanian, 2006). It is noted from the table that presently, PEDOT material was also been used as thermoelectric compound, hence has encouraged the investigation of thermoelectric properties in the modified PEDOT:PSS thin film in this work.

Table 1.2: Timeline of Thermoelectric and related research over the last 30 years.

YEAR RANGE	**THERMOELECTRIC EVENT**
1980s	- Minimum thermal conductivity and conducting polymer were discovered.
1990s to 2000s	- TE quantum well theory - Vacuum thermionic cooling - Glass-like heat flow (skutterudite) - Attempts of TE polymer-inorganic composites - Quantum well structures - Heterostructurethermionics - Crystals with complex electronic structures - Superlattice thin-film structures
2000s -2010s	- Bulk nanostructured materials - Polymer-CNT TE nanocomposites - Strained endotaxial nanostructures - PEDOT-Tos

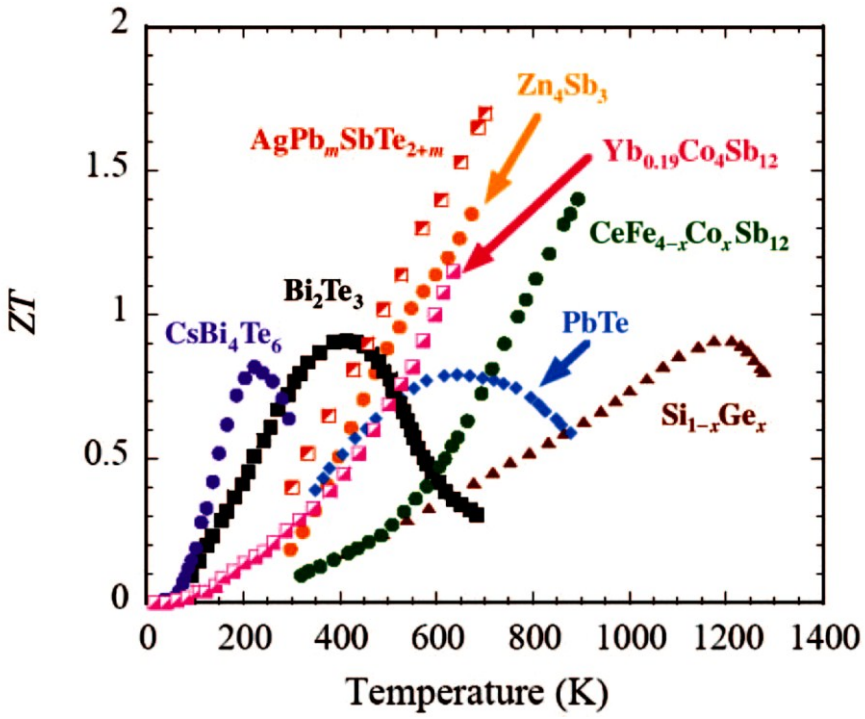

Figure 1.1: Figure of merit *ZT* shown as a function of temperature for several bulk thermoelectric materials.

1.3 Motivation for the research work

Although PEDOT:PSS is fully adequate due to its high transparency behavior, it is crucial to improve its electrical properties in order to become an efficient buffer layer in organic solar cell. A compromise is needed to obtain PEDOT:PSS thin film that can simultaneously exhibit high transparency and conductivity. The urgency to overcome this issue has forced the utilization of many methods including expensive and complex procedures. Nevertheless, many of such offer inconvenient effect to the technology where PEDOT:PSS involves as one of the major components in their manufacture products for example in organic solar cell and organic light emitting diode. This research is triggered by the need to seek for a green and simple method upgrading PEDOT:PSS performance for optoelectronic devices. Hence, the focus are on utilizing the non-toxic polymer conductive PEDOT:PSS, doping with non-toxic organic polar solvent, glycerol and non-toxic metal oxide (ZnO and AZO) as the chemical solutions for the green-assisted method.

Besides, it is well known that PEDOT:PSS can be the next potential candidate to replace ITO as a transparent conductive oxide layer. It is hoped that this work may provide new ideas on how to improve PEDOT:PSS as buffer layer utilizing a simple, economical and green technology friendly method.

Moreover, in the invention of green organic technology, thermoelectric device is another alternative to organic solar cell which offers approximate equal benefits as organic solar cell. Although, the thermal dependences of thermoelectric device has limited the efficiency achievement to be compared to organic solar cell, its solid state scalable technology found to be appealing enough and worthwhile to be study. Nonetheless, PEDOT:PSS does not only appear to be the main part in organic solar cell but also widely used as an efficient p-type material in organic thermoelectric device. Therefore, it is worthwhile to extend the study in this research by utilizing PEDOT:PSS in thermoelectric device.

Therefore, in this work, the research problem is addressed as:-

- The electrical properties of PEDOT:PSS was not compatible with high transparency ability in PEDOT:PSS. Although PSS particles has contribute in solving the insolubility issue in PEDOT solutions, the insulator behavior of PSS particles leads to the limitation in PEDOT electrical properties, specifically in terms of electrical conductivity. The raise in transparency of PEDOT:PSS lead to the decreasing in its electrical properties which shows unstable behavior in PEDOT:PSS to be applied in organic solar cell.
- The used of high maintenance, expensive, toxic and complex procedures in order to improve the electrical properties of PEDOT:PSS which may create corruption effect in environment and economical perspectives.

In general, the suggestion solutions to modify the optical and electrical properties of PEDOT:PSS thin film are consists of :-

- Introducing polar solvents of glycerol and ethylene glycol as the doped materials to PEDOT:PSS in order to modify the optical and electrical properties of PEDOT:PSS.
- Adding metal oxide of zinc oxide (ZnO) and aluminum zinc oxide (AZO) as the metal doped materials to PEDOT:PSS.
- Using a simple method of sol-gel process to prepare the mixed solutions of doped PEDOT:PSS and spin-coating technique to deposit thin film of doped PEDOT:PSS and also in the process of organic solar cell fabrication.

1.4 Research goal and objectives

The goal of this work is mainly to study the effect of types of dopant on the electrical and optical characteristics of PEDOT:PSS. Two types of dopant used in this study are organic and inorganic materials.

The organic polyol polar solvent materials used in this work are glycerol as the nontoxic candidate and ethylene glycol (EG) as the toxic candidate. The reason to use both opposite properties is because these two materials possess equal in molecular structure and chemical bonding, hence it is crucial to observe whether which material can contribute for a better electrical as well optical characteristics of PEDOT:PSS as buffer layer in organic solar cell.

Moreover, alternative materials of inorganic metal oxides are also investigated in this research, to be used as dopant in PEDOT:PSS. Zinc oxide (ZnO) and aluminum zinc oxide (AZO) produced by a simple sol-gel technique will be examined in term of their electrical, optical as well as microscopic properties. In this case the composite materials

called hybrid inorganic/organic material; by producing a metal oxide/PEDOT:PSS in solution form, which will then be used as buffer layer in organic solar cell. Towards the end of this research, the influence of modified PEDOT:PSS onto the thermoelectric behavior (temperature gradient) is also studied.

Hence in this work, the PEDOT:PSS were modified by doping with glycerol, EG, ZnO and AZO materials. The modified PEDOT:PSS were then deposited onto glass substrate as thin films. The optical, electrical as well as microscopic properties of the modified PEDOT:PSS thin films were measured by specific equipment to determine the best characteristics. Then, the organic solar cell were fabricated, utilizing the modified PEDOT:PSS as the buffer layer and compare the device efficiency with respect to the different dopant materials and variation percentage of dopant materials. Other than that, the electrical behavior of the modified PEDOT:PSS with respect to temperature gradient across the thin films were also been observed.

Thus, there are specific objectives need to be properly addressed as listed below:

i. To investigate the effect of doping various percentage of glycerol, EG, ZnO and AZO materials to the optical properties of PEDOT:PSS thin films.
ii. To examine the effect of doping various percentage of glycerol, EG, ZnO and AZO materials to the electrical properties of PEDOT:PSS thin films.
iii. To analyze the effect of doping various percentage of glycerol, EG, ZnO and AZO materials to the microscopic properties of PEDOT:PSS thin films.
iv. To study the efficiency of fabricated organic solar cell with respect to the different dopant materials and variation percentage of dopant materials in modified PEDOT:PSS as the buffer layer in the devices.
v. To observe the effect of temperature gradient across the modified PEDOT:PSS thin films with respect to their electrical behavior.

1.5 Thesis Outline

Overall, the contents of thesis includes the details of the procedures, analysis and achievements of the PEDOT:PSS with two organic materials and a metal oxide as the dopant materials.

In chapter 2, the background concept of organic solar cell is explained including the basic function of each component in the device. The hurdle experienced by the device also will be addressed in order to relate to the solutions taken by other researchers specifically on the approaches used to enhance the buffer layer properties of the device. Next, the detail introduction of PEDOT:PSS with the molecular structure, the chemical behavior and the advantages of PEDOT:PSS as buffer layer in organic solar cell were explained. Other than that, the weaknesses in PEDOT:PSS are also properly addressed and the options taken to improve PEDOT:PSS by other researchers are also elaborated in general. Then, the addition reviews on the thermoelectric concept and background of the thermoelectric device are explained to provide guidelines for the works of doped PEDOT:PSS on thermoelectric field and to relate with the thermoelectric module which is built exclusively in this work.

While in chapter 3, it begins with the detailed explanation on the sample preparation of the dopant materials followed by the doping processes and the preparation of doped PEDOT:PSS solutions will be discussed. Next, the fabrication of organic solar cell and the thermoelectric module are completely described and the specific measurements and calculation techniques are finally presented in this chapter. All of content descriptions in this chapter were assisted by specific diagrams, picture and equations to ease the understanding process for the research procedures and methodology in this work.

On the other hand, Chapter 4 consists of several subtopics which separated the characterization processes, initially the presentation of the optical properties results. Then

the results on the electrical properties are delivered followed by the explanation of the morphology of the studied doped PEDOT:PSS thin films. Consequently, the Raman spectroscopy results which provided the information on the chemical structure of the doped PEDOT:PSS are presented followed by the results on the organic solar cell efficiency. All segments are presented with the support of graphs, list of datas and mathematical values in specific tables and calculation details for analysis purposes.

Next in Chapter 5, elaborates on the results obtained from the experiment studies of the thermoelectric devices based on the doped PEDOT:PSS were described. Discussion of thermal gradient are laid in this chapter, with variation of dopant types used in PEDOT:PSS. Moreover, some results and values obtained using the commercially available high quality PEDOT:PSS; PH1000 are also presented and analysed for comparison.

Chapter 6 concludes the finding based on the obtained results and analysis of this study. Finally, some suggestions on future works are described.

CHAPTER 2

BACKGROUND STUDIES

Overview.

In this chapter, several topics in organic solar cell and thermoelectric were reviewed. The previous works reported by other researchers regarding organic solar cell, PEDOT:PSS material and thermoelectric were also described in details. This chapter begins with the background explanations on organic solar cell consists of the basic working principles and the view of the cross section of the device was also defined in details together with the description of the common materials used in each component in organic solar cell. The background of PEDOT:PSS material was also included to provide adequate knowledge about the subject material in this work. In addition, several materials which involved as doping substances in PEDOT:PSS were also described in details. This work was focused on using modified PEDOT:PSS as buffer layer in organic solar cell and in thermoelectric device. Hence the concepts of efficiency and performance of the organic solar cell and thermoelectric device were also elaborated in depth in this chapter.

2.1 Background of Organic Solar Cell Devices.

An organic electronic devices such as organic solar cell (OSC) and organic light emitting diode (OLED) have been widely fabricated due to its promising performance, having good flexibility, environmentally clean, and low fabrication cost. Many studies were implemented in order to improve the efficiency and stability of the devices which focusing on the main components of the devices. In both devices, the basic components consist of two electrodes, namely cathode and anode, active layer and buffer layer. The buffer layer

acts as the supportive medium incorporated the electrodes and active layer for the improvement efforts in the devices.

Polymer based-organic solar cell specifically focusing on organic solar cells made of active layer of the composite polymer materials become the main focus in this study. Such active layer of around 100 nm thick can be prepared via solution processing techniques. By referring to Figure 2.1, as light strikes on the glass substrate of the device, the photons pass via the transparent glass and anode layer before they reach the active layer. The absorption of photons in the organic active layer forms the bounds of electron-hole pairs known as excitons. The difference in work function between donor and acceptor layers in active layer will urge the separation of electron and hole in the excitons (Kietzke, 2007). The donor and acceptor materials used to determine the charge carrier transport after the diffusion process in the active layer of the organic solar cells. As a result of the diffusion process, the electrons will flow towards the cathode while holes move towards anode (Lin et al., 2012).

In polymer based-organic solar cell, the active layer normally consists of bulk heterojunction composite polymer of donor and acceptor materials where a conjugated polymer material such as P3HT acts as electron donor while fullerene derivative such as PCBM will act as electrons acceptor component. This heterojunction layer is able to form an interpenetrating network that provides a large interfacial area for charge separation and continuous pathways for charge transport (Mauger et al., 2012).

Both materials have differences in their highest occupied molecular orbital (HOMO) level of the donor (quasi Fermi level of the holes) and the lowest unoccupied molecular orbital (LUMO) level of the acceptor (quasi Fermi level of the electrons). This gradient in the chemical potentials of electrons and holes yields an internal electrical field

which defines the maximum open circuit voltage (V_{oc}) and leads to a field-induced drift of charge carriers assists by the internal electric field. Donor material has excess amount of holes that will be transported to the anode, while acceptor material having excess amount of electron that will be transported to the cathode after the diffusion of exciton to free electrons and holes.

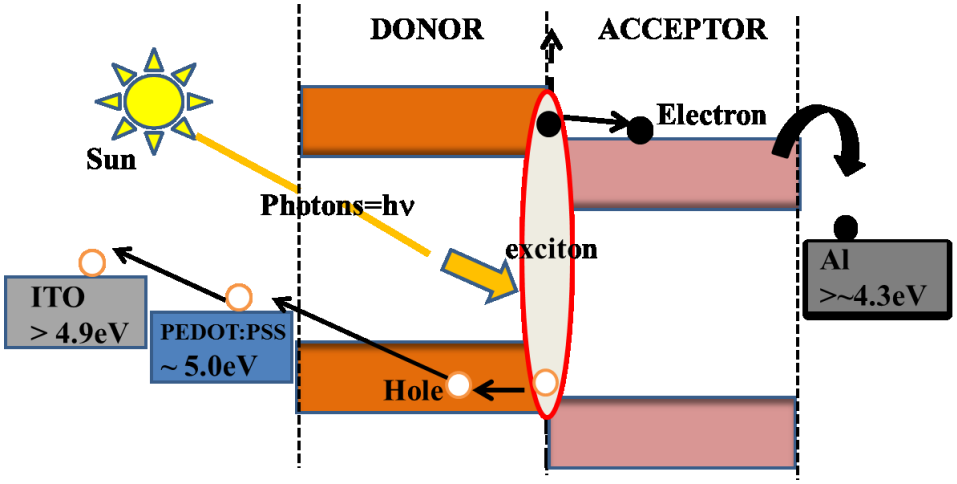

Figure 2.1 : Schematic diagram of the ideal operation in polymer:fullerene organic solar cell

In solar cell the efficiency is measured based on the amount of electric power of the device could produce and compared to the electric power of the device received from the sun. The measured electric power was produced by the collected electrons and holes when both free charge carriers flow accordingly from the organic solar cell to the external circuit. Specifically in organic solar cell, in order to ensure the smooth flow of free charges to each electrode, the efficient arrangement in the work function of the HOMO and LUMO levels of each component in the device is crucial. Both levels need to be arranged in a way that will permit a complete transportation of free charge carriers after receiving the sufficient energy from the sun. However, there is a possibility that the diffused charges of electrons

and holes will recombine back to exciton, which due to material defects or interface states hence decreasing the photocurrent generation and reduce the efficiency of photovoltaic device.

The recombination of free electrons and holes normally occur between the active and the cathode layers and also at the interfacial of donor and acceptor blend of active layer in organic solar cell. Therefore, to reduce the recombination of free electrons and holes, a buffer layer between electrode and active layer is introduced. A buffer layer which located between anode and active layer, should be able to block the electron away from anode by only allowing holes to pass through, such layer is also known as hole transport layer (HTL). In such way, the recombination of generated free charge carrier could be reduced, and the flow of holes to the anode can be increased. In particular, it can be suggested that a HTL is used for three reasons, firstly is to smooth the prickly surface of ITO, which can cause shorts, secondly is to create a link between the ITO (anode) and the active layer by providing alternating energy levels so that holes do not experience huge electrical barriers and lastly, it modifies the work function of the anode (Mauger et al., 2012).

PEDOT:PSS as semiconducting copolymer, is the most common used HTL material owing to several reasons and factors such as it is insoluble in organic solvents, conductive and it is transparent to visible light. Moreover, it possesses a stable work function, will accept holes from any polymer (regardless of its highest occupied molecular orbital (HOMO) and is electron blocking. This layer is significantly important because this electron blocking-layer improves device efficiency as it reduces dark current, which increases the open-circuit voltage of an organic photovoltaic (OPV) device (Mauger et al., 2012).

2.2 Poly (3,4-ethylene dioxythiophene): poly (styrenesulfonate) (PEDOT :PSS)

Poly(3,4-ethylenedioxythiophene) with its abbreviation, PEDOT is a well-known conductive polymer. In PEDOT chains there are charges or dipoles with specific structure called benzoid that is organized in curling order. A soluble PEDOT derivative was prepared by electrochemical polymerization method which yields an insoluble polymer with interesting properties of high conductivity and almost transparent in its thin and oxidized state of PEDOT film (Crispin et al., 2003).

Originally, it is impossible to form PEDOT pristine films in ambient condition because the pristine PEDOT is very unstable in its neutral state where the oxidation rate is high in air. Moreover it is insoluble in all common solvents hence by p-doping the PEDOT with high conductivity can be achieved. However PEDOT also can be over-oxidized where the oxidation may yield the traps that could cause drastic decreased in its conductivity values.

In order to overcome the poor solubility issue, a polyelectrolyte namely poly (styrene sulfonic acid) (PSS) was employed as primary doping material for PEDOT in order to ensure its solubility in water. PSS acts as a negative counterion to the positively charged PEDOT and results in the charge-balancing dopant of PEDOT:PSS combination (Cook et al., 2014). This mixture produced an aqueous dispersion of PEDOT:PSS with several advantages of forming a better film, higher conductivity, transmits higher visible light and good stability (Pathak et al., 2015). In addition, this polymer blend also possessed a stable polymer system which in return desires only a simple processing procedure such as spin coating technique to perform film on different substrate materials (Yan et al., 2009).

The simple description of the structure of PEDOT:PSS thin film is illustrated in Figure 2.2 where the image representing the aqueous solution of PEDOT:PSS. It is consists

of PEDOT rich particles and covered by PSS lamellas. The PSS portion developed thin top layer onto the PEDOT-rich particles which immersed beneath PSS after solid state processing (Xiong & Liu, 2012).

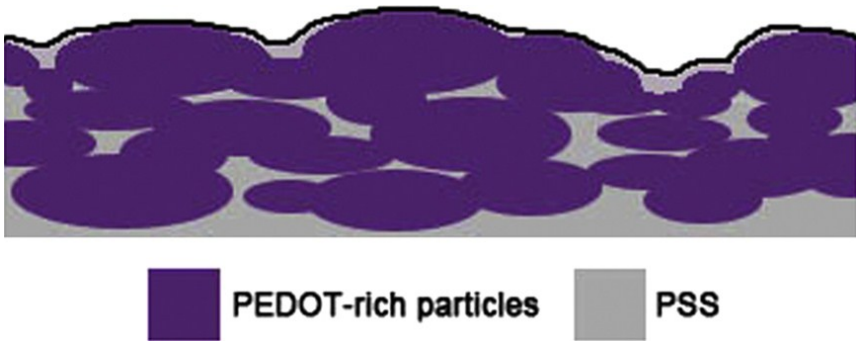

Figure 2.2 : Schematic of cross sectional morphological model of PEDOT:PSS thin film.

In addition to clearly visualize the chains condition of both polymers, J. Gasiorowski et al have described PEDOT:PSS in Figure 2.3 as a complex system where the PEDOT rich particles (blue) covered several parts of the isolated PSS rich chain(red) with a range of magnitude from micro to nano sizes. The aqueous PEDOT:PSS solution consists of polymer chains that form compact random coils of spherical nanostructure during the drying process in solid state films.However, in the case of the doped of DMSO into PEDOT:PSS, this spherical form of PEDOT:PSS shape was gradually transformed to an ellipsoidal arrangement (Gasiorowski et al., 2013).

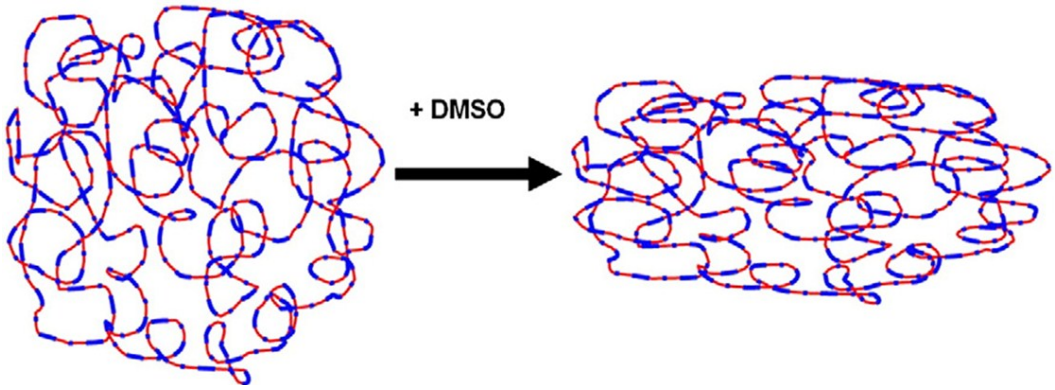

Figure 2.3 :Illustration of PEDOT:PSS polymer chains before doping and after doping to DMSO.

Although PEDOT is insoluble and owns a low molecular weight polymer but it is conductive, while PSS is an insulating polymer but yet possesses a high molecular weight. The combination of both polymers yields equilibrium in their chemical and physical properties which offers flexibility that required in PEDOT solution. Moreover, the electrostatic attraction of oligomer PEDOT portions to PSS chains have increases the solubility of the compound resulting in easier processing procedure (Laskarakis et al., 2013).

The chemical structure built in PEDOT consists of two resonant structures, benzoid and quinoid as demonstrated in Figure 2.4. The benzoid structure was based on two conjugated-electrons that form the C_α-C_β bond, while for quinoid structure no conjugated electrons on the C_α-C_β bond. The PEDOT structure may transform from benzoid to quinoid condition complemented by conformational adjustment in the chains from coil shape to linear or expanded-coil shape. This transformation happens to reduce the complexity of the structure and results in enhancement of the electrical properties of PEDOT (Wichiansee & Sirivat, 2009).

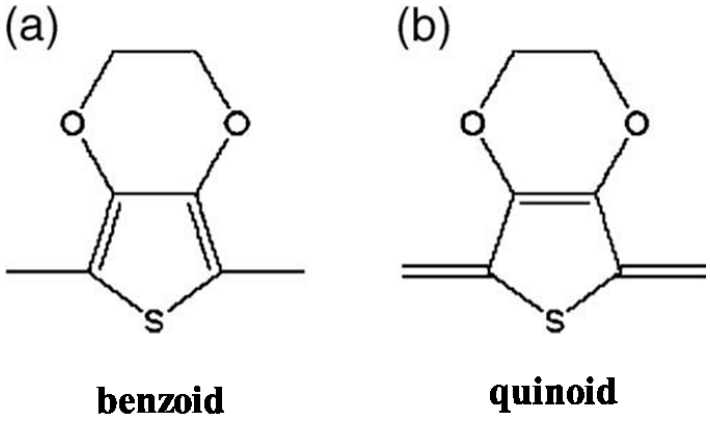

Figure 2.4 : Two kind of resonant structures exist within PEDOT.

Both structures of benzoid and quinoid may exist in PEDOT:PSS film. The benzoid structure seems to be the preferred structure for a coil conformation, while the quinoid structure could be the favored structure for a linear or expanded-coil structure. The transformation from curly-based structure of benzoid to the straight or extended coil of quinoid structure leads to the conductivity enhancement on the PEDOT chains (Teguh & Yeow, 2014).

Buffer layer can be important components in organic optoelectronic devices of both OSC and OLED in enhancing their electronic conduction ability. In OSC, the main purpose of buffer layer is to support the gathering of holes which were diffused in active layer to anode layer in order to generate electricity. PEDOT:PSS seems to be the most preferable material used as buffer layer due to several beneficial properties. Instead of having a direct contact arrangement of anode (ITO) and active layer, PEDOT:PSS can be used as the best solution to have the superior injection/collection of charge carrier which is located between the ITO (anode) electrode and bulk heterojunction active layer. This is due to the ability of

PEDOT:PSS in forming a uniform, conductive, transparent and stable thin film which results in a stable and smooth ITO surface. Therefore, the advantages of PEDOT:PSS leads to the improvement in the connection to the organic layer and support the hole injection to the electrode (Ouyang et al., 2004; Wichiansee & Sirivat, 2009).

2.3 Doping in PEDOT:PSS.

PEDOT:PSS possesses high transparency properties that permit a large amount of photons to pass through it and subsequently reach the active layer. However, the function of PEDOT:PSS as HTL is not only rely on the transmission of photons but also as a transport agent to usher the free holes from active layer to anode in organic solar cell. Hence the ability of PEDOT:PSS in assisting the flow of free holes from active layer is strongly depends on its electrical properties aspect. The efficient electrical properties of conductivity and mobility of PEDOT:PSS are the important factors in order to transport maximum rate of diffused free holes to the anode of the device.

Although PSS is the primary dopant for enable PEDOT to become soluble in water, the original nature insulation properties of PSS seems to create minor limitation for PEDOT conduction to perform as a good free charge transporter. Such discrepancy may be due to the lamellas structure of PSS surroundings the PEDOT causing the reduced in its electrical conduction. In order to overcome this limitation, several options were implemented to increase the electrical conduction of PEDOT:PSS. Grid deposition and soft lithography (Aernouts et al., 2004; Glatthaar et al., 2005) of PEDOT:PSS are among the methods that contribute to the enhancement of its electrical properties. However, the second option via doping process using the polar solvent into PEDOT:PSS is most likely to be an economical and environmental friendly. Among the potential secondary dopant that can be used for this

purpose are glycerol, ethylene glycol (EG), DMSO and sorbitol (Dimitiev et al., 2009; Huang et al., 2008; Ouyang et al., 2004; Rodriguez et al., 2011).

On the other hand, an inorganic metal oxide can also be used as an alternative dopant in PEDOT:PSS to increase its electrical conduction. The attempt on using ZnO or AZO as buffer layer were implemented which has been proven to enhance the performance of organic solar cell (Dong & Zhou, 2010) since zinc oxide own high electrical conduction properties and high transparency. Moreover, the metal oxide such as zinc oxide with aluminum (metallic) doped is believed to be able to improve the mobility and conductivity of zinc oxide itself. Hence, the mixture of both PEDOT:PSS and zinc oxide seems to be good potential combination in rising the electrical aspect of PEDOT:PSS thin film (Park et al., 2011;Dong & Zhou, 2010; Semaltianos et al., 2010; Sharmaa et al., 2009).

2.3.1 Glycerol doped PEDOT:PSS.

Glycerol in liquid state is under 3-OH group in plyol compound appears as colorless liquid, odorless and have a syrupy and sweet taste. The best part of glycerol is that it is a non-toxic material that has a high boiling point and can be used as plasticizer.

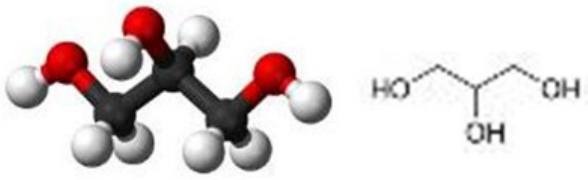

Glycerol

Figure 2.5 : Molecular structure of glycerol

As illustrated in Figure 2.5, glycerol was previously chosen as a secondary dopant in PEDOT:PSS in organic thin film transistor (OTFT). The deposition of glycerol doped

PEDOT:PSS was made by using ink jet printing process for OTFT fabrication. It was found that, with the addition of glycerol into PEDOT:PSS, It contributes not only in modifying the viscosity condition from ink jet process but also enhanced the electrical conductivity of PEDOT:PSS (Lee et al., 2010).

In addition of using glycerol doped PEDOT:PSS in OTFT, this combination seems to establish interesting performance in organic light emitting diodes (OLED) as well. Ana B. Rodriquez and her team suggested that glycerol exists as a cross-link agent which offers protection to PEDOT:PSS from water and moisture. Hence, the OLED device with glycerol doped seems to provide advantage in practical application results from high quality consistency of the device even after water immersion testing. However it is essential to control the addition of glycerol since the quality of the device performance is declined with larger amount of glycerol. The optimum amount of glycerol is suggested to be around 5% to promise a good performance of OLED device (Rodriquez et al., 2011).

Another work on using ink-jet method for glycerol doped PEDOT:PSS film printing have been performed by Zhaoting Xiong et al. In addition of thermal annealing process to the developed thin film, glycerol doped results in improving the film jetting process due to the change in ink viscosity. Moreover, the conductivity of PEDOT:PSS with glycerol also increase drastically 300 times compared to PEDOT:PSS without glycerol (Xiong & Liu, 2012).

The preheated treatment of glycerol doped PEDOT:PSS thin films was proved to exhibit better conductivity where it increased for over three orders of magnitude compared to the preheated pure (pristine) PEDOT:PSS (Yin et al., 2010). The enhancement of electrical properties also accompanied by the tremendous reduction in resistivity of PEDOT:PSS and the decreased in transmittance with the high heating temperature to the doped PEDOT:PSS. However in average, the decline of only about 1-3% at short

wavelength (300-600nm) in its optical properties is still in a reasonable and sufficient range for buffer layer application in organic solar cell (Tsai et al., 2008).

Glycerol doped PEDOT:PSS has also been utilized as a top electrode in the fabrication of inverted organic photodiodes by T.Nyberg et al. The device shows interesting outcome with glycerol doped PEDOT:PSS, poly (3-(4'-(1",4",7"-trioxaoctyl) phenyl) thiophene) (PEOPT) and bismuth as transparent anode, organic active layer and metal cathode, respectively. They claim that the successful process of spin coating the doping of glycerol to PEDOT:PSS onto the hydrophobic PEOPT is due to the glycerol existence and the silanize procedure upon PEOPT (Nyberg, 2004). Thus, their findings have encouraged high motivation to utilize glycerol as one of our doping candidate material in this work.

2.3.2 EG doped PEDOT:PSS.

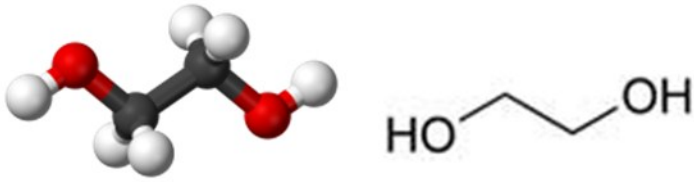

Ethylene Glycol

Figure 2.6 :Molecular structure of ethylene glycol

As shown in Figure 2.6, it is shown that EG is mostly identical with glycerol in its physical appearances which is odorless and colorless in liquid condition. The taste of EG is also syrupy and sweet and has a high boiling point. However compared to glycerol, EG comes from a 2-OH group in plyol component and is highly toxic material.

Work on EG as a dopant for PEDOT:PSS aqueous solution was implemented (Ouyang et al., 2004) where the conductivity of PEDOT:PSS was observed to be increased from 0.4 to 200 S/cm. In this case, the conductivity enhancement is believed to be strongly

dependent on the chemical structure and the EG treatment that lowers the energy barrier for charge hopping among the PEDOT chains. Their clear explanation on the enhancement of conductivity with EG doped PEDOT:PSS offers high motivation on this study. EG could to a drastic morphology arrangement with existence of large domains results in increasing the interchain interaction.

Moreover, EG treatment encourages the PEDOT chains transformation from the benzoidto the quinoid structure which leads to a conformation changes from the coil structure into expanded-coil or linear structure. Enhancement in conductivity of PEDOT:PSS with EG addition is due to the major impact in PEDOT chains which is registered as the conductive polymer chains. On the other hand, EG addition is likely to overcome the isolation effect of PSS in the PEDOT:PSS compound (Teguh et al., 2014).

Another interesting research was from W.Wichiansee and A.Sirivat work which strongly offers great support in the use of EG in the present work is the mixture of EG and PEDOT:PSS in certain volume ratios by casting process and dried in vacuum oven at 100°C. The drying processes at different range of temperatures of EG doped PEDOT:PSS contribute in water lossen, the loss of the residue solvent EG, the side chain degradation and the polymer backbone degradations of PSS and PEDOT chains. All transitions not only responsible in increasing the particle electrical conductivity of PEDOT:PSS but it also affects the electro-rheological properties of PEDOT:PSS blends (Wichiansee & Sirivat, 2009).

The used of EG in this work is important for the comparison purpose with the result from the used of glycerol as dopant since both were under the same alcohol group with almost the same molecular structure. However glycerol is very much less toxic than EG, therefore the study on EG seems to be a compliment to glycerol in order to investigate their ability as doping material in PEDOT:PSS.

2.3.3 Zinc Oxide and Aluminum Zinc Oxide doped PEDOT:PSS.

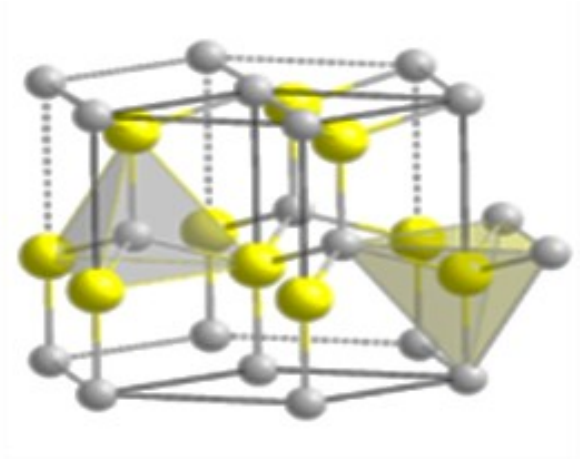

Figure 2.7 :Molecular structure of aluminum zinc oxide

The molecular structure of ZnO is shown in Figure 2.7. In effort to develop a hybrid organic device which merges the organic material and inorganic material, zinc oxide is suggested to become the high potential candidate to cooperate with PEDOT:PSS. The n-type properties of zinc oxide could increase the number of electrons in PEDOT:PSS and also reduce the energy band of PEDOT:PSS. As a result, the conductivity of PEDOT:PSS is expected to increase with the doping of this metal oxide.

The corporation of ZnO nanoparticles into PEDOT:PSS by laser ablation which was proven to enhance the electrical properties in double has offer major motivation of using this metal oxide as the inorganic doping material to PEDOT:PSS (Semaltianos et al., 2010). In addition, ZnO was also doped to the most well-known dopant material, aluminum which was expected to produce interesting outcome of conductivity enhancement. Other than that, several works involving ZnO and AZO as buffer layer in organic solar cell device also encouraged the usage of ZnO and AZO materials in this research (Godoy et al., 2010; Ju et al., 2009; Dong & Zhou, 2010; Sharmaa et al., 2009).

In another different work, zinc oxide nanoparticles have been used to replace PEDOT:PSS as buffer layer in organic solar cell. The buffer layer acts as a hole blocking layer to prevent recombination process of the charge carrier dissociation. Zinc oxide nanoparticle acts very well as a buffer layer although not much improvement is observed compared to the device with PEDOT:PSS as a buffer layer (Dong & Zhou, 2010).

Moreover, an encouraging result in a research using ZnO as buffer layer has been presented where ZnO was used as intrinsic buffer layer on AZO transparent electrode of organic solar cell. This buffer layer was successfully avoid the shunt path in the device and enhanced the device performance owing to the one without the intrinsic ZnO layer (Park et al., 2011).

Different approach has been reported by the use of double layer of ZnO as buffer layer inserted between ITO and PTA6/PCBM device and significant raising was found in the amount of free electrons from active layer to electrode. Although it only contributes to small increment in the efficiency of the organic solar cell, it demonstrates that this metal oxide material works well within organic material (Ju et al., 2009).

2.3.4 DMSO doped PEDOT:PSS.

Figure 2.8 illustrates the molecular structure of DMSO. To date, the doping of DMSO to PEDOT:PSS was reported where the conductivity of PEDOT:PSS PH1000 is successfully improved to 1000 $S.cm^{-1}$ (Gasiorowski et al., 2013) with the addition of DMSO. The finding is even more interesting since it also maintained the optical properties at a good range with the DMSO existence. Hence the modify PEDOT:PSS is in good condition to replace the shortcoming and expensive ITO in organic optoelectronic application in future (Gasiorowski et al., 2013).

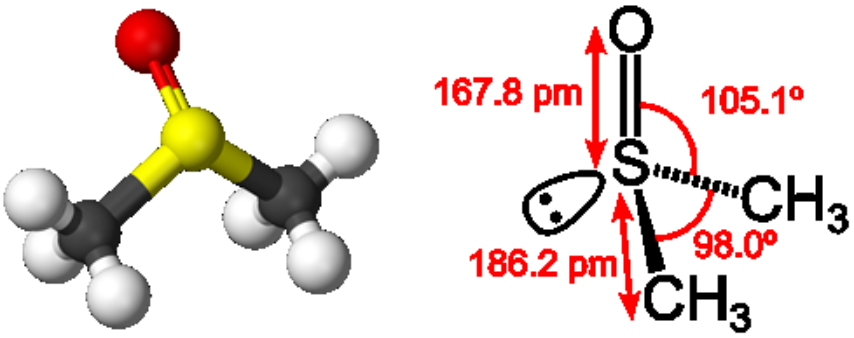

DMSO

Figure 2.8 : Molecular structure of DMSO

The post annealed treatment of DMSO doped PEDOT:PSS contributes to the efficiency of OSC up to two order of magnitude. The conductivity of pure PH1000 PEDOT:PSS is drastically increased from 1.65 to 866 $S.cm^{-1}$ with the present of DMSO. Hence it motivates the authors to imply this DMSO doped PEDOT:PSS as buffer layer in organic solar cell with P3HT/PCBM as the active layer organic material.

The variation in surface morphology with the existence of DMSO attributed to the improvement in electrical properties of PEDOT:PSS. Hence, the increase of charge carrier transport mobility contributes to the raise of the electrical conductivity of free holes from the active layer to the anode. Therefore, the improvement in buffer layer needs to be taken into account in ensuring the better efficiency in organic solar cell (Karagiannidis et al., 2012).

Due to the interesting outcome of efficiency in the device with DMSO doped PEDOT:PSS as buffer layer, the work on replacing ITO with this doped conducting polymer seems to be highly motivated. Seok-In Na et al shows that the use of DMSO doped PEDOT:PSS as polymer anode in organic solar cell exhibits comparable efficiency with the

conventional organic solar cell with ITO as anode layer. Hence the authors suggested that the issues of limitation and expensive ITO may be overcome with this alternative (Na et al., 2008).

In addition, O.P.Dimitriev et al compared the conductivity of DMSO doped PEDOT:PSS with EG doped PEDOT:PSS. They concluded that DMSO produced better performance in enhancing the electrical properties of PEDOT:PSS compared to EG. An equal amount of doping DMSO and EG is mixed with PEDOT:PSS which shows drastic difference in the conductivity value of the PEDOT:PSS. The conductivity of PEDOT:PSS is increased after the doping of DMSO and EG from 0.022 S/cm (in pristine) to 1.75 S/cm and 0.5 S/cm, respectively . Hence, the doping of DMSO to PEDOT:PSS seems to offer better performance for this conducting polymer in organic optoelectronic device application (Dimitriev et al., 2009).

However, carbon nanotube (CNT) seems to be a tertiary dopant after PSS (for soluble PEDOT), and DMSO (to improve conductivity). CNT gives further increase in conductivity by reducing the resistivity even more. The electrical conductivity is increased even more with the combination of DMSO with CNT as dopants for PEDOT:PSS by giving further advantage as a heat dissipation material for flexible electronic devices (Park et al., 2011). However, DMSO is a highly toxic material which is not really encouraged to be used for our work that mainly focus on low cost fabrication and green technology application (Elmoazzen et al., 2007; Ravindran et al., 2011).

2.3.5 Other addition to PEDOT:PSS.

Yijie Xia et al, enhanced the conductivity of PEDOT:PSS by treating itwith a fluoro compound, hexafluoroacetone (HFA). The interactions between amphiphilic HFP2OH of this compound and PEDOT:PSS is responsible in inducting thephase segregation of some hydrophilic PSSH from PEDOT:PSS. In addition the merge of HFA and PEDOT:PSS can also attributes to the conformational change of the conductive PEDOT chains. The conductivity drastically increases in four factor of magnitude with HFA by two significant interactions exclusively to PEDOT and PSS. The hydrophobic $–CF_3$ groups from the HFA compound reacted with the hydrophobic PEDOT chains while the hydrophilic of –OH groups of HFA compound reacted with hydrophilic PSS chains (Xia et al., 2012).

However, HFA is highly hazardous toxic that may harmful to the human breathing system and affected to the human skin as well. Hence, in spite of the interesting result in enhancing the conductivity of PEDOT:PSS, this is off listed in order to establish organic device in green technology.

2.4 Power conversion efficiency.

The components in organic solar cell based on substrate of ITO as the cathode, PEDOT:PSS as buffer layer, active layers of P3HT and PCBM and anode of aluminum. The materials were sandwiched in such an order according to their energy level to promise the flow of free charge carrier to cathode and anode. By referring to Figure 2.9, the work function of aluminum (Al) as cathode is arranged to be higher than the anode (ITO) level to urge the diffusion of free charges to flow on their respective ways, where electrons to cathode and holes to anode. PEDOT:PSS plays a role as a buffer layer where it is located at

the middle between ITO (anode) and the active layer of P3HT:PCBM bulk heterojunction which will act as a bridge for the transportation of holes to anode.

The difference in work function in active layer was reflected by the diode behavior of the device without any exposure to light. The open circuit voltage, V_{oc} was occur which due to the existence of internal electric field with the energy band difference. However as the device were exposed to light, the diffusion process of free charge carrier will generates the short circuit current with the light influence.

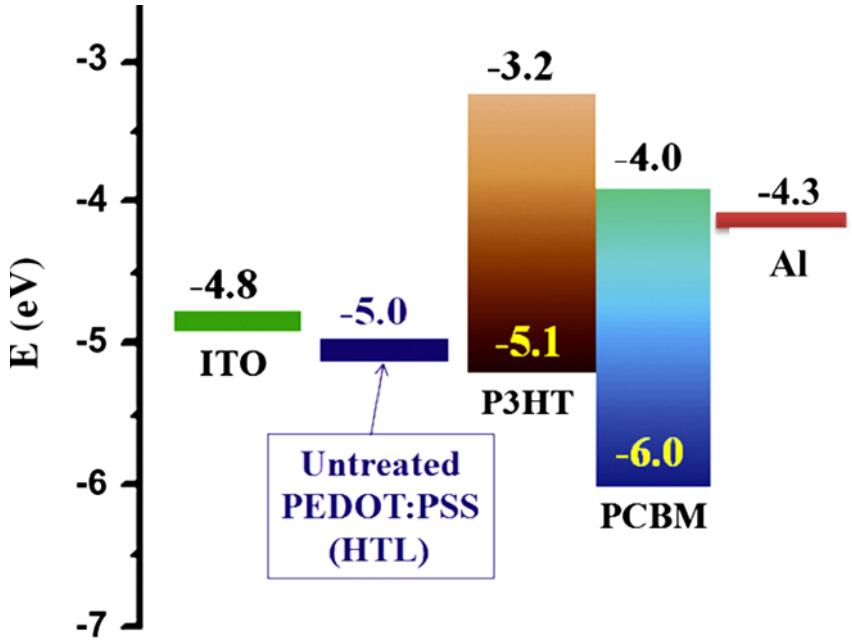

Figure 2.9 : Energy band diagram of the organic solar cell components(W. Zhang et al., 2014)

Figure 2.10 represents the current-voltage (I-V) plot of organic solar cell in dark condition, which forms a curve that obeys ideal diode behavior. The I-V measurement is a task to obtain the current versus voltage or resistance characteristics by providing voltage-current stimulus and measuring current-voltage reaction. It is a basic electric measurement and a fundamental way to discover behavior and characterize the semiconductor devices,

electronic devices and new materials. The I-V plot will provide the information on the electric power generates by the measured device.

The operating regime of the solar cell in which the cell generates power corresponds to the voltage range from 0 to V_{oc}, where the $V_{oc}$is the open circuit voltage. The V_{oc} value is normally influenced by the bias at the p-n junction of the device under light illumination condition.

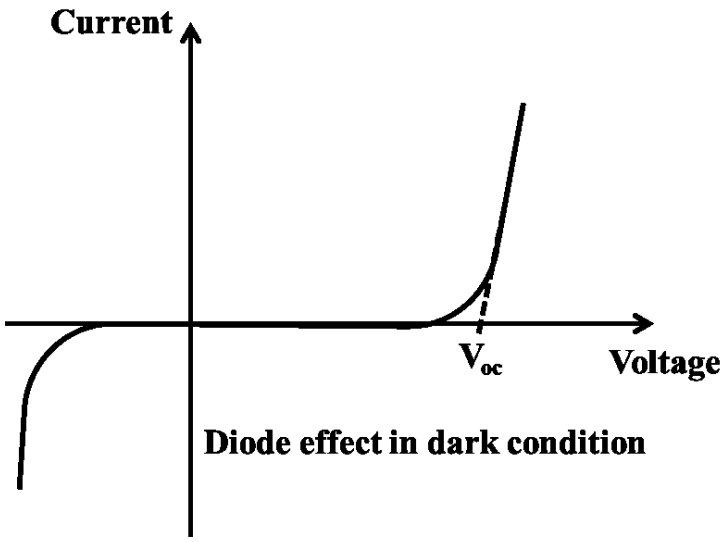

Figure 2.10: The current-voltage characteristics of an ideal organic solar in a dark condition cell (no light applied on the device).

Basically, the cell power, P is given by the product of the current (I) and voltage (V) produced by the organic solar cell. In addition, the device power, P reaches a maximum at the cell's operating point or maximum power point. This point occurs at a maximum voltage, $\boldsymbol{V}_{max}$and maximum current $\boldsymbol{I}_{max}$as illustrated in Figure 2.11.

Apart of V_{oc}, other quantities, namely short circuit current density, J_{sc}, fill factor, $FF$and device efficiency, η are the main parameters for the performance characteristics of a

solar cell and can be directly deducted from I-V plots under light condition as shown in Figure 2.11 (Benanti & Venkataraman, 2006).

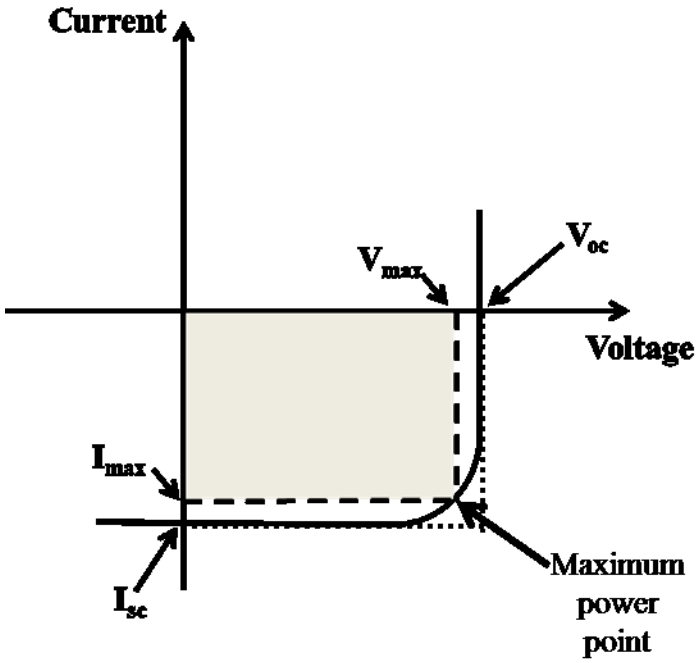

Figure 2.11 : The current-voltage characteristics of an ideal organic solar cell in light condition.

The J_{sc} is the current produced by the organic solar cell while no potential difference applied to the device. It occurs due to the short circuit in the device produced by the generation and collection of light-generated carriers. It is determined from the curve at the I-V plot together with the open circuit voltage, V_{oc}. The current density, J_{sc} is constructed by dividing the I_{sc} value taken from the I-V plot with the active area of the device approximately about 10 cm^{-2}.

The fill factor (*FF*) is defined as the ratio of the actual maximum power output to its theoretical power output if both current and voltage were at their maximum I_{sc} and V_{oc}, respectively. The FF is the key parameter to determine the cell performance and it is measured by the area at the fourth quadrant of the I-V curve as shown in Figure 2.11.

$$FF = \frac{J_{max}V_{max}}{J_{sc}V_{oc}} \quad 2.1$$

On the other hand, the power conversion efficiency, η of the cell is the power density delivered at operating points ($J_{sc}V_{oc}$ *x FF*) as a fraction of the incident light power P_i (Bin Yin, Qian Liu, et al. 2010). The efficiency is also determined as a percentage of the ratio of output power, P_o, produced by the device to the applied input power, P_i from the light illumination.

$$\eta = \frac{J_{sc}\times V_{oc}\times FF}{P_i} = \frac{P_o}{P_i} \quad 2.2$$

In addition, the efficiency is also determined as a percentage of the ratio of output power produced by the device to the applied input power from the light illumination.

2.5 Thermoelectric properties in doped PEDOT:PSS thin films.

The performance in thermoelectric device is based on the figure of merit (ZT) value which consists of:

$$ZT = \frac{\sigma.S^2}{\kappa}T \quad 2.3$$

This parameter is determined from the ratio of the product of electrical conductivity, σ, the Seebeck coefficient, S and the temperature, T to the thermal conductivities, κ of the materials used as p-type and n-type in the thermoelectric device.

The countless wasted heat produced in the surrounding which due to several processes in the active industrial productions have not been recycled properly. However the thermoelectric generation technology intends to conduct an efficient project using these low

grade wasted heats based on their solid-state energy conversion mode. It seems to be a high potential project due to its very low cost or even no cost in resources aspect which added extra benefit for energy-saving and emission reduction in the green technology in future (Gou et al., 2010).

In the thermoelectric device, the heating process of the aluminum top contact may influence the charge transport properties of the p-type and n-type materials. By the present of such thermal treatment, it may modify the structural characteristics of the organic semiconductors, due to the fact that the transport properties of semiconducting films are strongly depend on their structure of grain size and shape as well as the characteristics of the contact between them (Rusu et al., 1998). In addition, the heating at one side of the TE device constructs a temperature difference between both opposite sides which causes charge carriers in the material to diffuse from the hot side to the cold side. The separation of charge to the cold side creates an electric potential between two sides until it stops at the maximum value since the electric field is at equilibrium.

However, as the temperature gradient increases, it continues to collect the charged carriers onto the cold side which results in the growth of thermoelectric voltage and subsequently produce electric power in TE device. Therefore, it can be suggested that the variation of temperature gives Seebeck effect to the charge transportation in the material and subsequently contributes to produce electricity. The schematic diagram of thermoelectric device is illustrated in Figure 2.12.

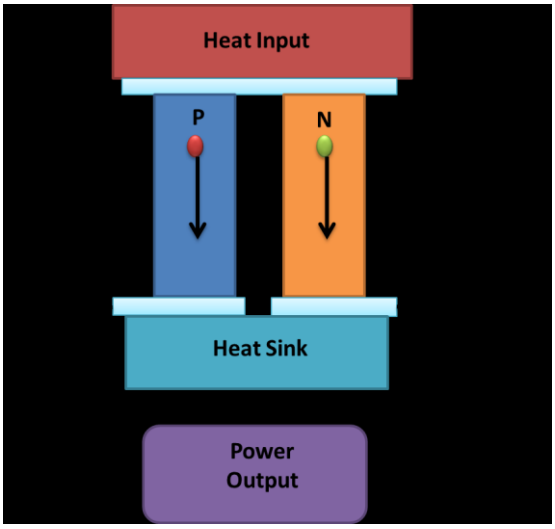

Figure 2.12 : Schematic diagram of the thermoelectric device and its external circuit.

One of the main characteristic of polymer materials that is low in thermal conductivity, κ is essential in thermoelectric concept in order to yield high performance in the device which is measured by the high ZTs. The studies on TE properties of PEDOT:PSS have started about a decade ago, in 2002 when J.Y.Kim et al discovered that the Seebeck coefficient decreased with the addition of dielectric solvent of DMSO (J.Y.Kim et al. 2002). Since the incorporation of PEDOT:PSS with DMSO has downgraded the TE properties, the mixture of this organic material with inorganic material such as Bi_2Te_3 and Te nanorods were implemented as an positive alternative. However, it results in a finding that the efficiency of TE properties is highly depends on the individual components, hence all compounds involve in PEDOT:PSS need to be enhanced in order to obtain high performance in TE properties (Tsai et al., 2011).

It is interesting that the conductivity of PEDOT:PSS can be enhanced drastically by the addition of various organic solvents such as glycerol, ethylene glycol and sorbitol. Hence, in addition to its low thermal conductivity, flexibility and great thermal stability, the high adjustable electrical conductivity of PEDOT:PSS hasbecomes a major advantage inapplying it as thermoelectric material (Feng-Xing et al., 2008).

Table 2.1: Electrical and thermoelectric properties of PEDOT:PSS.

Materials	Conductivity (S/cm)	Seebeck coefficient (μV/K)	Power factor, $S^2\sigma$(mW/m.K)
PEDOT:PSS P	~50	~13	8.45
PEDOT:PSS PH510	~300	~13	50.70
PEDOT:PSS PH1000	>900	~25	562.50

PEDOT:PSS has been widely studied in terms of its thermoelectric properties and has shown a good potential to be used in thermoelectric device. Table 2.1 tabulates the list of thermoelectric properties of several types of PEDOT:PSS. The types of PEDOT:PSS are listed in Table 2.1 as PEDOT:PSS(P), PEDOT:PSS(PH 510) and PEDOT:PSS(PH1000) with the conductivity of 50 $S.cm^{-1}$, 300$S.cm^{-1}$to 1000 $S.cm^{-1}$, respectively (Zhang et al., 2010). The upgraded PEDOT:PSS exhibit large increment in all thermoelectric parameters that consists of electrical conductivity, Seebeck coefficient and its power factor.

This is as to date such a common results produced for any conducting polymer that have been studied (Zhang et al., 2010). However the Seebeck coefficient of PH1000 has drastically increased with the increment in electrical conductivity. The conductivity in modified PEDOT:PSS were improved due to the alteration of charge mobility. Hence a significant increment in Seebeck coefficient can be ascribed to the growth of charge concentration amount in the solutions (Liu et al., 2010).

Due to these interesting performance, the study on the effect of doped PEDOT:PSS with glycerol, ethylene glycol (EG), zinc oxide (ZnO) and aluminum zinc oxide (AZO) in this presence work to their thermal behavior is studied and observed. Moreover,

PEDOT:PSS PH1000 is used as the p-type thermoelectric material and paired with two interesting organic materials, 3,4,9,10-Perylenetetracarboxylic dianhydride (PTCDA) and tris(8-hydroxyquinoline) (Alq_3) as n-type thermoelectric materials in a built in thermoelectric module. The present work was focused on the investigation on the Seebeck effect of these paired materials with respect to the temperature gradient across the thermoelectric module.

As shown in Figure 2.13(a), PTCDA is a n-type organic material of the small molecule group which has its own ordered crystalline structures. The charge transport is assumed to be more efficient for a higher electrons mobility (Zahn et al., 2006). This perylene derivative acted as a model system owing to its ability in constructing, well-ordered layers on a variety of substrates which is an important factor for providing effective electrical properties to PTCDA (Nicoara et al., 2006). As a result, PTCDA is likely to become a good candidate as n-type organic material in the TE device. To the best of our knowledge, this work is the starting point in studying PTCDA as n-type material for the TE device. The outcome of this work is expected to provide a useful information on organic TE technology for the future.

On the other hand, Alq_3 has attracted our attention for studying TE properties due to its very interesting properties as an electron transport material in organic light emitting diodes (OLED) (Meyers & Weck, 2004). As shown in Figure 2.13(b), Alq_3 is a small molecule material with ordered crystalline structures which is the significant requirement for an efficient transport of charge for a higher carrier mobility (Zahn et al., 2006). Best of our knowledge, Alq_3 has yet not been investigated as n-type material in the TE device. Therefore, Alq_3 has been introduced as n-type material in this work without any alteration or dopant treatment in order to investigate its own potential as n-type material in

thermoelectric device. The function of this study is to give some feedback on the preliminary attempt of using Alq_3 in thermoelectric device.

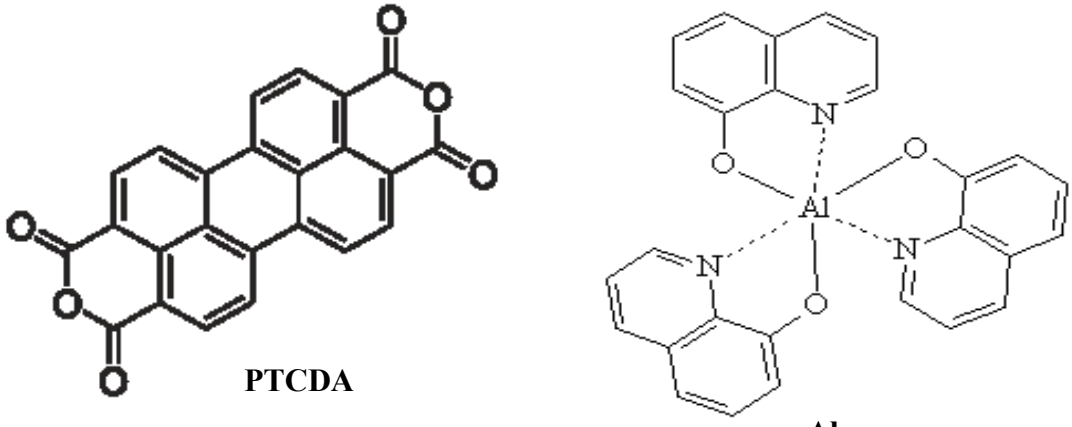

Figure 2.13 : Molecular structure of two organic materials used as n-type in thermoelectric module .

2.6 Conclusion.

This review provides general information in the modified PEDOT:PSS and their usage as buffer layer in organic solar cell. The demand to increase the efficiency of organic optoelectronic devices offers major requirement in modifying PEDOT:PSS since this conducting polymer is the main material for hole transport layer in the device. The addition process or so called secondary doping of PEDOT:PSS with organic solvent or other mechanical methods are crucial in order to upgrade its performance in organic optoelectronic devices. However due to the principle of green technology, the used of environmental friendly, nontoxic, cheap and a simple process material is highly suggested. Hence this work is specifically focused on glycerol, EG and doped zinc oxide as the doping materials to PEDOT:PSS.

Furthermore, the review also covered the thermoelectric concept and a brief introduction on the organic materials that were used in this work. Concise observation on the application of high conductive PEDOT:PSS and two n-type organic materials were also included to lead an advance work on another possible renewable energy device which is expected could be merge to organic solar cell in order to maximize the light source in two ways applications of solar energy and heat energy.

CHAPTER 3

METHODOLOGY

Overview

The organic semiconductor materials used in this study is presented in chapter 3, in detail. Besides, the thin film preparations as well as experimental setup are also described here. Finally, the mathematical operations and procedures used to determine the optical, electrical and performance of organic solar cell and thermoelectric device were explained in this chapter.

3.1 Preparation of samples.

The PEDOT:PSS brand Clevios PH500 (Series number:81076210) from **Heraeus Precious Metals GmbH & Co.** was used without any alteration. The solutions were filtered by using 0.5μm nylon filter on the glass syringe before being mixed it with the dopant materials.

3.1.1 Synthesis of glycerol and ethylene glycol doped PEDOT:PSS

Glycerol and ethylene glycol (EG) are the two alcohol based materials which have the identical physical properties such as colourless, odorless and liquidity. Both were used without any alteration and mixed with PEDOT:PSS solution. Glycerol and EG were purchased from Sigma Aldrich Sdn. Bhd. with code number of G7893 and 324558respectively.The doping amount of glycerol and EG were determined by volume rate ratio. For example, 2% doped glycerol mixed to PEDOT:PSS was based on the volume of PEDOT:PSS, e.g: 5ml. Hence, the volume of 2% glycerol is:-

$$\frac{2}{100} \times 5ml = 0.1ml \quad 3.1$$

The amount of glycerol and EG doped to PEDOT:PSS were varied from 0% (which also named pristine PEDOT:PSS) to 8% with 2% interval. Each doping material was mixed to 5ml PEDOT:PSS and was placed under ultrasonic bath at room temperature for 1 hour. Subsequently all solutions were aged for another 24 hours before the deposition process.

3.1.2 Synthesis Of Zinc Oxide (ZnO) and aluminum zinc oxide (AZO) doped PEDOT:PSS.

The aim of this process is to synthesize zinc oxide solution and three aluminum doped zinc oxide solutions with different aluminum doping percentage from 2% to 6% with 2% interval. Then the solutions were mixed with PEDOT:PSS liquid in a simple process of ultrasonic bath to assure complete mixing between the metal oxide and semiconducting polymer materials.

The ZnO and AZO solutions of each aluminum percentage were prepared using sol-gel technique. First, the precursor solution of zinc oxide (ZnO) was prepared using zinc acetate dehydrate, $Zn(CH_3CO_2)_2.2H_2O$ as astarting material and dissolved in 2-methoxyetahnol. Few drops of diethanolamine (DEA) were used as stabilizer. This solution was then divided into four different vials. While one of the solution remains undoped, the other three were added with aluminum which obtained from aluminum nitrate $Al(NO_3)_3.9H_2O$ precursor with variation of atomic percentage, 2.0, 4.0 and 6.0wt %. Then all solutions including the pristine (undoped aluminum) were stirred at 3000 rpm under magnetic stirrer for 2 hours, and annealed at 60^{o}C. The resultant solutions which were very

clear and transparent were then kept ageing in vials for more than 48 hours before film deposition process.

3.1.3 Preparation of doped PEDOT:PSS thin film.

The solution of all doped PEDOT:PSS were used in preparing the thin film on the cleaned glass substrate by spin coating technique. Since the solution is based on organic substance that tends to decompose with a heating treatment, this method is suitable owing to its process which operates only under room temperature. Moreover, this method is identified to produce a uniform and controllable thickness of the organic thin film.

The WS400B-6NPP-Lite spin coater instrument was used in this work which required a nitrogen gas to control the pressure to hold the sample on its disk plate. The spin speed, spin duration and spin mode can be adjusted and programmed in order to obtain the desired thickness of doped PEDOT:PSS thin film.

In the present work, the thicknesses of all studied doped PEDOT:PSS were intended to be approximately constant since the focus is to study the effect on different type of material doping and their doping amount to PEDOT:PSS. Thus the spin speed for all doping PEDOT:PSS solutions were maintained at 3000 rpm and spun for about 60 s which expected to form doped PEDOT:PSS thin films with thicknesses only in the range of 100 nm to 150 nm. This range is the optimum thickness for buffer layer component in order to assist the absorption of phonon light to the active layer region and as hole transport layer to anode electrode.

Firstly, the cleaned glass substrate was placed at the middle of the disk plate inside the spin coater. The glass substrate was holding on the disk plate under vacuum condition while the spinning process is in progress. The instrument was set-up at the desired speed and duration before the spin coating process started. After the deposition process completed

the glass substrate was dried at 120°C for 20 minutes to remove the moisture in the deposited thin film. Later, all doped PEDOT:PSS thin films were ready for the characterization.

3.1.4 3,4,9,10-Perylenetetracarboxylic dianhydride (PTCDA) as n-type in thermoelectric device

PTCDA powder was purchased from Sigma Aldrich and consists of a red powder in colour. It was deposited on cleaned glass substrates under vacuum environment by a thermal evaporation technique. The deposition pressure is 1 x 10^{-3} Mbar and the time taken for a deposition process was around 3 min. This process produced PTCDA thin films with the thickness approximately ~100 nm.

3.1.5 Tris(8-hydroxyquinoline) aluminum (III) (Alq_3) as n-type in thermoelectric device

The process of Alq_3 deposition is very much alike with PTCDA, where the yellowish Alq_3 powder which was purchased from Sigma Aldrich was deposited under vacuum pressure of 10^{-3} Mbar for about 3 min. The Alq_3 thin films with thickness around 100 nm were then deposited on the cleaned glass substrates under the thermal evaporation process.

3.2 Fabrication of electronic devices.

3.2.1 Cleaning Process of Glass and ITO Substrates.

The glass slides were cut into 2 cm x 2.3 cm in dimension for each glass substrate. The glass substrates were immersed in soap water before being inserted in an ultrasonic bath for 20 min at room temperature. Then the glass substrates were rinsed in distilled (DI) water, followed by acetone together with ethanol and then completing the cleaning process

with rinsed in DI water again. The wet glass substrates were purged under nitrogen gas to dry them completely prior to the deposition process.

On the other hand, in order to determine the electrical characteristics and the solar cell fabrication, commercial indium tin oxide (ITO) glass substrates with a sheet resistance of 7 Ω/sq cm were used. Prior to the cleaning process, the ITO films were cut into 2.0 cm x 2.3 cm. In order to maximize the efficiency of the studied organic solar cell, the ITO films were patterned by using etching technique. The etching processes involved coating of undesired ITO layer with cellophane tape and followed by spraying the exposed areas with an alcoholic commercial paint. The alcoholic paint was used to protect the chosen ITO area from being etched. The paint on ITO glasses were then leave to dry for a while and then the cellophane tape were taken off and exposed the undesired area for etching process. Afterwards, the ITO glass were fully submerged into diluted hydrochloric acid (HCl:H2O=4:6) and were heated at 60°C for about 20 minutes in order to remove the ITO layer at the exposed area. Later, the etched ITO glasses were taken for further substrates cleaning procedure.

The steps were identical with the procedure of cleaning the glass substrate. However, the alcohol cleaning part in glass substrate procedure was replaced with isopropyl for ITO cleaning process. After blow-drying the patterned ITO substrate, theywere ready for thin film preparation.

3.2.2 Synthesize of active layer solution for organic solar cell.

The active layer material consists of P3HT and PCBM substances, were blended together using chloroform (CH) and di-chlorobenzene (DCB) as the solvent. The ratio between P3HT and PCBM was fixed at 1:1 with concentration of 30mg/ml. The

blended solutions have been stirred using magnetic stirrer for about 24 hours and left for aging for a day prior to fabrication process oforganic solar cell (Yusli et al., 2009).

3.2.3 Organic Solar Cell.

The optimized metal oxide thin film was used in fabricating thepolymer solar cell which consists five main components, glass substrate, anode layer, buffer layer, active layer and cathode layer. All four components except the buffer layer will be fixed to the same material, where the patterned ITO acts as anode layer,P3HT will be the donor and PCBM the acceptor in active layer while aluminum functioned as cathode layer in the device. On the other hand the buffer layer was varied according to the doped PEDOT:PSS series as tabulated in Table 3.1.

Table 3.1 :List of doped PEDOT:PSS series as buffer layer in OSC device

DOPED PEDOT:PSS SERIES	**THE COMPONENT IN OSC DEVICE**
Pristine (Undoped) PEDOT:PSS	ITO/**pristine PEDOT:PSS**/P3HT:PCBM/Al
2% glycerol doped PEDOT:PSS	ITO/**2% G-PEDOT:PSS**/P3HT:PCBM/Al
4% glycerol doped PEDOT:PSS	ITO/**4% G-PEDOT:PSS**/P3HT:PCBM/Al
6% glycerol doped PEDOT:PSS	ITO/**6% G-PEDOT:PSS**/P3HT:PCBM/Al
8% glycerol doped PEDOT:PSS	ITO/**8% G-PEDOT:PSS**/P3HT:PCBM/Al
2% EG doped PEDOT:PSS	ITO/**2% EG-PEDOT:PSS**/P3HT:PCBM/Al
4% EG doped PEDOT:PSS	ITO/**4% EG-PEDOT:PSS**/P3HT:PCBM/Al

6% EG doped PEDOT:PSS	ITO/**6% EG-PEDOT:PSS**/P3HT:PCBM/Al
8% EG doped PEDOT:PSS	ITO/**8% EG-PEDOT:PSS**/P3HT:PCBM/Al
ZnO doped PEDOT:PSS	ITO/**ZnO-PEDOT:PSS**/P3HT:PCBM/Al
2% AZO doped PEDOT:PSS	ITO/**2%AZO-PEDOT:PSS**/P3HT:PCBM/Al
4% AZO doped PEDOT:PSS	ITO/**4% AZO-PEDOT:PSS**/P3HT:PCBM/Al
6% AZO doped PEDOT:PSS	ITO/**6% AZO-PEDOT:PSS**/P3HT:PCBM/Al

The standard OSC device consists of ITO/doped PEDOT:PSS/P3HT:PCBM/Al as shown in Figure 3.1. Apart of buffer layer being spin coated, the active layer which consists of the combination of P3HT and PCBM organic solutions also developed by the same technique while aluminum electrode was deposited under the thermal evaporation technique. The principle of spin coating technique has been elaborated in details in 3.1.3, however, the spin speed for buffer and active layers are varied based on the required thickness of each component layers. The fabrication processes started with the deposition of the doped PEDOT:PSS as the buffer layer which spun at 3000rpm for 60s onto the patterned ITO layer.

The steps followed with the deposition of active layer which consists of the combination of P3HT and PCBM solution and were spun at 3500 rpm for 45s to form thickness in the range of 100nm. Before the final layer deposition of aluminum electrode, the deposited glass substrate was heated at 130°C for 20 minutes on a hot plate to remove moisture and particles from the buffer and active layer component and also to enhance the interface contact between the respective deposited component layers. After the

deposition of aluminum electrode by thermal evaporator machine, the performance of organic solar cell device is ready to be measured. The current-voltage (I-V) characteristics of dark and light condition were utilized to determine the device properties by using Keithley 2400 System Measurement Unit (SMU) and solar simulator.

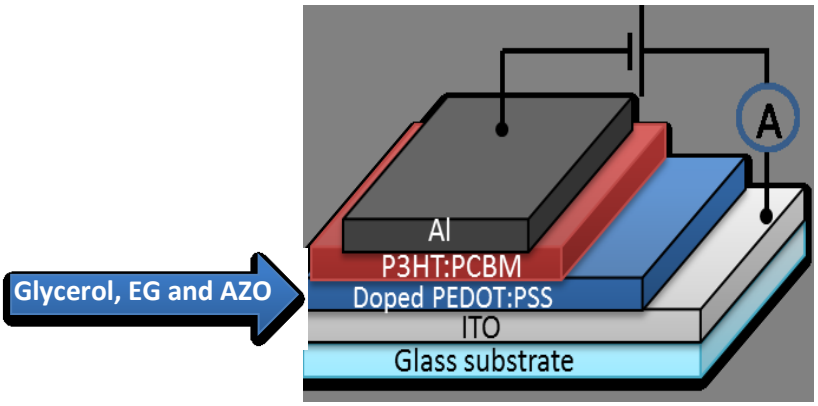

Figure 3.1 :Schematic diagram of fabricated organic solar cell

3.2.4 Aluminum deposition process by thermal evaporation technique.

As illustrated in Figure 3.2, thermal evaporation system consists of a built-in vacuum chamber which includes a shadow mask, a sample holder, a pair of electrodes and a connected valve to pump the pressure in the chamber. The chamber is connected to the controller for pressure adjustment and pumping procedures. In addition, a pair of electrodes in the chamber was connected to the power resource which supplies electric current to heat the tungsten filament in order to evaporate the respective metal material, e.g: aluminum, gold or silver. The desired deposit metal was tightly clamped on the tungsten filaments, in a specific amount which approximately enough to evaporate to the desired areas at the doped PEDOT:PSS thin films samples which were placed above the shadow mask.

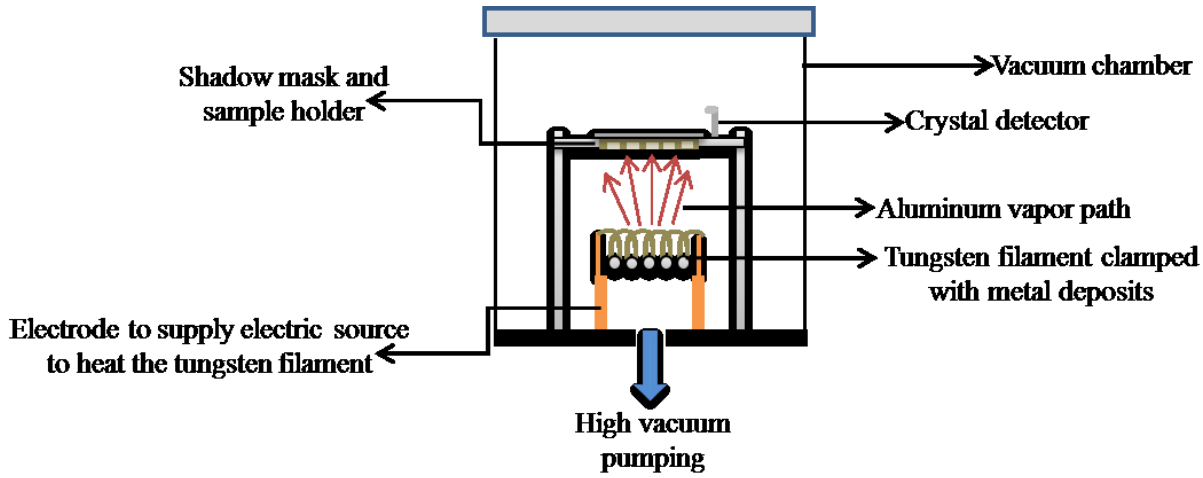

Figure 3.2 :Schematic diagram of thermal evaporation system

The deposition process started with the warming session to stabilize the rotary pumping system. In the meantime, the aluminum wire and the tungsten filament were placed under ultrasonic bath in acetone acid to remove particles in the cleaning process. All deposited substrate which are the target films in this process were located on the shadow mask and transfer to the vacuum chamber. The cleaned aluminum wire was then dried under nitrogen gas and was cut into small pieces and was hung tightly on the tungsten filament. Subsequently, the tungsten filament with metal deposit of aluminum was clamped at the two electrodes in the vacuum chamber. Subsequently, to provide a good vacuum condition inside the chamber, the evaporator system is required to be fine –pumped to pump out all of the air from the chamber.

In order to ensure the successful of aluminum evaporation process, the pressure in the vacuum chamber needs to be at least at 5.0×10^{-5} mbar. Pressures lower than 10^{-5} mbar are essential to ensure that most of the evaporated metal will travel in the straight path to reach the target films within the vacuum chamber. Hence, the pumping process was sustained in order to achieve 10^{-5} mbar. After the system is under this pressure, the current

is slowly supplied to the electrode until the aluminum at the tungsten started to melt when the current reach about 20 A.

The shutter which protects the sample was removed to allow the aluminum to evaporate on the samples and in the meantime the supplied current was simultaneously increased to 24 A. This value of current is supplied to confirm that all molten aluminum was evaporated to the samples. The deposition time taken is approximately about two minutes and this duration was found to be appropriate to develop aluminum contact with the thickness around 120 nm. Subsequently, the system was switched off and left for cooling while venting the air in which increased the system pressure to about 2.0×10^{-2} Mbar. Finally, the chamber is allowed to open and the complete organic solar cell devices were removed from the chamber before the I-V measurements to determine their device performance.

3.2.5 Preparation on doped PEDOT:PSS to observe the effect on temperature gradient.

The doped PEDOT:PSS thin films with several percentages of glycerol, EG and AZO were also studied in terms of the effect on their current-voltage measurements according to the temperature gradient, ΔT. The thin films were prepared where aluminum layer were deposited between the doped PEDOT:PSS thin films and were connected as shown in Figure 3.3. Both aluminum acts as the thermal connection where one side as the hot region and another is the cold region. The temperature gradient of doped PEDOT:PSS thin films between these two sides of aluminum was measured by connecting both region to FLUKE 116 True-rms digital multimeter by using thermocouple copper wire.

Another two probes were touched to either sides of aluminum and connected to Keithley for I-V measurements while the temperature gradients drops across the

PEDOT:PSS thin films. The heat source comes from the boiling water which placed on the left aluminum layer, while the cooling source created by ice cubes which located on the right side of the aluminum layer. The temperature gradient *(ΔT)* was changed according to the temperature drops of the boiling water placed at the hot region and by temperature increase in the ice cubes at the cold region. The I-V measurements were recorded every 2 minutes to obtain the trend of I-V plots with respect to the changes in their temperature gradient.

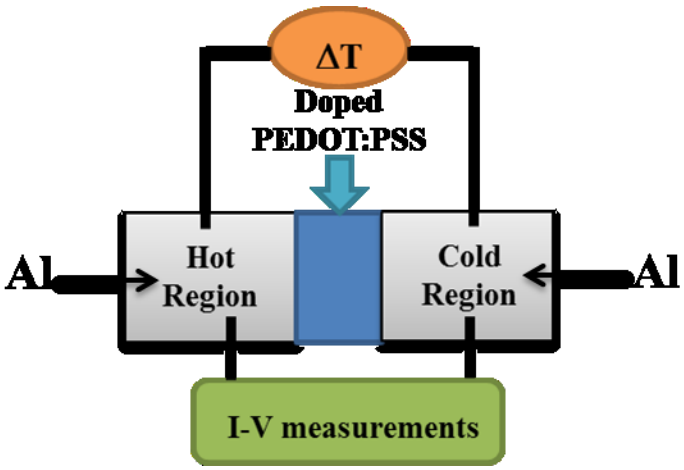

Figure 3.3 :Set-up equipment for thermal gradient versus I-V measurement

3.2.6 Thermoelectric Module.

The thermoelectric (TE) module has been exclusively designed with very much concern on a simplest and economic fabrication process. The fabrication of the TE module begins with the deposition of aluminum contacts on a glass slide of a design shown in the schematic diagram in Figure3.4. The device structure consists of two parts, the first part is the hot region of heat input (Q_i) which connected to the n- and p-type regions, while the second part is the cold region of heat sink/loss (Q_o). PEDOT:PSS was deposited by drop-cast in agap between the aluminum contacts whereas PTCDA and Alq_3 were deposited by thermal evaporation technique at a pressure of 10^{-3}Mbar in the other gap. The thicknesses

of the PEDOT:PSS thin films approximately ~100 nm while PTCDA and Alq_3films were estimated to be around 120 nm.

The hot area supplied by the heat from boiling water while the cold area was maintained with ice cubes attached to two opposite sides of the device. The changes in the temperature gradient was corresponded to the decreasing temperature of boiling water and the increasing temperature of the ice cubes which were finally converted to cold water.

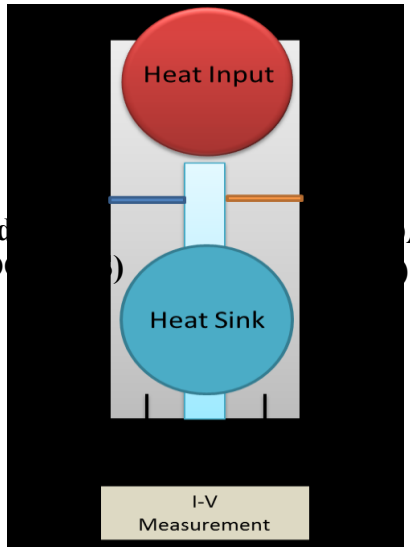

Figure 3.4 :Schematic diagram of a simple thermoelectric module

To measure the Seebeck coefficients (*S*) of both materials, each material was deposited on the approximately 200µm gaps created between the two aluminum electrodes. The applied temperature difference between the electrodes was measured together with the current-voltage plotting to observe the influence of changing in temperature difference with the electrical behavior using thermocouple. The voltages produced under temperature difference were measured using a FLUKE 116 True-rms digital multimeter.

3.3 Measurement techniques.

The present study focuses on the functions of anode layer in polymer solar cell. Thus,high level of transparency and conductivity of metal oxide is essential in order to absorb as much sunlight as possibleand to efficiently transport the converted free charge carriers (holes) to external circuit. In order to obtain the optimum metal oxide sample, several measurements have to be implemented.

3.3.1 UV-Vis Spectroscopy.

The investigation on the optical properties of doped PEDOT:PSS is important due to the application of these materials as buffer layer in organic solar cell device. Optical properties of any thin film consist of the reflection, absorption or transmission ability of the mediums upon the light incident. In this device, the capacity to absorb light of all medium isan essential factor to the betterperformance of the device.

As shown in Figure 3.5, theabsorption and transmission of doped PEDOT:PSS thin films were obtained by using Jasco V-570 UV/VIS/NIR Spectroscopy. The procedure of the measurement is started by placing two cleaned glass substrate on the sample holders as references. A deuterium discharge tube and a tungsten iodine lamp were used to apply light in the range of 190 nm to 350 nm and 340 nm to 2500 nm.

Figure 3.5 :Jasco V-570 UV/VIS/NIR Spectroscopy

The light was travelled through a grating in the monochromator and divided into two when it passed through the two light paths on both glass substrates at the sample holder. The photodetector detects the transmitted light. The lights were then assembled at the photomultiplier and were transferred to the amplifier for electric signal decoding process. The schematic diagram of the working principle of this equipment is shown in Figure 3.6. Subsequently, a built-in software converts the signals and produces the transmission spectra. These spectra create a baseline as a reference to be used when measuring the transmission of any thin film on the glass substrate. Then the measurement of the doped PEDOT:PSS was performed after one of the glass substrate was removed and replaced with the sample. All transmission and absorption spectra were then recorded and were used in the analysis process.

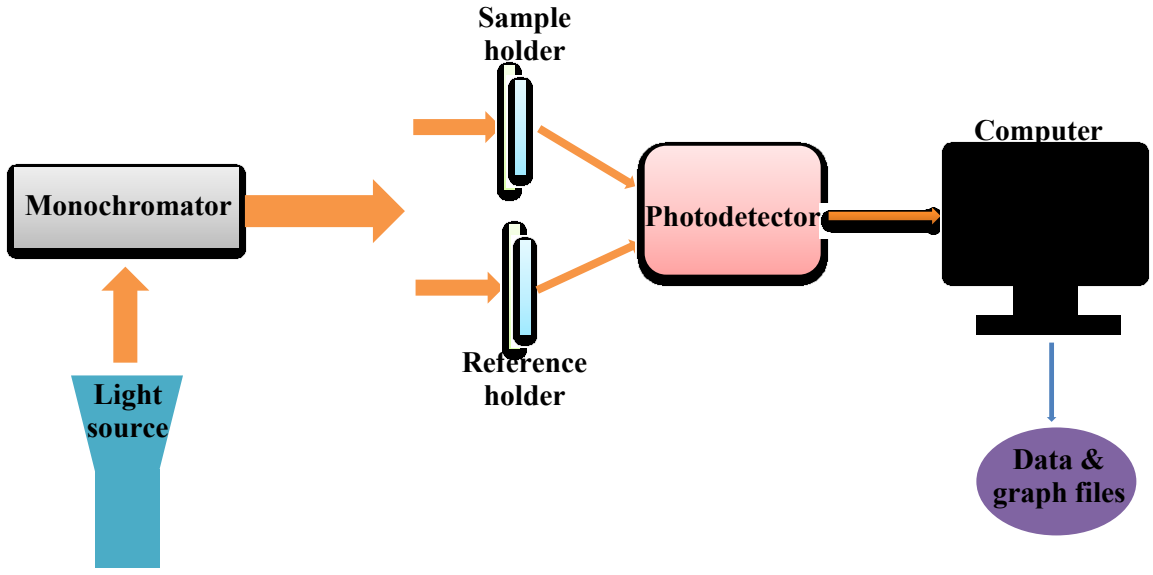

Figure 3.6 :Basic working principle in Jasco V-570 UV/VIS/NIR Spectroscopy

As shown in equation 3.2, by using Lambert's law, the transmission spectrum were used to obtain the absorption coefficient of all doped PEDOT:PSS thin films. α is the absorption coefficient, t is the film thickness and T is the transmittance of the thin film.

$$\alpha = \frac{1}{t}\ln(\frac{1}{T}) \qquad 3.2$$

The absorption coefficient and photon energies (hv) were related to the optical band gap, E_g by using Tauc's relation written in equation 3.3. The E_g is deducted with an assumption that a direct transition of electron was occurred between the edges of the HOMO and LUMO level ($n=0.5$), which produced variations in the absorption coefficient due to the increment in photon energy.

$$\alpha hv = \alpha_o(hv - E_g)^n \qquad 3.3$$

As illustrated in Figure 3.7, the E_g value was determined from the graph of $(\alpha hv)^2$ versus hv and the extrapolating of the linear potion near the onset of absorption edge to the hv axis.

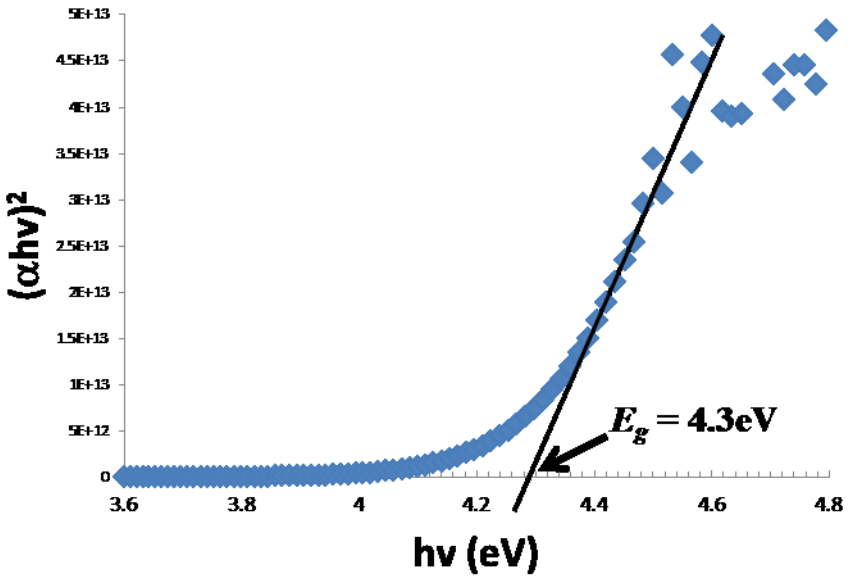

Figure 3.7 :Example plot of $(\alpha hv)^2$ versus hv to obtain Eg from the extrapolation line.

3.3.2 Four-Point-Probe.

The measurement of electrical properties were conducted to doped PEDOT:PSS thin films in order to determine the sheet resistance and conductivity of the thin films. The four point probe model in Figure 3.8(a) consists of four highly conductive probes that touched the top surface of the film or material. The four probes are in lines or linear and have a constant spacing. Upon connected with the power supply from the Keithley system measurement unit (SMU), the applied current (I) flows via the two end probes and voltage (V) can be measured between the two center probes as illustrated in Figure 3.8(b).

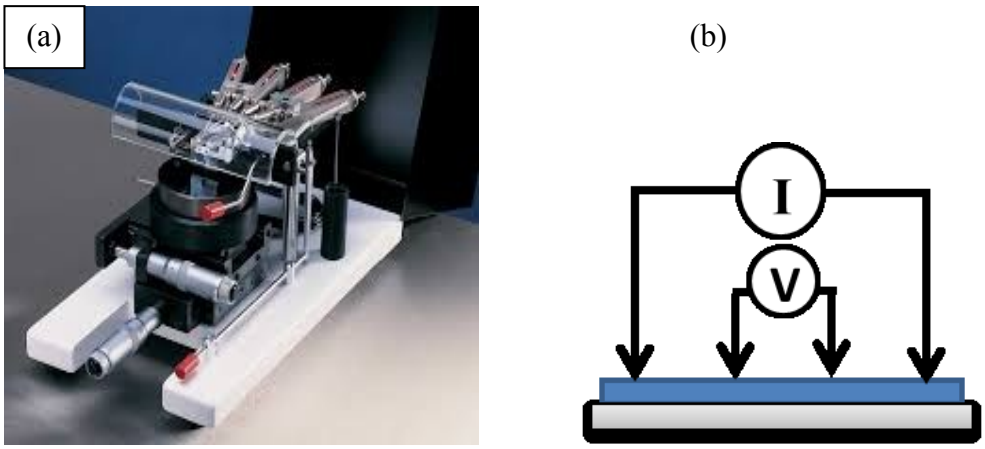

Figure 3.8:(a) Four-point-probe model , (b) Schematic diagram of the four-probes measurements.

Thus the measurement will provide current versus voltage plot across the thin films. The plots were used to determine the sheet resistance which was extracted to calculate the conductivity of the thin films. From the I-V plot, the resistance, R_s was obtained by using equation 3.4 where the current and voltage are related to the average resistance by the slope of the linear graph (V/I) multiplied with the ln π. This concept is based on the Haldor

Topsoe theories which explained in details about the relations of the sample geometric with the spacing between the probes used (Topsoe,1968) . Therefore, this concept is valid if the conducting sheet infinite in the horizontal directions and the thickness of the thin film is smaller than 40% of the spacing size of the probes. Consequently, to find the conductivity value, the resistivity, ρ of the doped PEDOT:PSS was deducted by using equation 3.5 where t is the thickness of the studied thin film or material:-

$$R_s = \ln \pi \frac{V}{I} \quad \text{(ohms/sq)} \qquad 3.4$$

Later, the conductivity, σ of the samples was determined from the reciprocal of resistivity from equation 3.6.

$$\rho = \frac{R_s}{t} \text{(ohm-cm)} \qquad 3.5$$

$$\sigma = \frac{1}{\rho} \qquad 3.6$$

3.3.3 Atomic Force Microscopy (AFM) Measurement

Figure 3.9 :Veeco 3000 AFM instrument.

The morphology variation of the thin film with respect to the treatment changing is measured by using AFM spectroscopy. In this work, the AFM instrument model Veeco 3000 (Figure 3.9) is used to determine the surface roughness and morphology of all doped PEDOT:PSS thin films. The AFM measurement can be implemented in several different modes. For example, the tip can be in constant contact with the sample, or may be placed slightly above the sample, or it also can be operated in "tapping" mode, alternatingly tapping tenderly on the sample. The latter mode method works well with soft samples that might be damaged if the tip remained in contact. Thus, due to the sensitive condition of our polymer thin films, the tapping mode of AFM measurements were employed to all samples.

The measurement principle of AFM is based on activating a probe to scan back and forth over the surface of a sample. But instead of using an electrical signal, the AFM measurement is based on forces between the atoms in the tip and in the sample. As demonstrated in Figure 3.10, the probe of the AFM is represented by a flexible cantilever with a tip attached to its bottom. In general, while the tip scans the sample, the force between the tip and the sample surface is examined. In order to maintain the force magnitude, the cantilever is moving up and down, alternatively. A reflected laser beam which acts as a detection device will measure the cantilever vertical motion, which matches to the physical structure consists of hills and valleys of the film surface. Consequently, a computer converts this observed vertical movement of the cantilever into an AFM image.

Other than the surface morphology, the information on friction between the tip and the sample surface and also the elasticity or softness of the film can also be obtained from the AFM measurement. In this work, the surface roughness were measured for all doped

PEDOT:PSS thin films in order to investigate the influence of each doping material with different percentages to the morphology structure of PEDOT:PSS thin film.

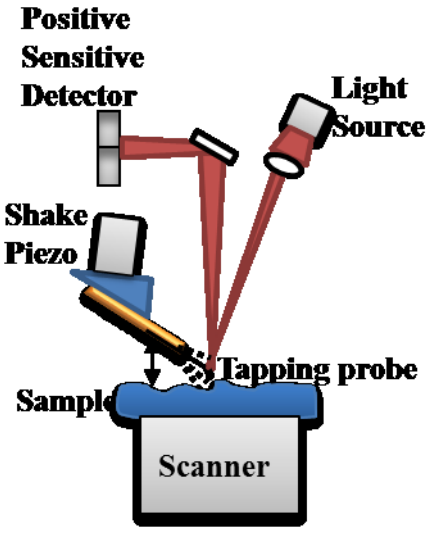

Figure 3.10 :Working principle of typical AFM instrument.

3.3.4 Raman spectroscopy measurement.

Figure 3.11 :Renishaw in Via Raman Microscope.

Raman spectroscopy is used due to its unique vibrational information that relates to the chemical bonds and symmetry of molecules. Specifically for organic material, raman spectra is similar to infrared spectra in that they have regions that are useful for functional group detection. Hence, it provides a fingerprint by which the molecule is able to be

identified. In this work, Renishaw in Via Raman Microscope in Figure 3.11 is used to obtain the raman spectra of all doped PEDOT:PSS thin films.

The origin of Raman spectra is markedly different from that of IR spectra. In Raman spectroscopy, the sample is irradiated by intense laser beams in the UV-visible region and the scattered light is usually observed in the direction perpendicular to the incident beam. The scattered of light consists of two types; (i)Rayleigh scattering which is strong and has the same frequency as the incident beam and (ii)Raman scattering which is very weak with frequencies $v_o \pm v_m$ that based on the Stokes lines as demonstrated in Figure 3.12. $v_m$represents the vibrational frequency of a molecule which is measured from the Stokes (v_o-v_m) and anti-Stokes (v_o+v_m) lines. Basically, Raman spectra are observed for vibrational and rotational transitions, however, it is also possible to observe Raman spectra of electronic transitions between ground states and low-energy excited states (John R. Ferraro , et al. 2003)

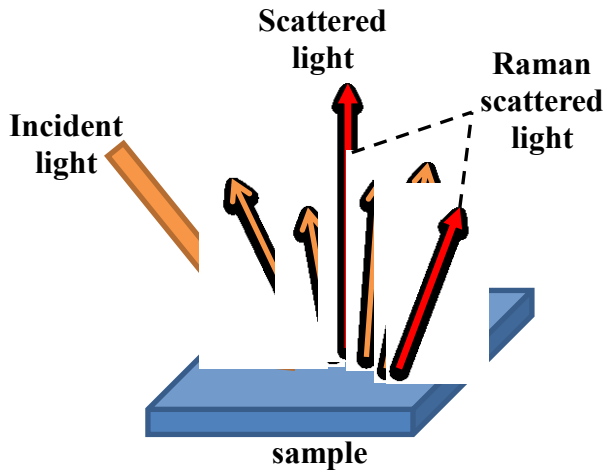

Figure 3.12 :Diagram of the Raman scattering light occur on a sample.

Based on Raman spectra, types of chemical bonding were assigned normally according to the frequency where the maximum peak occurs. Each frequency represents the specific chemical bonding and the assignment bands of Raman spectra can be obtained.

The chemical bonding type describes the behavior of the normal vibrations between polyatomic molecules of the material. For example, the symmetric (in-phase) stretching vibration refers to the motion of three molecules bonded together which were move back and forth along the bond direction after being stretched and released simultaneously.

For a specific condition where two of the molecules being stretched and the other bonding is deformed, the normal vibration that occur after released is called the antisymmetric (out-of-phase) stretching vibration. For all three molecules which moved in perpendicular direction and released simultaneously, this type of vibration is called the symmetric bending vibration. All these three examples possess their own frequency and will be detected by the maximum peak in the Raman spectra.

3.3.5 Surface Profilometer.

KLA Tensor P-6 surface profilometer as illustrated in Figure 3.13 (a) was used to determine the thickness of the doped PEDOT:PSS thin films in this work. Upon the measurement process, several scratching traces are made on the thin film surface. These scratches act as the steps which will be detected by the instrument scanning probe upon the measurement process. As demonstrated in Figure 3.13 (b), the thin film was inserted on the sample platform where the scratched trace is placed near the middle point indicating the probe location. The scratched trace will provide obvious height difference which will differentiate the surface height of the thin film to its bottom.

Subsequently, the scanning probe will move along the surface of the thin film from left to the right, while scanning the vertical or height differences along the film and display it as an analog signal for analysis. This signal will then be converted to a plot showing the height differences with certain XY- coordinate scales to determine the actual difference magnitude between the high and low level of the step. Theoretically, the height difference obtained from this plot representing the thickness of the measured thin film.

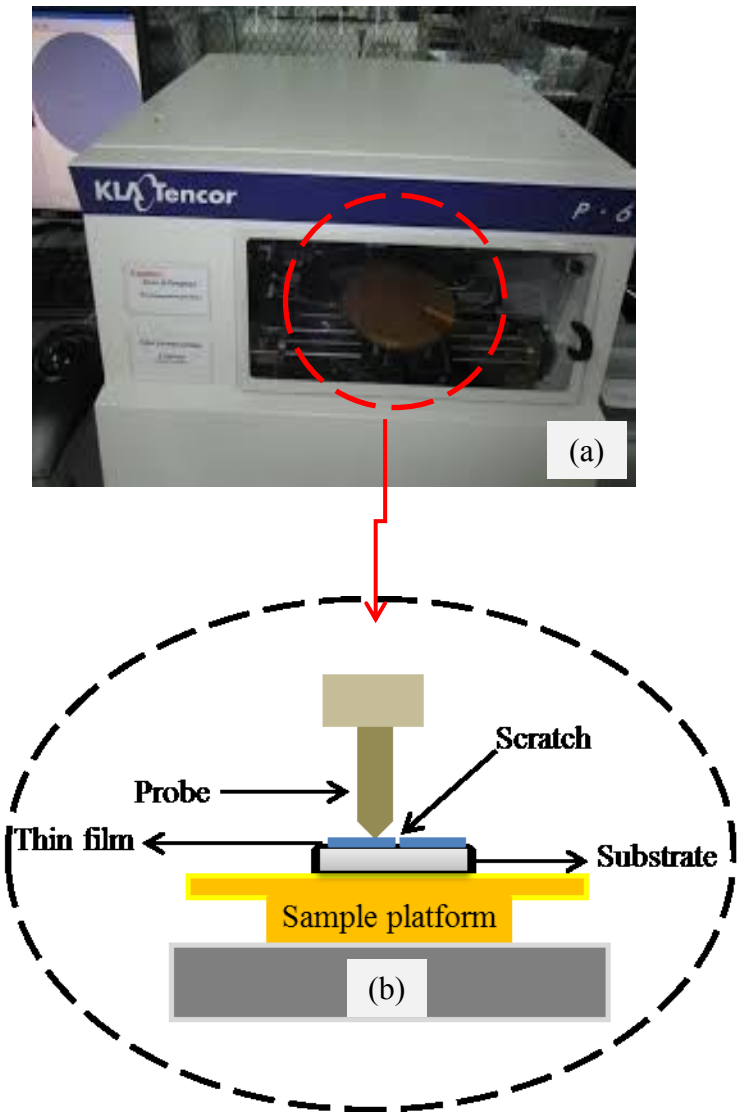

Figure 3.13:(a) KLA Tensor P-6 surface profilometer, (b) The schematic diagram of the surface profilometer.

3.3.6 Current – Voltage (I-V) Characterisation.

Current-voltage characteristics were measured with a Keithley 2400 high voltage source measurement unit (SMU) in the dark and under AM1.5 solar illumination with an intensity of 100 mW cm^{-2} for measurement under light condition. The I-V measurements under dark and light condition are essential to determine the performance of the studied organic solar cells. The performance of organic solar cells can be evaluated fromthe fill factor (FF) and the power conversion efficiency (η) that expressed mathematically in equation 3.7 and 3.8, respectively.

$$FF = \frac{I_m V_m}{I_{sc} V_{oc}} \quad 3.7$$

$$\eta = \frac{I_{sc} V_{oc}}{P_{in}} FF \quad 3.8$$

In detail, I_m and V_m represent the current density and voltage of the maximum output power, respectively. The I_{sc} , V_{oc} and P_{in} are the abbreviation of short circuit current, open circuit voltage and the incident light power from solar illumination, respectively. The ideal I-V plot is shown in Figure 2.11 in Chapter 2.0 where it shows the typical curve produced under light condition measurement which demonstrates the I_{max} , V_{max}, I_{sc} and V_{oc} properties.

3.3.7 Thermoelectric properties of doped PEDOT:PSS thin films.

In this work, the behavior of a simple thermoelectric device with a high conductive PEDOT:PSS PH1000 as the p-type material and two organic n-type materials(PTCDA and Alq_3) were observed by using current-voltage (I-V) plot.

The main concept of any thermoelectric device is that the charge carriers in n- and p-type material will diffuse from hot region to cold region due to the temperature gradient across them. Hence, the diffused charge carriers of opposite charge type were then tend to flow to external circuit that has been connected earlier which results the production of electrical power to the circuit. Therefore, the I-V measurement is expected to detect the changes provided by the TE device while experiencing temperature gradient during the measurement.

The V_{oc} and I_{sc} will be deducted from the I-V plot according to the changes occur in the temperature gradient across the TE device. Subsequently, the output power, P_o representing the respective TE device will be calculated from equation 3.9 and presented in a plot versus the temperature gradient.

$$P_o = I_{sc}V_{oc} \tag{3.9}$$

CHAPTER 4

RESULTS AND DISCUSSIONS OF THE DOPED PEDOT:PSS THIN FILMS AND THE ORGANIC SOLAR CELLS

Overview.

Chapter 4 discussed the effects of modified PEDOT:PSS with the doping materials of polar solvent, ethylene glycol (EG) and glycerol with different concentrations of 2%, 4%, 6% and 8%. Apart of that, metal oxide such as zinc oxide and the doped aluminum zinc oxide with different percentage of 2%, 4% and 6% have been used as doping materials. The studies on the optical and morphological properties of the modified PEDOT:PSS thin films have been performed. In addition, the electrical characteristics of modified PEDOT:PSS as a buffer layer in organic solar cell with the construction structure of ITO/modified PEDOT:PSS/P3HT:PCBM/Al have also been investigated. In this chapter, the results of characterisation are separately reported according to the most important properties of optical followed by electrical, morphological, Raman and finally the performance of the organic solar cell devices.

4.1 Optical properties.

The optical properties of modified PEDOT:PSS thin films were measured using UV-Vis-NIR Spectroscopy of Jasco V-750 to study the absorption and transmission of the modified PEDOT:PSS thin films.

4.1.1 Optical properties of glycerol doped PEDOT:PSS

Figure 4.1 shows the transmission spectra of all thin films in the range between 270 nm to 800 nm. The pristine and glycerol doped PEDOT:PSS thin films show high transmission above 80% in ultraviolet range. All transmittances started at about 290 nm and continuously increase beyond the near infrared region. However with the existence of glycerol, an obvious increment in transparency is noticeable as compared to the pristine transmission.

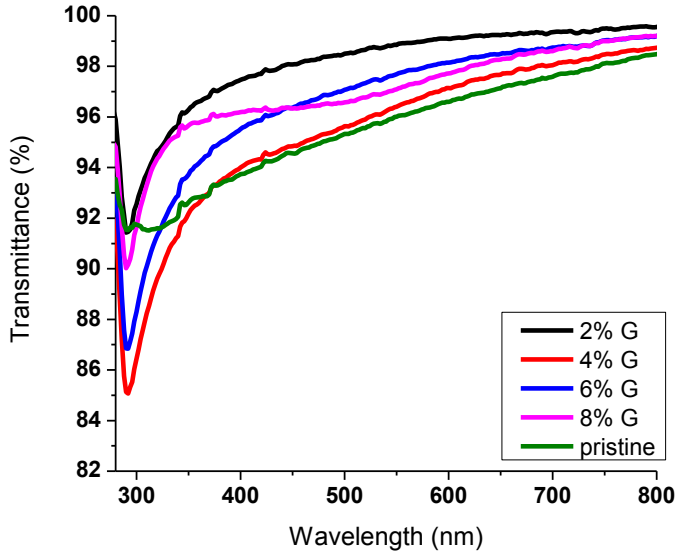

Figure 4.1 :Transmission spectra of glycerol doped PEDOT:PSS compared to the pristine.

Apparently, the most transparent film is the 2% glycerol doped PEDOT:PSS while the 4% doped PEDOT:PSS seems to transmit the same amount of photon energy as the pristine thin film. However, in general all of the pristine and glycerol doped PEDOT:PSS thin films exhibit transmission beyond 90%. The difference of transmission among the thin films were acceptable since the percentage were maintained under the best range for optical propose in the optoelectronic device.

Glycerol itself is a transparent material and with the doping process, specifically at 2% glycerol doped, the transparency of PEDOT:PSS thin film has been enhanced for about 3% higher than the pristine film. Glycerol doping to PEDOT:PSS may be responsible in rearrangement of the PEDOT polymer chain and PSS lamellar which results in homogeneous and uniform distribution to allow larger transmission effect in the PEDOT:PSS (Chen et al., 2009).

The transmission region indicates the range of photon energy owned by the respective material in order to assist the electron excitement from the π-bonding level to the anti-π bonding level. The ultraviolet and visible regions are able to provide adequate photon energy to excite electron to the anti-bonding phi level and the below, which may cause in the enhancement of the electrical properties of the PEDOT:PSS. An obvious transmission increment can be observed in near ultraviolet region for all doped glycerol of PEDOT:PSS compared to that of the pristine one. Furthermore, in the visible region, all of the films can be able to transmit light more than 90%.

The influence of glycerol doping level on the absorption spectra of PEDOT:PSS is demonstrated in Figure 4.2. It can be observed that all of the glycerol doped PEDOT:PSS thin films produce a strong absorption in near UV wavelength range from 230-330 nm with the maximum absorption peak of all films is located at around 290 nm. The solvents involve in the modification of these PEDOT:PSS most likely possess a consistent factor which allows the absorption peaks maintained at this wavelength region. Hence, glycerol solvent contributes in enhancing the absorption intensity at the same wavelength region which gave advantages in increasing a sufficient energy to excite electrons in π orbitals to π* antibonding orbitals or n electrons to π* or σ* antibonding orbitals (Robinson, 1975).

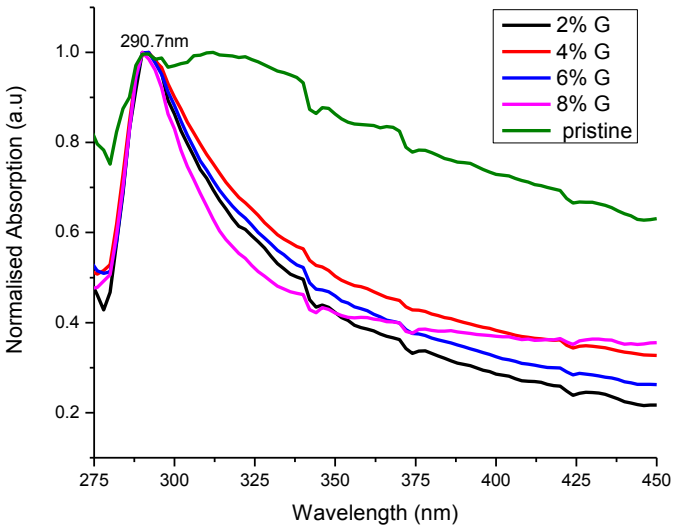

Figure 4.2 :Absorption spectra of glycerol doped PEDOT:PSS compared to the pristine.

All spectra exhibit an intense and sharp absorption peak without wavelength shift, indicating that the absorption in modified PEDOT is not affected by the amount of solvent added. The result is in agreement with study done by Mermazadeh et al where the absorption peaks at 290nm indicate the existing and rearrangement of PSS lamella chain with the glycerol doping (Mermazadeh et al., 2012). Hence, the changes of PSS may have been affected by the structure of the molecular chains between PEDOT and PSS. Thus, these changes attributed to the conformation of the PEDOT chains which produce a sharp and focus absorption spectra relative to that of the pristine in the absorption spectrum .

Other than absorption coefficient (α), optical band gap (E_g) is also an important parameter for the measurement of hole transport efficiency in the PEDOT:PSS thin films as future anode layer of OSC. Values of optical band gap (E_g) and the ideality factor ***n*** are calculated based on Tauc's relation (Muhammad & Sulaiman, 2011). The variation in optical band gap, E_g obtained upon glycerol doping in PEDOT:PSS is tabulated in Table 4.1. It can be seen that there is a drastic rise in $E_g$upon glycerol doping compared to the

pristine. However the variation in glycerol amount seems does not contribute significant change in E_g which lies within a small range of 3.70 to 3.80 eV.

As discussed earlier, the existence of glycerol tends to restructure the PEDOT molecules and PSS lamella which results in more organised and homogenous films. Moreover, doping glycerol may also affect the molecular bonding by separating the ionic bonds between PEDOT and PSS chains. This separation would cause PSS chains(which bear the negative charge carriers) to repel with each other, hence produce a better organized alignment (Xiong & Liu, 2012).

Subsequently, with the increase addition of glycerol, the elliptic particles of PEDOT:PSS become round shape and bigger thus exhibiting more severe aggregation which performed the broaden optical gap. Hence, it indicates that thelarger energy is needed to absorb photons if compared to the pristine PEDOT:PSS thin film (Xiong & Liu, 2012).

Table 4.1: Values of optical band gap ($\boldsymbol{E_g}$), ***n*** and thickness for pristine and glycerol doped PEDOT:PSS.

Material/ Parameters	Absorption Coefficient (10^3 cm^{-1})	Optical Band Gap (E_g) (± 0.01 eV)	Thickness (± 0.5nm)	*n* (Direct = 0.5 In-direct = 1.5)
Pristine	11.09	2.80	151.2	0.5
2% G	11.11	3.80	152.6	0.7
4 % G	20.01	3.73	150.1	0.9
6 % G	17.64	3.70	148.6	0.7
8% G	12.97	3.85	152.2	0.8

Figure 4.3 shows the variation in the optical band gap and the absorption coefficient with respect to the percentage of glycerol added into PEDOT:PSS. Absorption properties of a thin film is highly influenced by the optical band gap between conduction and valence band or between the HOMO and LUMO levels in organic material. PEDOT:PSS is a conjugated polymer, that possess the extended π-bond system of conjugated polymers (single and double bond structure) along the chain.

Hence, this structure affects the properties of the material, including their optical properties. The conjugation length of the bond is strongly correlated to the optical band gap and the absorption wavelength. The presence of doping material, which in this case is glycerol has adjusted the PEDOT:PSS conjugation length to some extent, thus alter the optical band gap. The increase in the conjugation length is correlated to the decrease in the adjacent energy levels (Skotheim et al., 1998). Nevertheless, in this study, the presence of glycerol has increased the E_g, indicating a substantial reduction in the conjugation length of the PEDOT:PSS bonding. Unfortunately, larger energy gap of PEDOT.PSS would not favor the charge transport properties as electrode in organic solar cell.

Moreover, alteration of conjugation length also contributes in controlling the range of absorption wavelength range (Skotheim et al., 1998). Despite the dramatic increase of the absorption coefficient with the glycerol doped, no shift of wavelength is observed in the glycerol doped PEDOT:PSS. Thus, glycerol likely acts in minor modification of the conjugation length which only affect the E_g while maintaining the absorption in ultraviolet at 290nm.

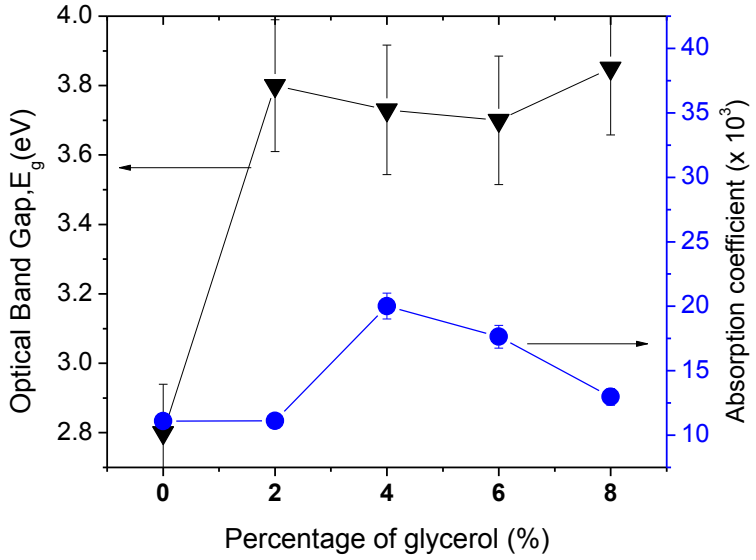

Figure 4.3 :Correlation of optical band gap ($\boldsymbol{E_g}$) and absorption coefficient (α) with respect to the percentage of glycerol doped PEDOT:PSS.

All of the samples were prepared at a constant spin speed, with the identical thicknesses (~150nm) as tabulated in Table 4.1. By extracting from Tauc plot shown in Figure 4.4 and utilizing equation 3.3, the ideality factor *n* value can be calculated.

The values of *n* and E_g of the modified PEDOT:PSS and the pristine are presented in Table 4.1. The *n* value indicates that the energy gap of PEDOT:PSS is a direct band gap referring to the value which is around 0.5 to 1.0. Such values are in agreement to those reported in other organic thin films (Karabulut et al., 2014; Muhammad et al., 2010; Pejova, 2014; Zarrinkhameh et al., 2014). This is corresponds to the fact that the excitation of electron from π band to π*(anti-phi) band needed no other band as a bridge due to the sufficient energy enhanced by the existence of glycerol and the high transparency properties of the material.

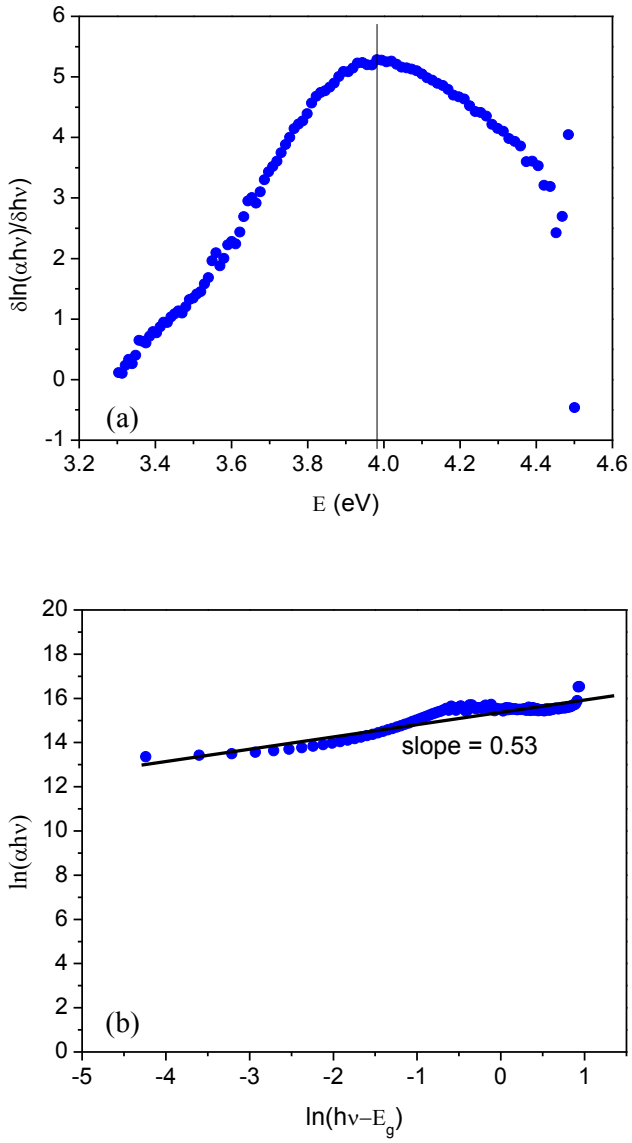

Figure .4.4: Extraction from Tauc equation, (a) $\delta ln(\alpha h\nu)/\delta h\nu$ versus$E$ and (b) $\ln(\alpha h\nu)$ versus ln $(h\nu - E_g)$.

4.1.2 Optical properties of ethylene glycol (EG) doped PEDOT:PSS

Ethylene glycol (EG) is another high potential polar solvent that contributes in enhancing the performance of PEDOT:PSS in electronic devices. The EG doped PEDOT:PSS thin films were measured under UV-Vis spectroscopy to evaluate their absorption and transmission properties.

Figure 4.5 shows the effect of EG doping levels on the transmission spectra of modified PEDOT:PSS thin films. It is found that the films have allowed more than 90% of light to be transmitted in near ultraviolet range. At longer wavelength of visible region, the transmittance increases upon EG doping, but approaching saturation level nearly 100% at near infrared region. It is favorable that with greater transmittance within the respective range in the doped PEDOT:PSS may permit more absorption of photons in active layer of the solar cell which may produce higher J_{sc} in organic solar cell (Huang et al., 2013).

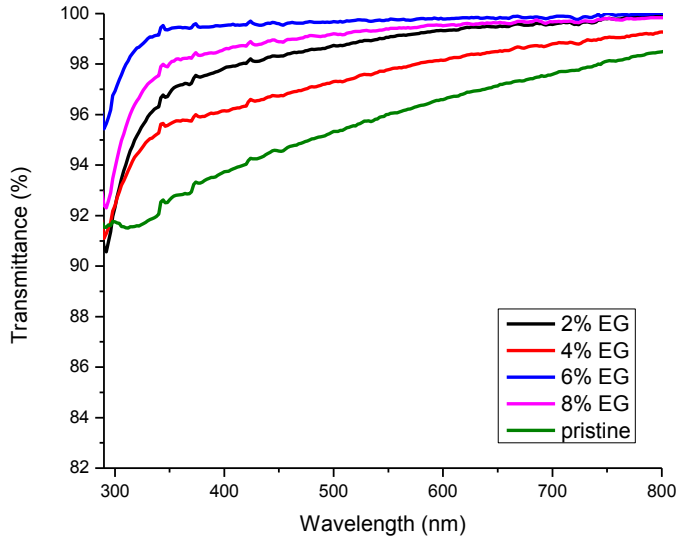

Figure 4.5 : Transmittance spectra for EG doped PEDOT:PSS thin films.

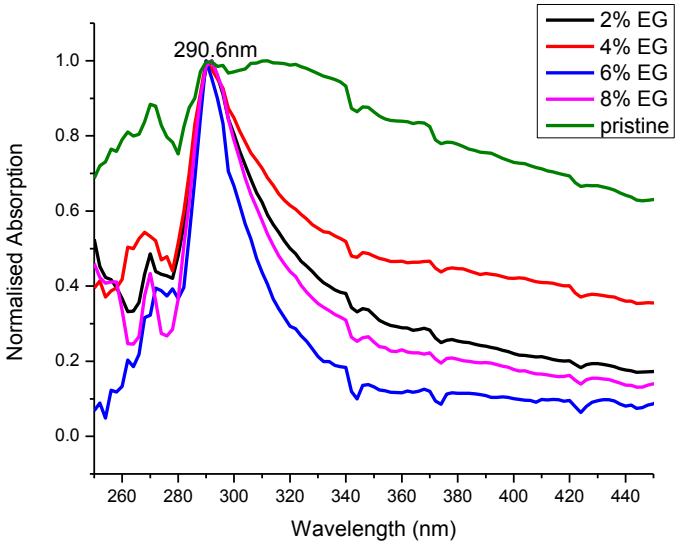

Figure 4.6 : The absorption coefficient spectra for EG doped PEDOT:PSS thin film.

Figure 4.6 demonstrates the absorption spectra of the EG doped PEDOT:PSS which found to be sharp, tense and clearly settled at 290.6 nm. The wavelength region of all absorption spectra are located within ultra-violet region, which mostly correlated to the doping of PEDOT:PSS material with polar solvent (Huang et al., 2013).

Table 4.2 tabulates the optical properties of EG doped PEDOT:PSS thin films. The optical band gap,$E_g$increases from 2.80 eV to 3.0 eV upon doping with 2% EG. The EG existence has affected in rearranging the molecular structure of both PEDOT and PSS, which results in the conformational modification of the molecular structure. This conformational modification will be discussed in later section of Raman spectra, Section 4.4.1. It is believed that the modification in molecular structure is responsible for the formation of the interchain interaction. The E_g seems to be almost consistent for all variation of EG doping in PEDOT:PSS, indicates that the addition of EG of more than 2%, does not alter the energy level of PEDOT:PSS polymer chain. Generally, it is noted that such finding in the EG doped PEDOT:PSS, is in contrast to the result of energy level for the glycerol doped PEDOT:PSS.

Table 4.2 : Optical properties of EG doped PEDOT:PSS thin films.

Material/ Parameters	Absorption Coefficient (x $10^3 cm^{-1}$) at max peak (~ 290nm)	OpticalBand Gap (E_g) (± 0.01 eV)	Thickness (± 0.5nm)	*N* (Direct = 0.5 Indirect = 1.5)
Pristine	11.09	2.80	151.2	0.5
2% EG	12.31	3.0	155.0	0.5
4 % EG	11.55	2.95	153.0	0.5
6 % EG	5.73	3.0	153.3	0.5
8% EG	9.90	3.0	155.6	0.5

The correlation between optical band gap and the maximum absorption coefficient of EG doped PEDOT:PSS is shown in Figure 4.7. It is obvious that a similar increasing pattern can be observed in both E_g and absorption coefficient for the percentage of EG below 4%. It seems that the optical properties of PEDOT:PSS is improved with only small amount of EG in the range between 2% and 4% doping. This attributes tothe stable increment of absorption coefficient with broader E_g. Larger amount of EG may interfere the PEDOT:PSS molecules, since the addition of EG is able to increase the diameter and also capable in forming clusters of the PEDOT:PSS primary colloidal particles (Yan & Okuzaki, 2009), hence reduce the ability of film to absorb light.

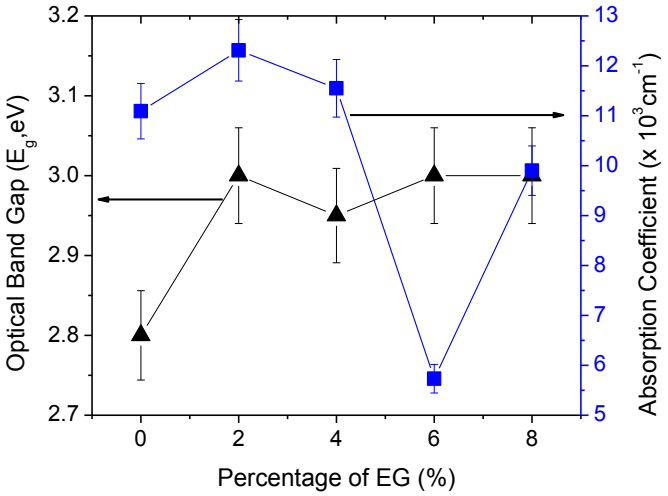

Figure .4.7 : Correlation of optical band gap (E_g) and absorption coefficient (α) with respect to the percentage of EG doped PEDOT:PSS.

4.1.3 Optical properties of aluminum zinc oxide (AZO) doped PEDOT:PSS.

Aluminum zinc oxide (AZO) was used as one of the dopant materials in PEDOT:PSS in order to obtain the optimum optical and morphological properties. The optimized PEDOT:PSS film then may be used to enhance the electrical characteristics.Figure 4.8 shows the transmittance spectra of AZO doped PEDOT:PSS thin films. All films exhibit transmittance beyond 90% which shifted more towards the visible region. The transparent behavior of the modified PEDOT:PSS with ZnO has been slightly improved. However with aluminum presence in zinc oxide to form AZO, this dopant material has strong effect in improving the transmittance of PEDOT:PSS.

In this case, the highest transmission of thin film is obtained from the modified PEDOT:PSS 6% AZO content. Other researchers (Pearton et al., 2004) reported that the high transparency of PEDOT:PSS has been achieved by adding AZO substance. Therefore the AZO-doped PEDOT:PSS may be used as one of the alternative electrode for application in organic solar cells.

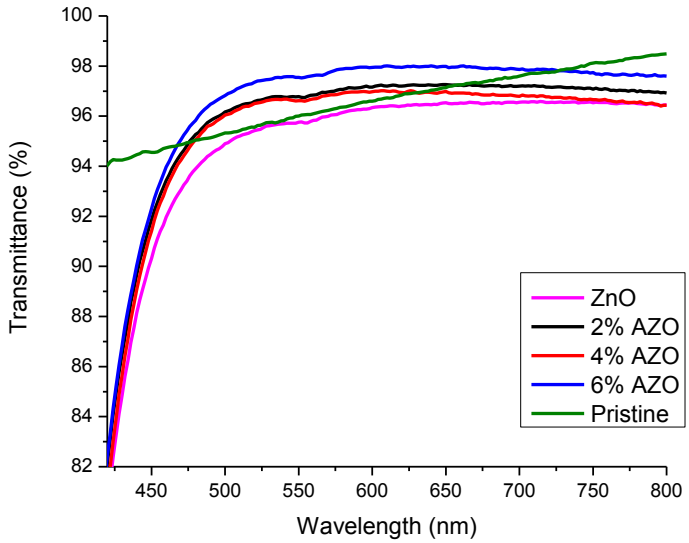

Figure 4.8 : Transmittance spectra for AZO doped PEDOT:PSS thin films.

Figure 4.9 illustrates the effect of AZO doping amount on the absorption spectra. The pristine and ZnO doped PEDOT:PSS are also shown as comparison. Generally, the peak for ZnO doped PEDOT:PSS is located at 345 nm, whilst the pristine PEDOT:PSS film has a broad absorption range between 300 and 320 nm. Thus, the result indicates that ZnO has influenced to some extent of absorption in PEDOT:PSS after doping process. In the meantime, all AZO doped PEDOT:PSS films demonstrate an intense narrow peak at 351 nm. Hence, it shows that AZO component has large contribution in modifying the absorption properties of PEDOT:PSS film.

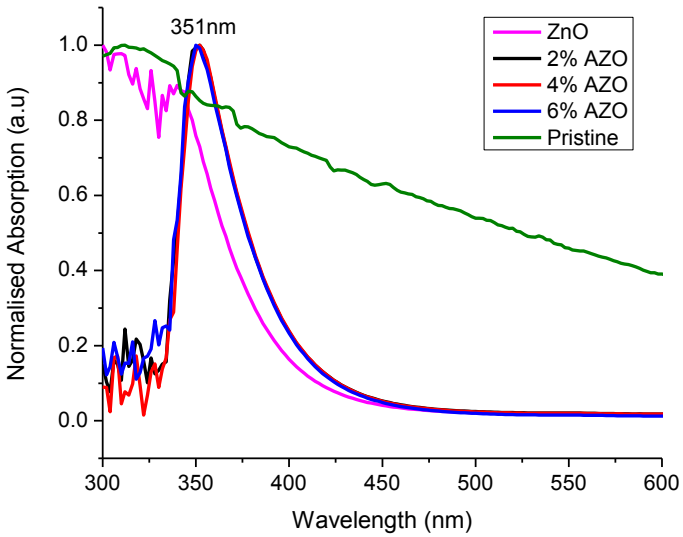

Figure 4.9 : Absorbance spectra for AZO doped PEDOT:PSS thin films.

Table 4.3 tabulates the optical properties of ZnO doped and AZO doped PEDOT:PSS. The optical band gap,$E_g$is obtained from the Tauc's relation, similar to the method discussed earlier. By comparing the E_g of pristine film of 2.80eV, andZnO-doped of 4.03eV, distinguish result is found. In the fabrication of organic electronic devices, a huge modification of optical band gap of ZnO doped PEDOT:PSS might be utilized.

Table 4.3 :Optical properties of ZnO, pristine PEDOT:PSS and AZO doped PEDOT:PSS thin films.

Material/ Parameters	Absorption Coefficient ($10^5 cm^{-1}$) at max peak (~ 352nm)	Optical Band Gap (E_g) (± 0.01 eV)	Thickness (± 0.5nm)	*n* (Direct = 0.5 In-direct = 1.5)
Pristine	0.11	2.80	151.2	0.5
ZnO	1.63	4.03	155.0	0.5
2 % AZO	1.04	3.74	153.0	0.5
4 % AZO	1.13	3.41	153.3	0.5
6% AZO	1.13	3.52	155.6	0.5

Studies have shown that ZnO itself is a n-type oxide semiconductor material with a direct wide of optical band gap of 3.37eV (Tang et al., 2013). However, the optical band gap in ZnO may be broaden with respect to the increase in doping percentage of aluminum (Wang et al., 2009).

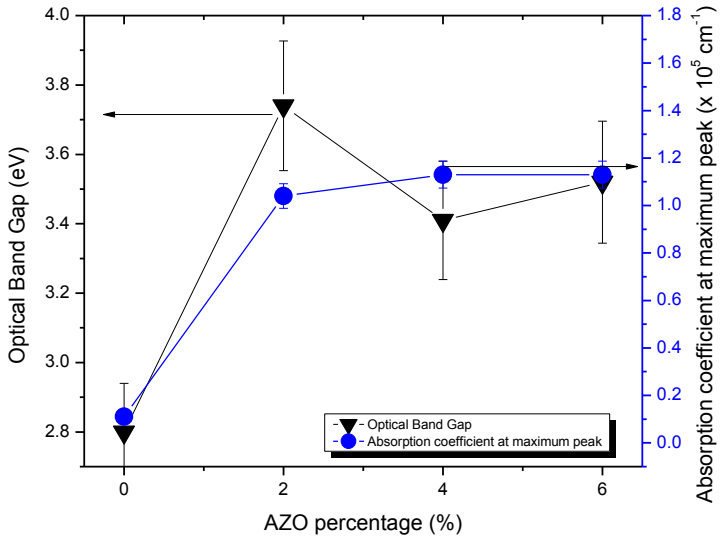

Figure 4.10 : Correlation of optical band gap (E_g) and absorption coefficient (α) with respect to the percentage of AZO doped PEDOT:PSS thin films.

The variations in the optical band gap and the peak absorption coefficient are shown in Figure 4.10 with respect to the percentage of AZO doped PEDOT:PSS. Aluminum atoms doped to ZnO lattice results in reducing the grain size hence break up the continuous energy bands into discrete levels which leads to a broaden optical band gap (Wang et al., 2009). In the present study, it is shown that the optical band gap of AZO doped PEDOT:PSS increases with the content of dopant. Thus, it is believed that this behavior is due to the Burstein-Moss effect in which the expand in energy band gap is attributed to the increasing of carrier concentration in AZO material (Kumar & Rao, 2012; Mamat et al.,

2010). The widening in optical band gap (E_g) is strongly related to the carrier concentration (n_e) through equation 4.1 (Fournier et al., 2008) :-

$$\Delta E_g = \left(\frac{h^2}{8m^*}\right)\left(\frac{3}{\pi}\right)^{2/3} n_e^{2/3} \qquad 4.1$$

Where, h is Planck's constant and m^* is the electron effective mass in conduction band. Therefore, it is suggested that with AZO doping contributes in broadening the optical band gap due to the increase in carrier concentration of AZO in PEDOT:PSS.

The result shows that there is a strong correlation between both parameter of optical band gap and the peak absorption coefficient. The changes in both parameters occur parallel with the increased of AZO quantity in PEDOT:PSS. Notably, the contribution of ZnO and AZO as the dopants in PEDOT:PSS is quite significant. The enhancement of the optical parameters in the modified PEDOT:PSS films has been achieved via this method. Comparison between the absorption spectra of all the dopants used in this study i.e. the alcohol polar solvents of glycerol and ethylene glycol; metal oxide of zinc oxide and aluminum doped zinc oxide is presented.

The trend of absorption spectra between the alcohol polar solvent of glycerol and ethylene glycol, metal oxide of zinc oxide and aluminum doped zinc oxide show obvious difference where the spectra shifted to blueshift range where the peak moves 70 nm towards visible range with AZO components in PEDOT:PSS. As stated by Wang et al, the doping of aluminum to zinc oxide thin film attributes to a distinct blueshift of the absorption edge where it is due to more amorphous Al_2O_3 and smaller crystallites of Al in ZnO (Wang et al., 2009).This is in a good agreement with results occur in this work where the same effect also appears in AZO doped PEDOT:PSS thin film.

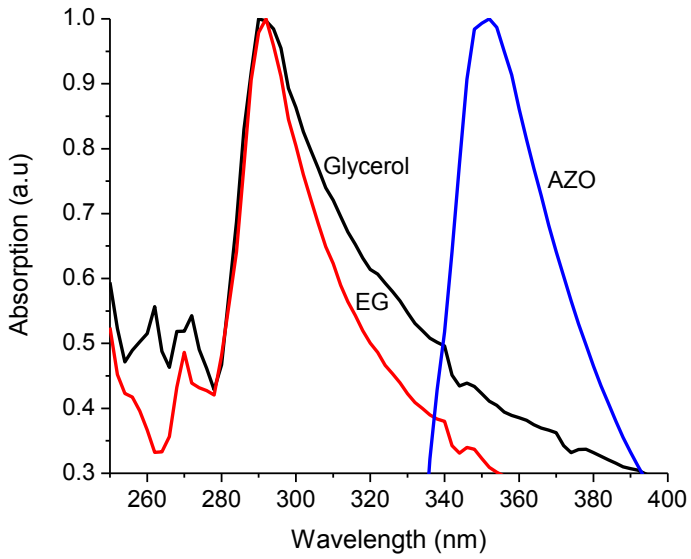

Figure 4.11 : Absorbance spectraof AZO doped PEDOT:PSS thin films.

The absorption peak is blue shifted with increasing Al doping concentration which results from the broadening of the optical band gap. The widen E_g is due to the Moss-Burstein shift where with Al doping, the donor which occupied the bottom of the conduction band possesses additional energy to be excited to higher energy in conduction band. It is caused by the Pauli principle which tends to avoid the double occupied of electrons in the energy states and also due to the vertical optical transition between the energy level in the thin film (Lee et al., 2009). Hence, it is observed that AZO doping offers strong effect in modifying the optical properties of PEDOT:PSS thin film.

4.2 Ele ctrical properties.

4.2.1 Electrical Properties of Glycerol doped PEDOT:PSS

Figure 4.12 shows the plot of sheet resistance of the glycerol doped PEDOT:PSS compared to the pristine PEDOT:PSS. Generally, a dramatic decrease was observed with the doping of glycerol where the sheet resistance was reduced to about a factor of two. The sheet resistance of pristine which is about 36.3 ohm/sq decreased to the lowest of about 9.1

ohm/sq with 2% glycerol doped to PEDOT:PSS. However, as the glycerol concentration increases to 6%, the sheet resistance increases a bit before drastically rose to 40.8 ohms/sq for 8% doped glycerol of the thin film. Hence the optimum amount of glycerol shall not be more than 6% in order to minimise the sheet resistance of the thin film.

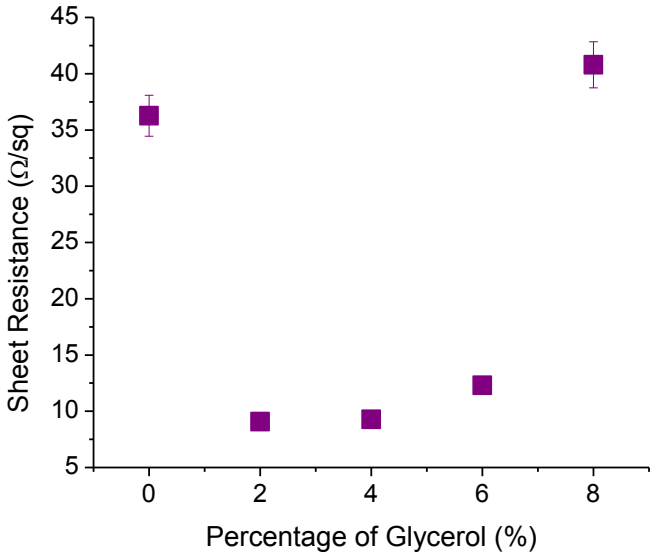

Figure 4.12 : Sheet resistance versus percentage of glycerol doped PEDOT:PSS.

The decreased in sheet resistance may due to the increase in charge carrier concentration which indicates by the widen in optical band gap of glycerol doped PEDOT:PSS compared to pristine PEDOT:PSS (Fournier et al., 2008). The reduction of sheet resistance is favorable in enhancing the electrical conductivity of PEDOT:PSS with glycerol. On the other hand, the drastic increase in sheet resistance for 8% glycerol doped to PEDOT:PSS is most likely due to the degraded surface morphology (Park et al., 2011).

The degrading surface morphology was referring to the size of particle engorgement which was decreasing and has allowed the PSS insulator to fill the gap between PEDOT particles. This condition leads to the higher sheet resistance for more than 6% of glycerol

doped of PEDOT:PSS. Hence it is notable that the electrical properties of the glycerol doped PEDOT:PSS are strongly related to the surface morphology. The effect on surface morphology of PEDOT:PSS thin films with respect to the glycerol doping percentage was discussed in details in section 4.3.1 where above 6% doped glycerol, the surface roughness were reduced 33% from its highest surface roughness at 4% doped glycerol PEDOT:PSS.

It is noteworthy that due to this matter it can be concluded that the interaction between PEDOT:PSS and glycerol becomes significant for low percentage of glycerol concentrations and thus the conductivity is enhanced accordingly (refer to Figure 4.13). However, when the amount of glycerol is sufficient to form a continuous conducting phase of PEDOT:PSS, the interaction between them becomes less significant (Park et al., 2011).

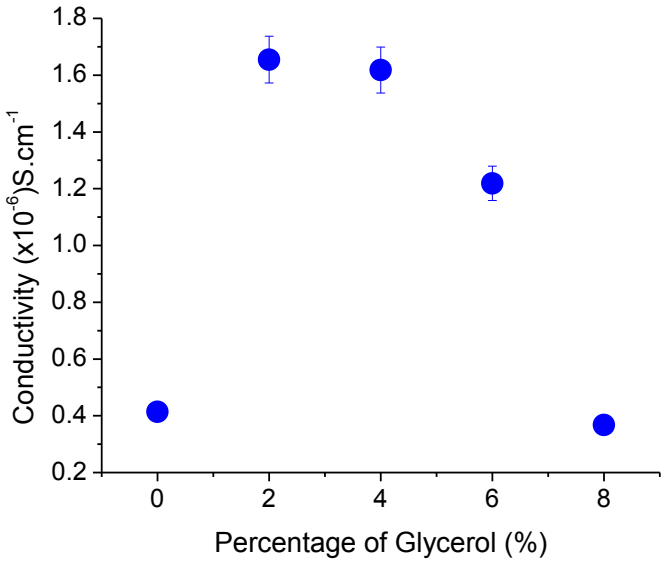

Figure 4.13: Conductivity versus the percentage of glycerol doped PEDOT:PSS.

Pertaining to the sheet resistance, the effect of glycerol in the PEDOT:PSS thin films was then studied by DC conductivity measurement at room conditions with the four-point probe technique. Figure 4.13 shows these results to various concentrations of glycerol

in the aqueous dispersion of PEDOT:PSS. We can observe that the conductivity increases rapidly as a function of glycerol concentration up to a maximum value of 1.62×10^{-6} S/cm for 4% glycerol doped and then, it gradually reduces with the further concentration of the doping glycerol.

It is reported that the electrical conductivity of PEDOT:PSS thin films strongly depends on the extent of aggregation of the constituent polymer nanoparticles (Xiong & Liu, 2012). It is also attributed to the swelling and interconnection of the conducting clusters in the film (Laskarakis et al., 2013). There was an opposite reaction occurred between the PEDOT particles and PSS lamella bonding in the thin film with the existence of glycerol. In the combination of PEDOT with PSS, where PSS lamella bonding is an insulator while PEDOT grain is the conductive element, the solution of PEDOT:PSS conductivity is limited by the large insulating barrier occurred with the PSS lamellas on the surrounding of PEDOT grains. The existence of glycerol assists in widening the average grain size of the PEDOT particles which results in the reduction of insulating barrier of the PSS between the PEDOT grains. Thus, the energy barrier was narrowed, hence creating extra spaces for charge hopping that leads to the increase in conductivity in the thin film (Cruz-Cruz et al., 2010).

It is apparent that, the electrical properties of conducting polymers are strongly dependent on their film morphology and structure. As the morphology of the films changes with the glycerol doping, the grain size and granular connectivity of the PEDOT and PSS may have been affected in which some way reduces the number or the height of the barriers. Thus, this leads to the variation of conductivity of the glycerol doped PEDOT:PSS (Huang et al., 2003).

Note that at 4% concentration of glycerol, the conductivity increases one order of magnitude, from 4.14 x 10^{-7} S/cm in pristine to 1.62 x 10^{-6} S/cm in 4% glycerol doped PEDOT:PSS. However, after the optimal concentration, a gradual decrease in the conductivity is observed with more glycerol concentration. It is suggested that when we doped the PEDOT:PSS with glycerol and as the concentration of glycerol increases to 4%, the obstruction issue of the electronic charge transport through the material were overcome with the rising of the charge transportation spaces.

However, after reaching an optimum concentration of glycerol, the further increase of the glycerol concentration allows further growth of the PEDOT domains to longer distances to each other which delay the charge transportation process in the thin film that results to the reduction of the films conductivity (Laskarakis et al., 2013).

Although the conductivity has reduced after 6% glycerol doping, it is retain higher than the conductivity of the pristine PEDOT:PSS film showing the significant of glycerol doping in order to improve the electrical properties of the PEDOT:PSS thin film (Cruz-Cruz et al., 2010). Thus, it is noteworthy that the existence of polar solvent as glycerol in the PEDOT:PSS has strongly assisted in enhancing the charge carrier hopping between different polymer grains. Therefore it revealed the information on the charge carrier mechanisms and their dependence with the polar solvent concentration in the solution (Laskarakis et al., 2013).

4.2.2 Electrical Properties of ethylene glycol doped PEDOT:PSS.

The main purpose of doping PEDOT:PSS with polar solvent is to enhance its electrical conductivity. The electrical conductivity enhancement may be due to from the increase in the charge-carrier mobility which result from the conformational changes of the

PEDOT chains. Ethylene glycol (EG) is another high potential polar solvent that contributes to the enhancement of performance of PEDOT:PSS in electronic devices. The conductivity of PEDOT:PSS aqueous solution was enhanced by adding EG because EG reduces the conductive PEDOT:PSS particle size and makes the insulating PSS layer around the conductive particles becomes very thin (Sharmaa et al., 2009).

Figure 4.14 shows the variation in the sheet resistance upon different amount of the EG being mixed in the PEDOT:PSS thin films compared to the undoped (pristine) PEDOT:PSS thin film. The sheet resistance values were obtained from the four-point probe measurement. The plot shows that there is a huge reduction in sheet resistance recorded by the 4% EG doped PEDOT:PSS. The sheet resistance value is reduced from 36.3 ohm/sq (pristine sample) to 9.1 ohm/sq (4% EG). However, the sheet resistance is increased with further addition of EG at 8% concentration.

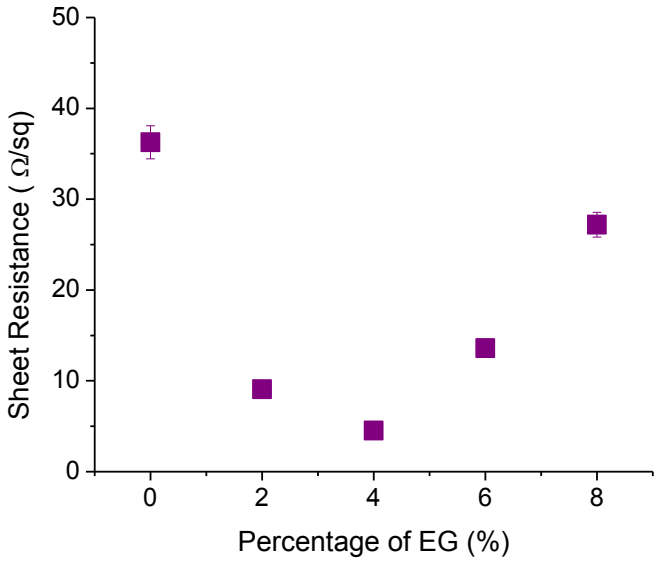

Figure 4.14 :Sheet resistance of the modified PEDOT:PSS with different percentage of EG.

Indeed, the reduction in sheet resistance of PEDOT:PSS thin films would significantly contribute to the increase in conductivity of a material. As shown in Figure 4.15, the electrical conductivity of the PEDOT:PSS thin film enhanced with EG doping. The conductivity values for EG doped PEDOT:PSS thin films are between 5.5 x 10^{-7} S/cm and 3.3 x 10^{-6} S/cm. It is shown that, the small percentage of EG has strongly contributed to the improvement of the conductivity of doped PEDOT:PSS. However, as observed in the conductivity of glycerol doped PEDOT:PSS, the similar trend has occured in EG doped PEDOT:PSS. Further increased in EG percentage of 8% has reduced the conductivity to a magnitude power of two.

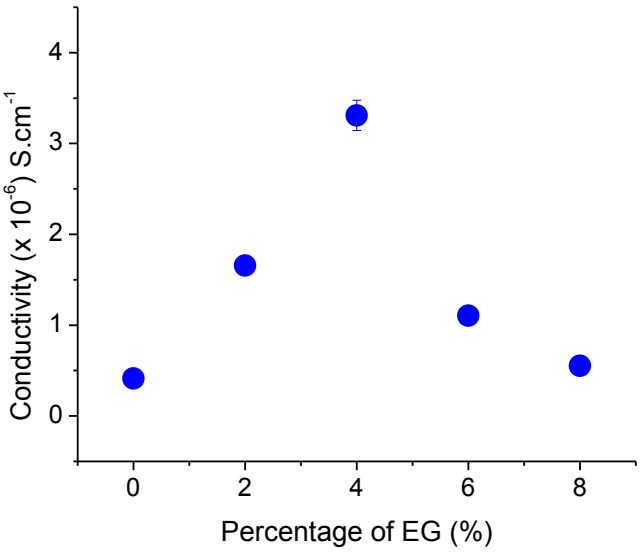

Figure 4.15 :Conductivity of the modified PEDOT:PSS with different percentage of EG.

EG has two polar groups in a molecule:one polar group may form a hydrogen bond to the sulfonate or sulfonic acid group of PEDOT/PSS , while another polar group may reside very close to the PEDOT chains. These two polar groups may create the interaction of different dipole moment or generate the positive charge on the PEDOT chains. Hence, it

is thought that the interaction between EG and the PEDOT chains, become the driving forces for the conformational changes (Wichiansee & Sirivat, 2009).

Furthermore, the second conformation change may result from the transformation of the chemical structure of PEDOT. There are two kinds of resonant structures, the benzoid and the quinoid structures that exist within PEDOT, as discussed in Chapter 2.0 (refer Figure 4.16).

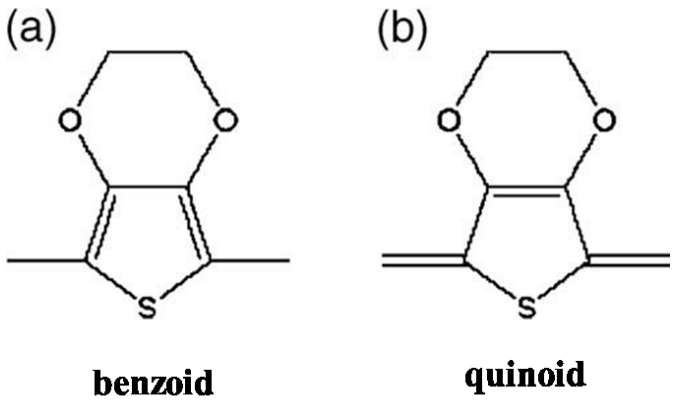

Figure 4.16 : Two kind of resonant structures exist within PEDOT.

For the benzoid structure, there are two-conjugated-electrons that form the C_α-C_β bond. For the quinoid structure, there is no conjugated-electrons on the C_α-C_β bond. After the secondary doping of EG, the benzoid structure transform into the quinoid structure and the quinoid structure becomes dominant within the PEDOT/PSS chains. The transformation of the chemical structure of PEDOT chains is generally accompanied by a conformational change. Coil and linear or expanded-coil conformation are possible for PEDOT. Thus such conformational changes may induce the rise in EG-doped PEDOT:PSS.

The obstacle in low conductivity of PEDOT:PSS (in the range of 10^{-6} S/cm) is likely to be due to the nature of its structure. The core of the molecule is rich of the conductive PEDOT moiety, however, it is surrounded by the shell of the insulating PSS

moiety. As to enhance the conductivity of the PEDOT:PSS, the main concern is to reduce the thickness of the PSS insulating shell. This will lower the energy barrier of the interchain and inter-domain charge hopping, hence the electrical conductivity of the PEDOT:PSS can be improved (Xia et al., 2012).

EG doping has shown some impacts in improving the electrical conductivity of the PEDOT:PSS thin films. The enhancement may due to the increase in charge-carrier mobility resulting from the conformational changes of the PEDOT chains (Ouyang et al., 2005). The contact between EG and PEDOT:PSS is claimed to be the driving force that contributes in the conformational changes. EG with its two polar groups in a molecule possess a strong factor to develop interaction that could enhance the conductivity of the PEDOT:PSS. The connection occurs where one polar group of EG form a hydrogen bond to the sulfonate or sulfonic acid group of PEDOT/PSS while another polar group may reside very close to the PEDOT chains between the dipole moment of the polar group and the dipole moment or the positive charge on the PEDOT chains (Ouyang et al., 2005).

Moreover, the conductivity of PEDOT:PSS also suggested that the increase is mainly due to the screening effects of polar solvents (Kim et al., 2002). The screening effect is referring to the modification of chemical structure in PEDOT:PSS with the addition of EG. At the same time the excess insulating PSS part was washed away from the surface of the PEDOT:PSS grains in the film, leading to a better connection between the conductive PEDOT:PSS grains (Jönsson et al., 2003).

4.2.3 Electrical Properties of AZO doped PEDOT:PSS.

As shown in Figure 4.17, a different trend is observed in R_s obtained for AZO doped PEDOT:PSS. Initially, the introduction of ZnO doping to PEDOT:PSS thin film yield a small reduction of R_s. However, as the AZO doping percentage increased up to 4%,

the R_s drastically declined until the lowest value of 4.1 ohm/sq. Nevertheless, with further increased to 6% of AZO has caused the R_s to increase to 6.8 ohm/sq. This indicates that the 4% amount of AZO is optimum amount of AZO to enhancethe electrical properties of AZO doped PEDOT:PSS.

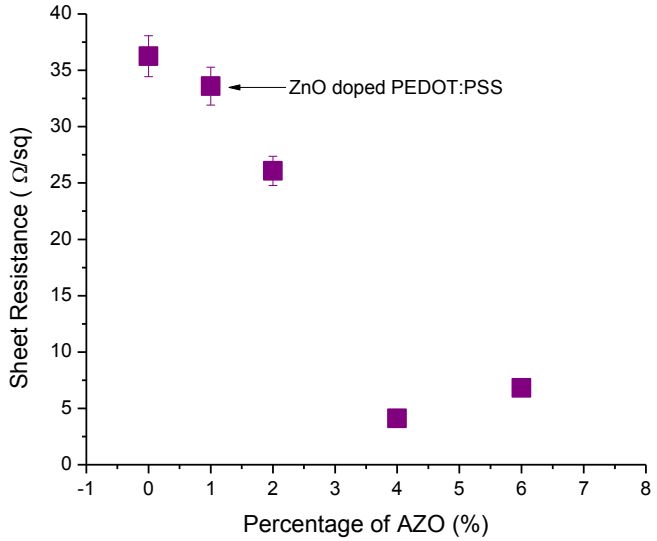

Figure 4.17 :Sheet resistance of the modified PEDOT:PSS with different percentage of AZO.

Hence, as illustrated in Figure 4.18, the conductivity of AZO doped PEDOT:PSS as an inverse trend of the sheet resistance R_s (plot in Figure 4.17) has recorded the highest conductivity of 3.6 x 10^{-6} S/cm by 4% AZO doped to PEDOT:PSS. The conductivity of ZnO doped PEDOT:PSS is around 4.5 x 10^{-7} S/cm which value is laid between the conductivity of pristine PEDOT:PSS (0%) and 2% AZO doped PEDOT:PSS.

An interesting enhancement in conductivity with AZO in PEDOT:PSS thin film illustrates high potential of upgrading the electrical properties of polymer by a hybrid mixture with metal oxide. In the present work, zinc oxide and AZO are likely to become the important compound in modifying and enhancing the electrical properties of PEDOT:PSS.

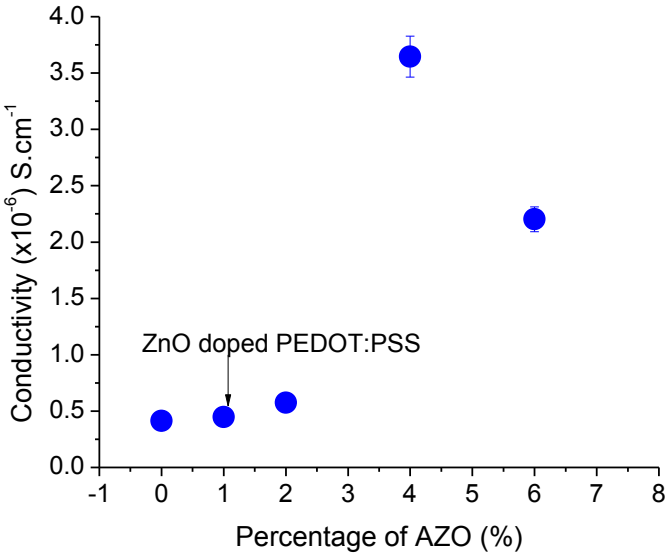

Figure 4.18 : Conductivity of the modified PEDOT:PSS with different percentages of AZO.

Zinc oxide and AZO are known as n-type material with electrons as the majority charge carriers (Tseng et al., 2010). The electrical conductivity of ZnO is directly related to the number of electrons which formed by the ionization of the interstitial zinc and the oxygen vacancies. By introducing aluminum as a dopant in zinc oxide (6%) to form AZO, the carrier concentration is increased with the decreasing of resistivity. However, further doping of aluminum beyond the optimum value may increase the electrical resistivity which related to the segregation of dopants at the grain boundary. In this case, large amount of aluminum dopant become impurity which give drawback to the electrical properties of the materials (Kuo et al., 2006).

In the present work, 4% of AZO concentration in PEDOT:PSS thin film is sufficient in reducing the sheet resistance, therefore increases the conductivity of the PEDOT:PSS thin film. Combination between n-type material, AZO and p-type PEDOT:PSS attributed to the conformational changes in the macromolecular polymer chains from a coil conformation to extended coil or a linear conformation (Xia & Ouyang,2011). The changes

of conformation may be originated from the dipole moment interaction. This inorganic:organic hybrid may produce inhomogenoues and unbalance distribution of positive and negative charges due to the dipole interaction between a dipole moment of ZnO or AZO with the dipole moment of the ethylenedioxythiophene in PEDOT. Hence, the change in conformation may be the significant factor in upgrading the electrical properties of the AZO doped PEDOT:PSS (Semaltianos et al., 2010).

4.3 Morphological properties.

One of the factor to accomplish an optimum performance of bulk heterojunction device is to control the morphology of the multilayer structure of the device. Fundamentally, each layer of the device is connected by the interfaces. Hence an optimum morphology is favorable to form a well-dispersed system which is crucial for efficient charge separation between the interface of active layer and the electrodes. Moreover, a phase separation on a large scale also essential to improve charge transport from the active layer to the electrode of the device (Beek et al., 2005).

Hence, the atomic force microscopy (AFM) measurement with a tapping mode was implemented to investigate the effect of surface morphology of the PEDOT:PSS thin film with the doping of glycerol, EG and AZO. The root-mean-square (R_{rms}) roughness is a quantitative value for describing the surface roughness of the dopedPEDOT:PSS thin films.

4.3.1 Morphological properties of glycerol doped PEDOT:PSS.

The topographical images of glycerol modified PEDOT:PSS compared to the 0% glycerol (pristine) are shown in Figure 4.19 . The AFM image of pristine PEDOT:PSS clearly shown that the morphology of the un-doped sample is smooth and conquered by short curved structure which attributes to the existing of polymer nanoparticles from

aqueous dispersion (Hau et al., 2009). The surface morphology of PEDOT:PSS films consist of grains for PEDOT-rich regions and large areas among them appear almost featureless for PSS-regions (Semaltianos et al., 2010). However, upon the addition of glycerol, a dramatic effect on the surface roughness of the thin films is shown.

As a high boiling point solvent, glycerol has a potential to reduce the evaporation rate of the PEDOT:PSS solvet hence results in forming a flat thin film surface which may encourage in reducing the surface roughness of the PEDOT:PSS thin films (Tekin et al., 2004; Xiong & Liu, 2012). As observedin 2% glycerol modified PEDOT:PSS thin films, the aggregation of PEDOT-rich particles which have been generated due to the small amount of glycerol can result in an increase roughness on the film surface. The surface morphology of the glycerol doped PEDOT:PSS became more inhomogenous than the pristine PEDOT:PSS.

Figure 4.20 presents the effect of glycerol-doped PEDOT:PSS on the surface roughness. The values of root-means-square surface roughness (R_{rms}) and the mean of surface roughness, R_a are tabulated in Table 4.4. It can be seen that the surface roughness of PEDOT:PSS increases upon glycerol doping up to 4%.

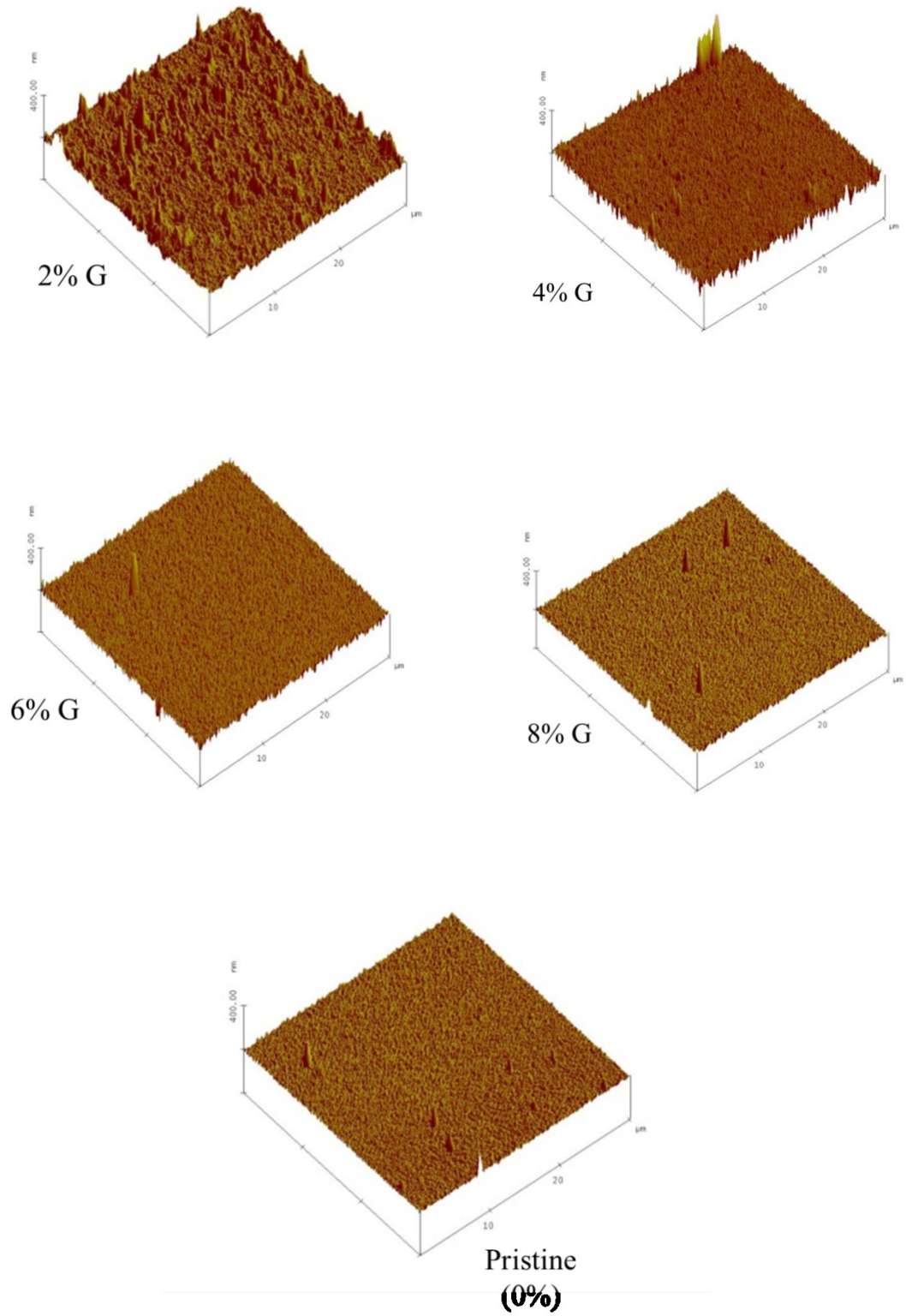

Figure 4.19 : AFM images for glycerol doped PEDOT:PSS compared to pristine PEDOT:PSS.

Such rise could be explained in terms of the broken ionic bonds that formed between PEDOT and PSS chains with the doping of glycerol to PEDOT:PSS which leads to the repulsion of negative charges on PSS chains. As the glycerol amount increases, it results in more severe aggregation in PEDOT chains which may cause the increase in the surface roughness of the PEDOT:PSS thin films (Xia & Ouyang, 2011).

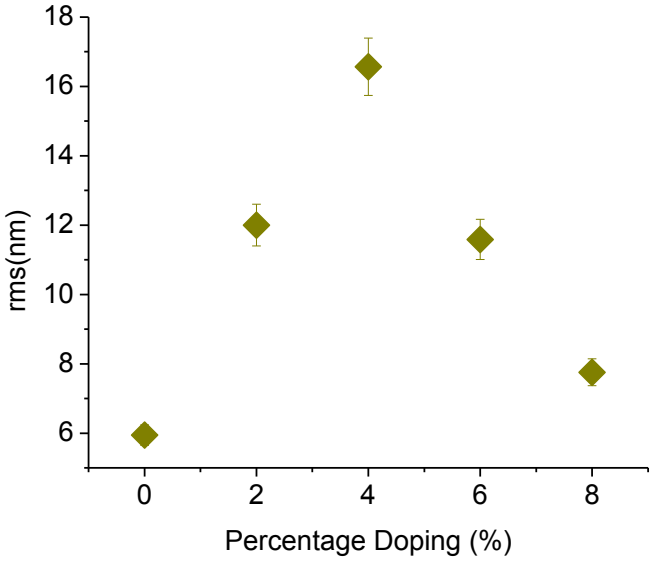

Figure 4.20 : R_{rms} roughness for glycerol doped PEDOT:PSS thin film.

Table 4.4: Root-mean-square roughness and mean surface roughness for glycerol doped PEDOT:PSS.

Sample Name	Root-mean-square roughness, R_{rms}(nm)	Mean-surface roughness, R_a (nm)
Pristine	5.946	4.813
2 % Glycerol	12.001	8.720
4 % Glycerol	16.567	12.618
6 % Glycerol	11.587	9.179
8 % Glycerol	7.757	6.289

However as the percentage of glycerol increases (up to 8%), the PSS lamella layer reacted with glycerol where the negative charges on the PSS chains repulse each other. This

repulsion forms a better organized alignment to produce a smoother surface with further percentage of glycerol (Xiong & Liu, 2012). Moreover, glycerol that acted as a plasticiser upon addition to PEDOT:PSS results in the engorged colloidal particles thus in return, improved the conductivity between the conductive region of the films (Lee et al., 2010).

Hence, the smoothen surface of 8% doped PEDOT:PSS thin film contributes accordingly to increase the sheet resistance of the thin films as discussed in section 4.2.1 thus reduced the conductivity of 8% glycerol doped PEDOT:PSS thin film. The smoothen surface reduced the engorgement effect of PEDOT:PSS particles which leads to the increasing of surface contact between the PEDOT particles. As this allowed insulator of PSS to fill in between the PEDOT particles result in the increment of sheet resistance of the PEDOT:PSS thin films.

4.3.2 Morphological Properties of EG doped PEDOT:PSS thin films.

Atomic force microscopy images of the ethylene glycol (EG) doped PEDOT:PSS are shown in Fig. 4.21. By adding EG to PEDOT:PSS, the surface morphology of the thin films has changed. The variation was claimed to be related to the conformational modification which responsible in raising the interchain interaction (Ouyang et al., 2004). An additive effect shows that the granular structure becomes smaller with a sharper engorgement generating the higher surface roughness value compared to the glycerol modified PEDOT:PSS.

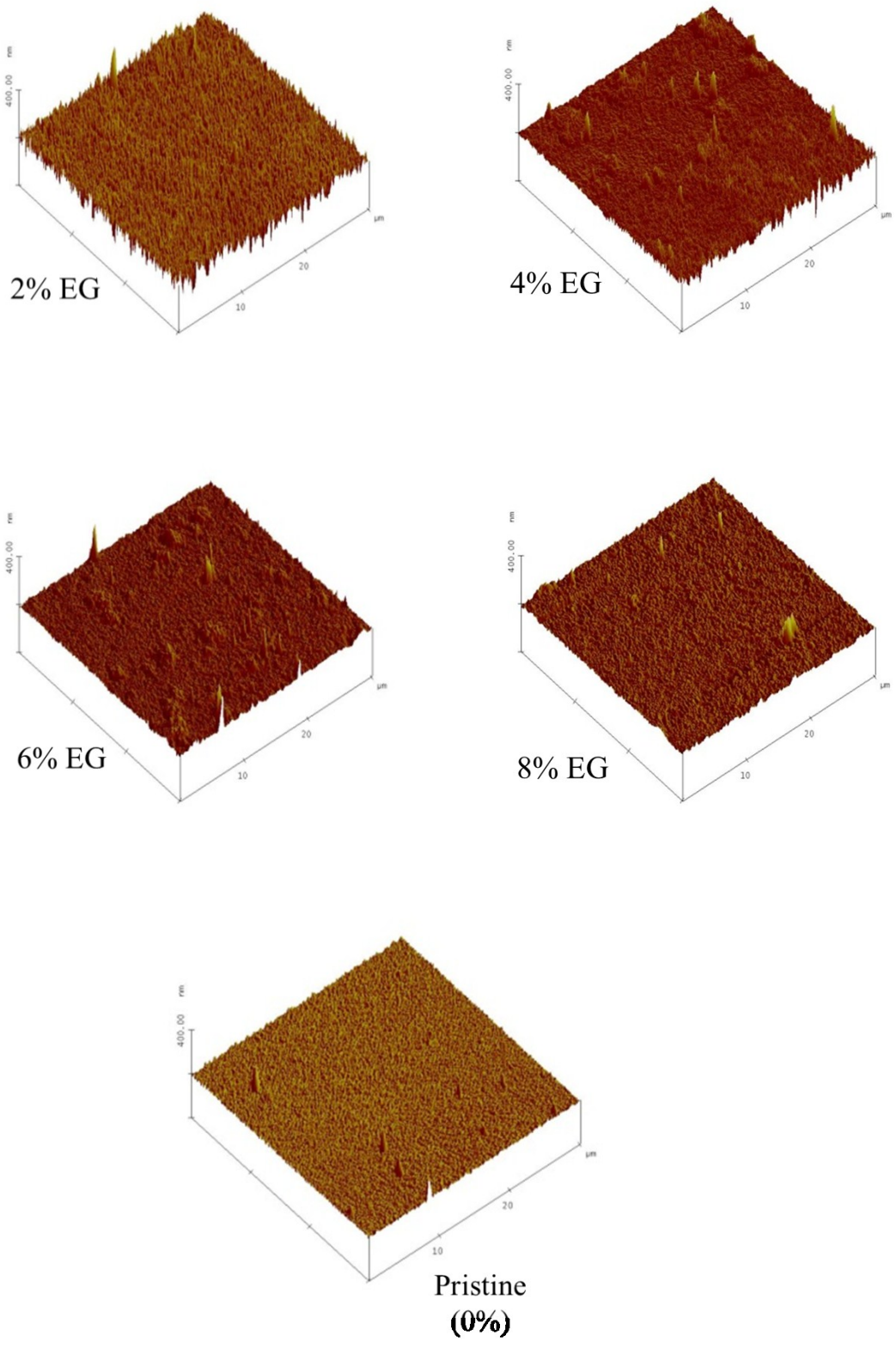

Figure 4.21 :AFM images for EG doped PEDOT:PSS compared to pristine PEDOT:PSS.

As tabulated in Table 4.5, the addition of 2% and 4% of EG content has caused the extreme surface roughening. The mixture of 2% and 4% of EG into PEDOT:PSS molecules created non-homogeneous distribution of the PEDOT and PSS species within the grains. Figure 4.22 presents the effect of EG-doped PEDOT:PSS on the surface roughness. This result could be due to the migration of solvent component to the films surface and produced an uneven surface of film. However, with 6% and 8% amount of EG doped has gradually smoothen the film surface to exhibit a granular morphology consisting of PEDOT:PSS particles. Other researchers have also reported the similar observation on the EG-doped PEDOT:PSS (Karagiannidis et al., 2012).

According to the AFM images, it is obvious that the morphology of the pristine (undoped PEDOT:PSS) is significantly affected by the presence of EG. Upon doping of solvent, the PEDOT:PSS molecules become elongated oriented.It forms a long stretched network that results in increase of surface roughness (Laskarakis et al., 2013). In addition, H.Yan et al proposed that the roughness of the film surface was considerably become rougher upon EG addition due to the formation of clusters with several primary particles (Yan & Okuzaki, 2009).

Moreover, as shown in Figure 4.21, the existence of white granular on 6% EG and 8% glycerol modified PEDOT:PSS thin films indicates the island formation on the film (Mauger et al., 2012). The results obtained in this AFM observation, also in agreement to the images observed by Crispin et al. The existence of elongated islands was explained by the phase separation upon addition of diethylene glycol (DEG) in PEDOT:PSS (Crispin et al., 2003).

Table 4.5 :Root-mean-square roughness and mean surface roughness for EG doped PEDOT:PSS

Sample Name	Root-mean-square roughness, R_{rms}(nm)	Mean-surface roughness, R_a (nm)
Pristine	5.946	4.813
2 % EG	12.750	9.717
4 % EG	23.574	18.399
6 % EG	7.110	4.287
8 % EG	4.597	3.779

Further addition of EG contributes to the reduction of the excess PSS on the PEDOT/PSS grains or film by phase separation (Sharmaa et al., 2009). In the PEDOT and PSS clusters, the size of the primary particle can be decreased by removing the excess PSS layer. The polar solvent tends to wash away the PSS molecules from the surface region. Hence the PEDOT:PSS film become thinner with the increase of EG amount beyond 4%.

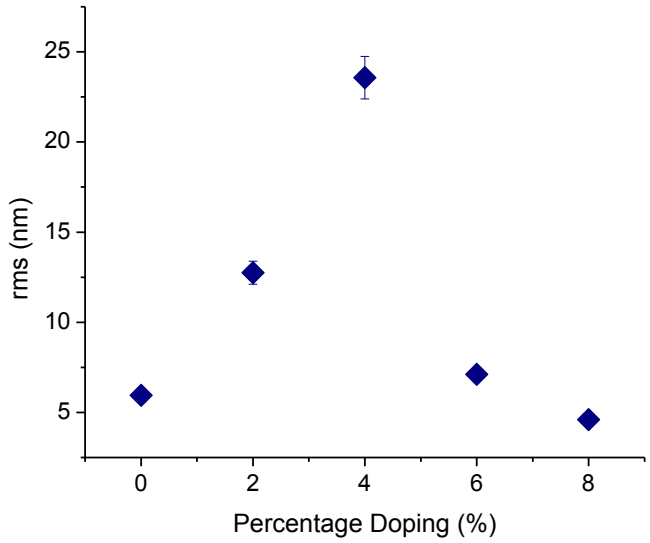

Figure 4.22 :$R_{rms}$of ethylene glycol (EG) modified PEDOT:PSS thin film.

Nevertheless, it is in contrast with the AFM results by J.Gasiorowski et al where in their observation, the trend indicates that roughness slightly increases upon increasing the concentration of EG at certain values. Initially, they found that, the layer without EG showed relatively smoother surface with granular structure of PEDOT:PSS. However with an increasing concentration of EG, a noticeable increase of the roughness of the films had been observed. They suggested that the significant increase of roughness with EG concentration may due to the fact of formation of small grains within PEDOT:PSS (Gasiorowski et al., 2013).

Another work also suggested that the EG doping has increased the thickness of the PEDOT:PSS (Yan & Okuzaki, 2009). They referred that such thicker film was caused by the increasing of the primary particle diameter or the aggregation of two or three primary particles or cluster. Hence it is concluded that the EG doped PEDOT:PSS in the present work mainly contributes in reducing the PSS layer as well as adjusting the PEDOT particles for the elongated and better oriented thin films for EG concentration beyond 4%. Such contradictory results may due to the different type of EG grade used in their study.

4.3.3 Morphological properties of AZO doped PEDOT:PSS thin films.

Morphologies of the different AZO doped PEDOT:PSS thin films are shown in Figure 4.23. AFM images of pristine, ZnO doped and AZO doped PEDOT:PSS are also shown as comparison. In general, the surface morphology in all thin films is reasonably smooth, with uniform grain distribution. The obvious variation of roughness with the present of AZO may results from the conformational changes of the macro molecular polymer chains of PEDOT:PSS with AZO doping. The coil conformation structures have been converted to a linear or expanded coil conformation with the incorporation of AZO

(Semaltianos et al., 2010).The structure conversion from coil conformation to linear or expanded coil altered the surface morphology by increasing its roughness hence this may leads to the better connection among the conductive PEDOT chains.

The root mean square roughness (R_{rms}) and the mean surface roughness (R_a) are tabulated in Table 4.6. It can be seen that the root mean square roughness of PEDOT:PSS thin film with AZO doping rises twice compared to that of the pristine thin film, from about 5.946 nm up to 12.323 nm for 6% AZO doped PEDOT:PSS thin film. Figure 4.24 shows this drastic change in upon 4% AZO amount compared to the pristine film.

One can notice (from Table 4.6) that there is no changes occur in the roughness of the ZnO doped PEDOT:PSS thin films compared to the pristine sample. Nevertheless the exist of aluminum in zinc oxide (to form AZO) strongly contribute in a drastic increase of the surface roughness with respect to AZO doping.

The variation of surface roughness in ZnO doped- and AZO doped PEDOT:PSS (as shown in Table 4.6) rather steadily occur compare to the glycerol doped and EG doped which likely forming drastic changes with their doping material. ZnO and AZO material are n-type material which basically possessed dominant carriers of negative charges. Hence, the doping process to a p-type PEDOT:PSS has established an electrostatic interaction between PEDOT chain and the AZO components (Heo et al., 2013). It is also noted that the gradual increase in rms roughness of the AZO doped PEDOT:PSS thin films may due to the effect of aluminum content in zinc oxide compound leading in the transformation to a linear conformation of PEDOT:PSS structure.

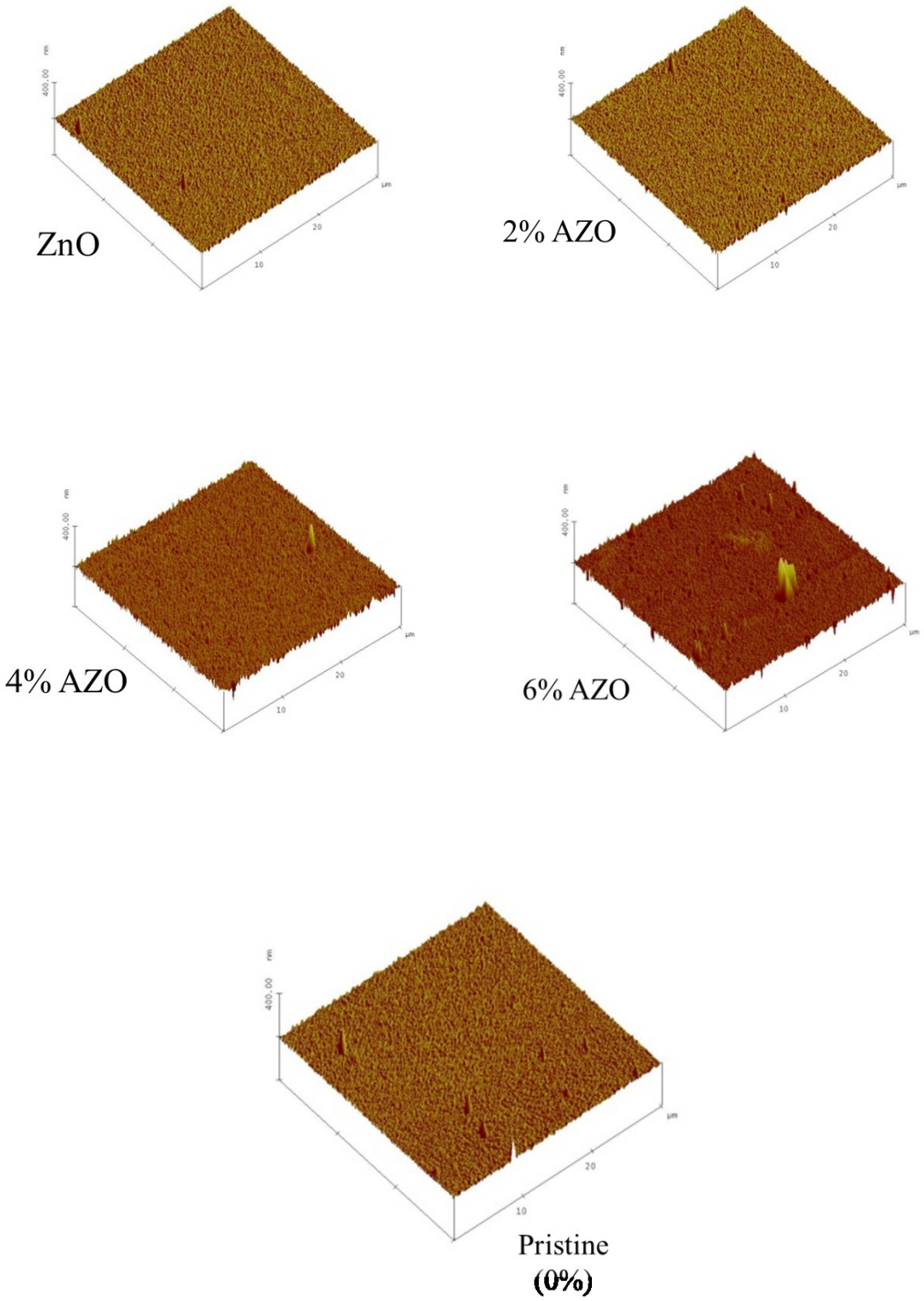

Figure 4.23: AFM images for AZO doped PEDOT:PSS compared to the undoped (pristine) PEDOT:PSS.

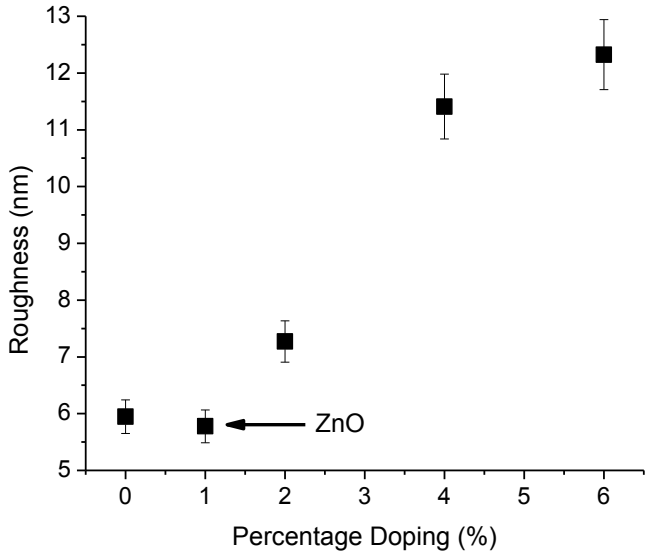

Figure.4.24: Roughness, rms for AZO modified PEDOT:PSS compared to the pristine PEDOT:PSS.

Table 4.6 :Root-mean-square roughness and mean surface roughness for AZO modified PEDOT:PSS compared to the pristine PEDOT:PSS.

Sample Name	Root-mean-square roughness, Rq(nm)	Mean-surface roughness, R_a (nm)
Pristine	5.946	4.813
ZnO	5.778	4.639
2 % AZO	7.270	5.580
4 % AZO	11.408	8.963
6 % AZO	12.323	7.227

4.4 **Raman studies**.

Raman spectroscopy studies is normally used due to the unique vibrational informational which is specifically relates to the chemical bonds and symmetry of molecules. Specifically for organic material, Raman spectra are similar to infrared spectra in that they have regions that are useful for functional group detection. Hence, it provides a fingerprint by which the molecule is able to be identified.

4.4.1 Raman studies of glycerol doped PEDOT:PSS

The Raman spectra for pristine and glycerol doped PEDOT:PSS are shown in Figure 4.25.As an overall, the bands observed and their assignments are in good agreement with the one obtained by other researchers (Schaarschmidt et al., 2009); Semaltianos et al., 2010; Tamburri et al., 2011). The fingerprint spectra of PEDOT:PSS with the most clear, intense and well-shaped peaks were produced for these polymer chain groups of glycerol doped PEDOT:PSS. The main fingerprint peaks which provide identification of the polymer material as PEDOT:PSS were appeared in the Raman band spectra and are summarized in Table 4.7 together with their peaks and assignments of their chemical bonding.

As illustrated in Figure 4.25, the spectrum of the reference pristine (green curve), a band with a strong intensity is centered at 1426 cm^{-1} which corresponds to the symmetric stretching mode of the aromatic C=C band within the PEDOT chemical structure . Three other important bands found at 1530, 1365 and 1261 cm^{-1} which are related to the antisymmetric C_α-C_β stretching, C_β-C_β stretching deformations and C_α-C_α inter-ring stretching vibrations, respectively (Schaarschmidt et al., 2009).

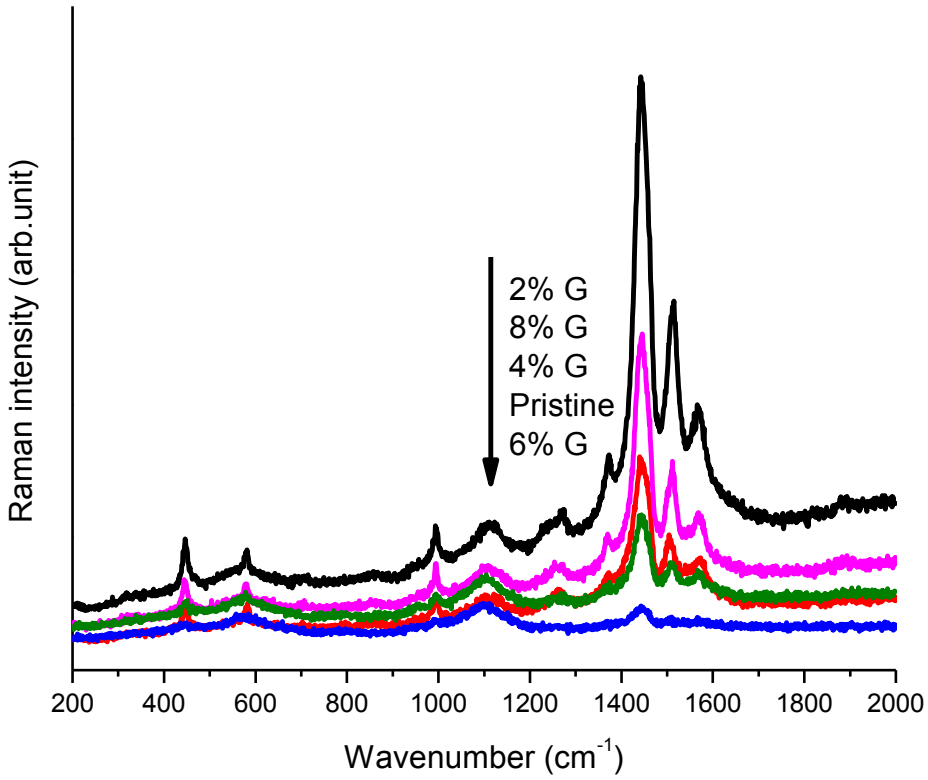

Figure 4.25 : Raman spectra for pristine and glycerol doped PEDOT:PSS in the frequency range 200 – 2000 cm^{-1} .

Table 4.7:. List of band position, band assignments and the type of raman active modes of glycerol doped PEDOT:PSS raman spectras

Band Position (cm^{-1})	Band assignment	Raman active modes
1569 -1574	C_α- C_α	Antisymmetric stretching
1504-1514	C_α - C_β	Antisymmetric stretching
1444	Aromatic C1/4	Symmetric stretching
1369-1374	C_β- C_β	Stretching deformation
1269	C_α- C_α	Inter-ring stretching vibrations
1104-1120		C-O-C deformation
990-995		Oxyethylene ring deformation
576-581		Oxyethylene ring deformation
446-451	SO_2 bending	

From the Raman spectra, it is observed that the location of the aromatic C=C bands (at 1443 cm^{-1}) of the glycerol-doped samples are not shifted upon doping of glycerol. It is also noticeable that the Raman intensity at 1443 cm^{-1} of the films have changed to some extent, with respect to the variation of the glycerol percentage. The effect of glycerolon Raman intensity is tabulated in Table 4.8. For the PEDOT:PSS film with 2% glycerol, the band reaches the highest intensity, while at 6% doping exhibit lowest intensity.

Table 4. 8 : Raman peak at 1443 cm^{-1} of the glycerol doped PEDOT:PSS.

Glycerol doped (%)	Raman absolute intensity
0	2514.20
2	9657.00
4	3413.68
6	1021.29
8	5493.80

The variation in Raman intensity upon glycerol doping exhibit the alterations in the PEDOT polymer chain doping and the PSS ionic strength caused by the conformational change in the PEDOT:PSS thin films (Schaarschmidt et al., 2009; Tamburri et al., 2011). However the Raman peak originated from the PSS structure cannot be detected in this study, probably due to the non-conjugated backbone (Nguyen & Vos, 2004).

Figure 4.26 shows Raman spectras of glycerol doped PEDOT:PSS in the range of wavenumber from 1300 cm^{-1} to 1600 cm^{-1} which provides clear view on the finger-print peak locations to observe the shifting phenomena due to the glycerol doping procedure to the PEDOT:PSS. Several peak locations which show shifting results due to the doping of glycerol are at 1372 cm^{-1} and 1510 cm^{-1}. However at raman peaks locations of 1444 cm^{-}

[1]and 1571 cm^{-1} show no shifting effect but only changes in their intensity with respect to different doping percentage of glycerol.

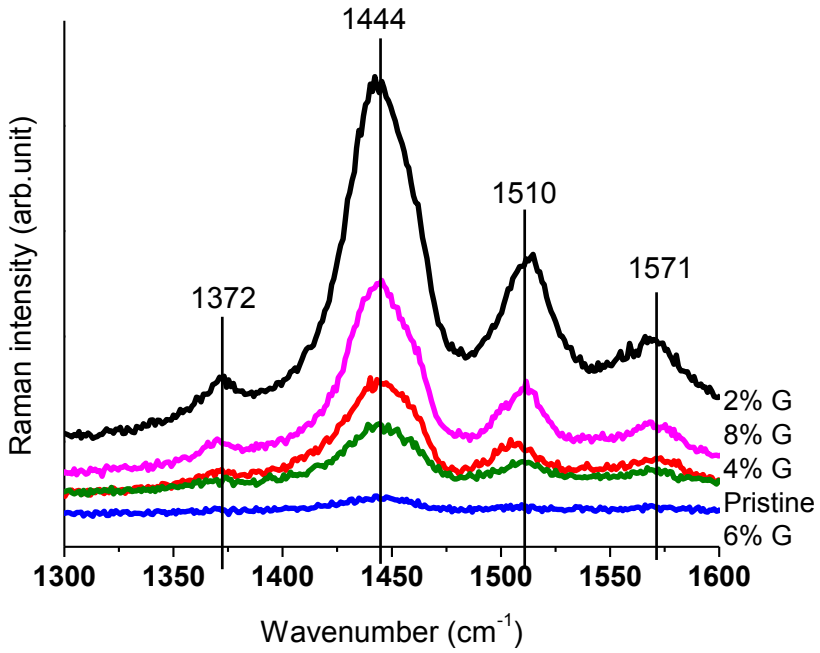

Figure 4.26 : Raman spectras of the pristine PEDOT:PSS and modified PEDOT:PSS with glycerol doped in the range 1300 cm^{-1} to 1600cm^{-1}.

The peak at 1372 cm^{-1} is referring to the stretching formation of C_β- C_β bonding and the doping effect of 2%, 4% and 8% shows that the peak were shifted to the left with respect to the peak by the pristine thin film, which shown the decreasing of the raman wavenumber. The peak at 1510 cm^{-1} also shows shifting effect with the doping of glycerol where 4% doped peak moved backwards which the wavenumber were reduced while the peaks of 2% and 8% doped glycerol moved forwards and were increased in their raman wavenumbers.

The shifting and broadening effect upon glycerol doping process are correspond to the stretching vibration of $C_\alpha = C_\beta$ on the five-member ring of PEDOT. It is suggested to be attributed to the resonant structure of PEDOT chain which changing from a benzoid to a

quinoid structure (Ouyang et al., 2004). Hence in this study, the shifting peaks of 2%, 4% and 8% glycerol doped PEDOT:PSS may relate to the vibrations of C_α=C_β antisymmetric stretching and the deformation of $C_\beta = C_\beta$ stretching bonding which correspond to the structure deformation from benzoid to quinoid structure.

As discussed in section 2.2 (page 23), the change to linear or expand coil of quinoid structure results in the enhancement of electrical properties of PEDOT:PSS. Thus this results was in good agreement with the electrical properties of 2% to 4% glycerol doped PEDOT:PSS which shows increasing in conductivity of PEDOT:PSS with 2% and 4% glycerol doped PEDOT:PSS (Section 4.2).

It should be noted that the two peaks at 1095 and 572 cm^{-1} bands in all Raman spectra correspond to the glass substrate and not originated from the doped PEDOT:PSS thin films. For the same measurement condition, the absolute Raman intensity spectrum is the function of the optical properties of the analyzed materials, mainly the colour and the clearness (Colomban & Slodczyk, 2009). The intensity of the scattered light can decrease significantly because of the weathering effects such as the appearance of microcracks, pits, salts, precipitates and corroded silica rich layer at the upper surface exposed to different polutions.

Hence, due to the intensity difference with respect to the doping percentage of glycerol indicates the presence of impurities and defects which increases with the higher amount of glycerol in PEDOT:PSS thin film. This is in a good agreement with the surface morphology of glycerol doped PEDOT:PSS discussed in section 4.3.1 which shows rise of rms roughness with the addition of glycerol, specifically in the range of 2% to 6% of glycerol doped to PEDOT:PSS thin films. It is noted that the variations in rms roughness

were not in order with the differences in Raman intensity. Hence, the increase of rms roughness were suggested to be only partly related to the existence of defects on the surface of the doped PEDOT:PSS thin films.

4.4.2 Raman Properties of EG doped PEDOT:PSS thin films.

Since the EG doping shows interesting changes in PEDOT:PSS thin films specifically in their optical and morphology properties, hence further investigation on the effect of this dopant to the molecular structure and polymer chains is crucial. In this section, Raman spectroscopy measurement is discussed. Figure 4.27 presents the Raman spectra of the EG doped- PEDOT:PSS thin films.

In this work, the Raman spectra for EG doped samples consist of several intense bands. The correspond Raman bands to the bonding modes of the EG doped-PEDOT:PSS spectra are tabulated in Table 4.9. The spectra obtained from this study is almost identical to the Raman spectrum reported by the other researcher (Tamburri et al., 2011). It can be noticed that the presence of an intense band at 1446 cm^{-1} corresponds to the symmetrical C_α=$C_\beta$stretching modes. The asymmetrical C_α=C_β stretching mode actually splits into two bands located at 1504 and1564cm^{-1}, respectively.

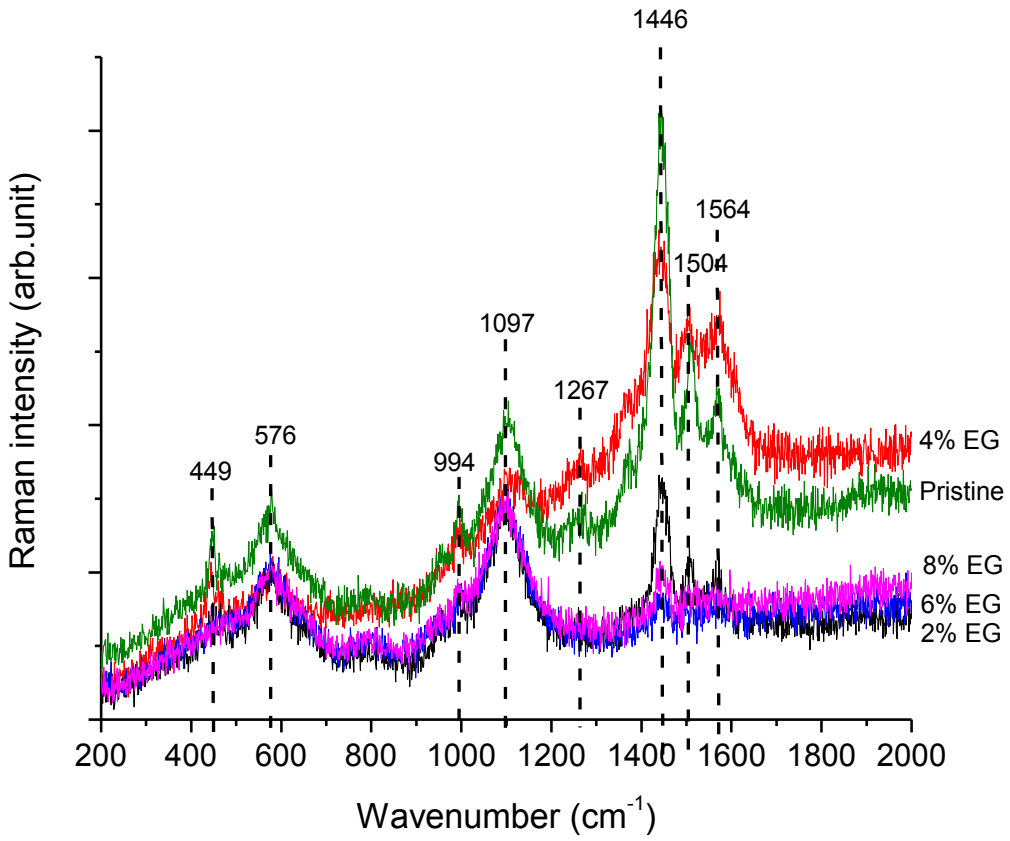

Figure 4.27 : Raman spectra of the pristine PEDOT:PSS and modified PEDOT:PSS with EG.

Moreover a tiny band attributed to C_α-C_α stretching at about 1267 cm^{-1} is also found in this study. This spectral feature has been widely recognized in literature and ascribed to the oxidized form of the polymer. However, generally, their bands are broader and shifted to higher frequency with respect to those detected for the undoped PEDOT:PSS polymer form (Tamburri et al., 2011). The broader band was suggested due to the changes from coil to linear chain structure which leads a transformation from benzoid to the quinoid molecular structure.

Raman spectroscopy of EG doped PEDOT:PSS has provided information on the molecular transformation upon the addition of EG. It is suggested that the conformational of the PEDOT chains is altered by EG doping in PEDOT:PSS (Ouyang et al., 2004). The driving force for the conformational change is the dipole-dipole interaction of EG dipole and PEDOT chains in PEDOT:PSS. The rearrangement of polymer chains in PEDOT:PSS with EG doping provides a strong influence in electrical properties, as discussed earlier.

It is notice from Table 4.9 that by EG doping, the 1369 cm^{-1} band has disappeared. This band corresponds to the C_β-C_β stretching deformation and with more than 2% of EG addition, has diminished this type of bonding structure in PEDOT:PSS. The missing bonding may reflects the different structure of studied EG doped PEDOT:PSS thus affected in different properties compared to the EG doped PEDOT:PSS by other research work (Singh et al., 2014).

Table 4.9: List of band position, band assignments and the type of Raman active modes of EG doped PEDOT:PSS

Band Position (cm^{-1})	**Band assignment**	**Raman active modes**
1564	C_α- C_α	Antisymmetric stretching
1504	C_α - C_β	Antisymmetric stretching
1444	Aromatic C1/4	Symmetric stretching
1267	C_α- C_α	Inter-ring stretching vibrations
1097		C-O-C deformation
994		Oxyethylene ring deformation
576		Oxyethylene ring deformation
449	SO_2 bending	

Wichiansee et al claimed that EG may involve in the second conformation change due to the transformation of the chemical structure of PEDOT (Wichiansee & Sirivat, 2009). Two kind of the resonant structures exist within PEDOT which consists of benzoid and quinoid structure which involve the deformation chains of C_α- C_β as shown in Figure 4.28 (Yoo et al., 2014). In the benzoid structure, the C_α - C_β bond is formed by two conjugated electrons while in quinoid structure there is no conjugated-electrons on the C_α - C_β (Wichiansee & Sirivat, 2009). The difference in intensity and the shifting of Raman peaks were highly due to the doping behavior in PEDOT:PSS according to the doping material (Han et al., 2011).

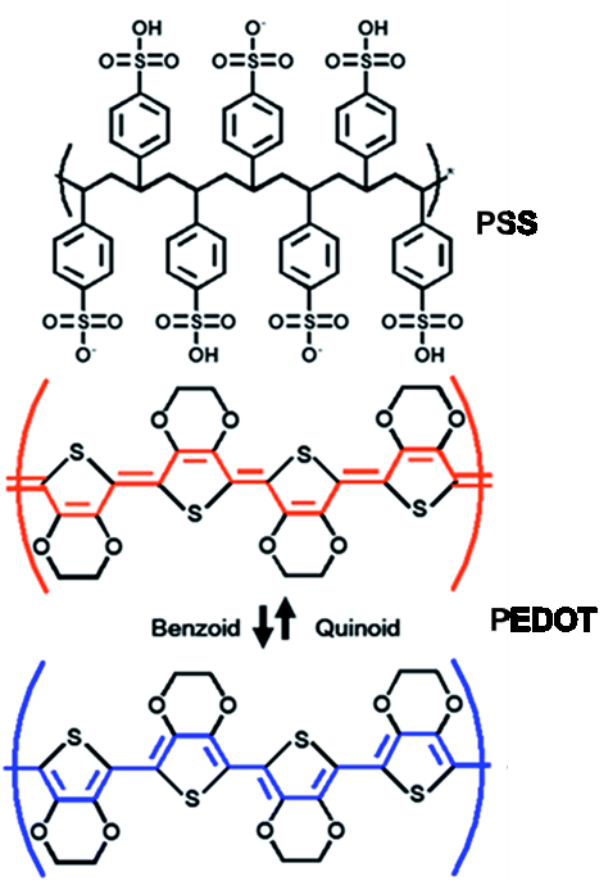

Figure 4.28 : The transformation in chemical structure of PEDOT:PSS from benzoid to quinoid structure.

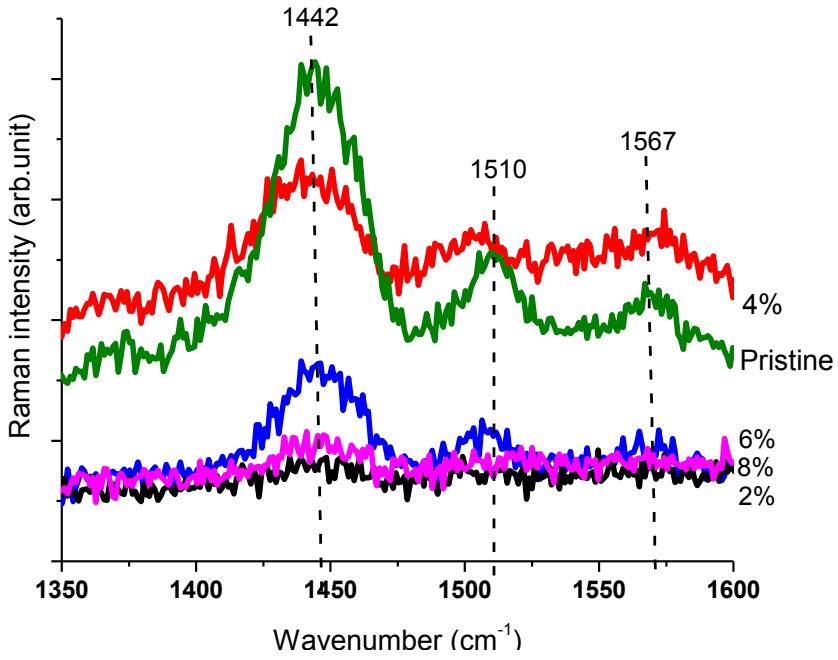

Figure 4.29 : Raman spectra of the pristine PEDOT:PSS and modified PEDOT:PSS with EG in the range of 1350 cm^{-1} to 1600 cm^{-1} .

Figure 4.29 shows the raman spectras of EG doped PEDOT:PSS in the wavenumber range of 1350 cm^{-1} to 1600 cm^{-1}. Apparently, the peaks at 1442 cm^{-1} shows no shifting effect while obvious peak shifting were observed at 1510 cm^{-1} and 1567 cm^{-1} with respect to the raman spectras of the pristine PEDOT:PSS. 4% and 6% EG doped PEDOT:PSS shows the backwards shift of wavenumbers relative to the pristine peak at 1510 cm^{-1}. However 2% and 8% EG doped PEDOT:PSS shows almost none raman peak at this wavenumber which indicating the weak bonding of C_α- C_α and C_α - $C_\beta$antisymmetric stretching.

4.4.3 Raman Properties of AZO doped PEDOT:PSS.

The Raman spectra for zinc oxide and AZO doped PEDOT:PSS are shown in Figure 4.30. Generally, as demonstrated in the plot, the band spectra and the peaks location of AZO doped PEDOT:PSS thin films are all in good correlation with the pristine

PEDOT:PSS. The most clear, intense and well-shaped peaks are produced for the polymer chain groups of AZO doped PEDOT:PSS. The summary of the Raman peak and their correspond active modes is tabulated in Table 4.10.

For zinc oxide and AZO pristine thin films, the Raman peaks appear in the range between 250 cm^{-1}and700cm^{-1} (Manounia et al., 2006). From the plot, there was no clear appearance of these respective peaks occur. Hence, no obvious modification in PEDOT:PSS structure upon mixing with AZO compound.

It is also noticeable that peak 1370 cm^{-1} also invisible in these Raman spectra. This indicates that C_{β}-C_{β} bonding also not exist in AZO doped PEDOT:PSS which means no stretching deformation occur between the molecular structure of PEDOT:PSS after its collaboration to metal oxide of zinc oxide and AZO material.

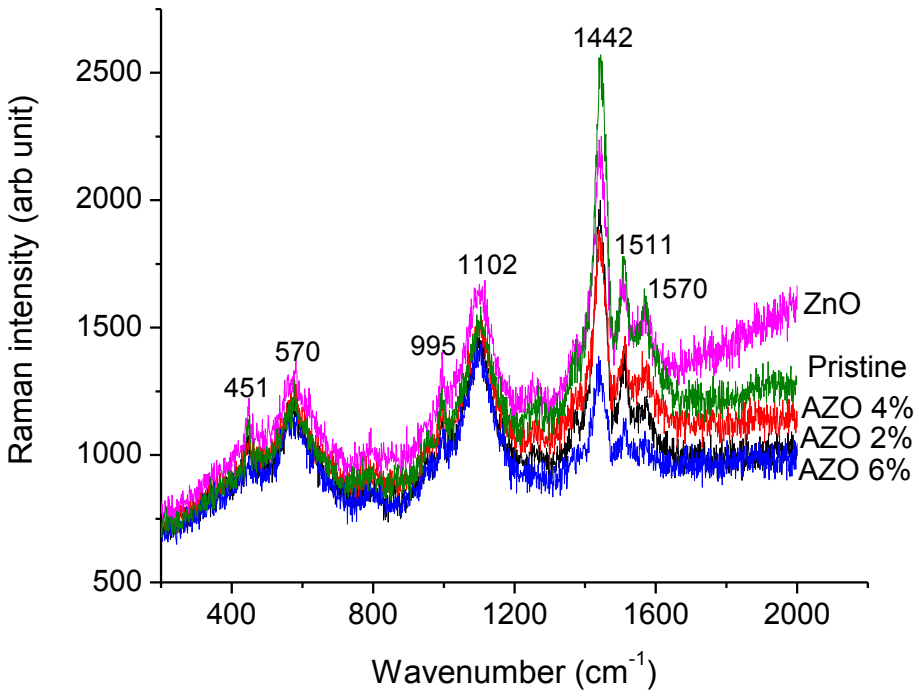

Figure 4.30 :Raman spectra of the pristine PEDOT:PSS and modified PEDOT:PSS with AZO.

Table 4.10. List of band position, band assignments and the type of raman active modes of AZO doped PEDOT:PSS

Band position (cm-1)	Band Assignment	Raman Active Modes
1570	C_α-C_α	Antisymmetric stretching
1511	C_α-C_β	Antisymmetric stretching
1442	Aromatic $C_{1/4}$	Symmetric Stretching
1267	C_α-C_α	Inter-ring stretching vibrations
1102		C-O-C deformation
995		Oxyethylene ring deformation
570		Oxyethylene ring deformation
451	SO2 bending	

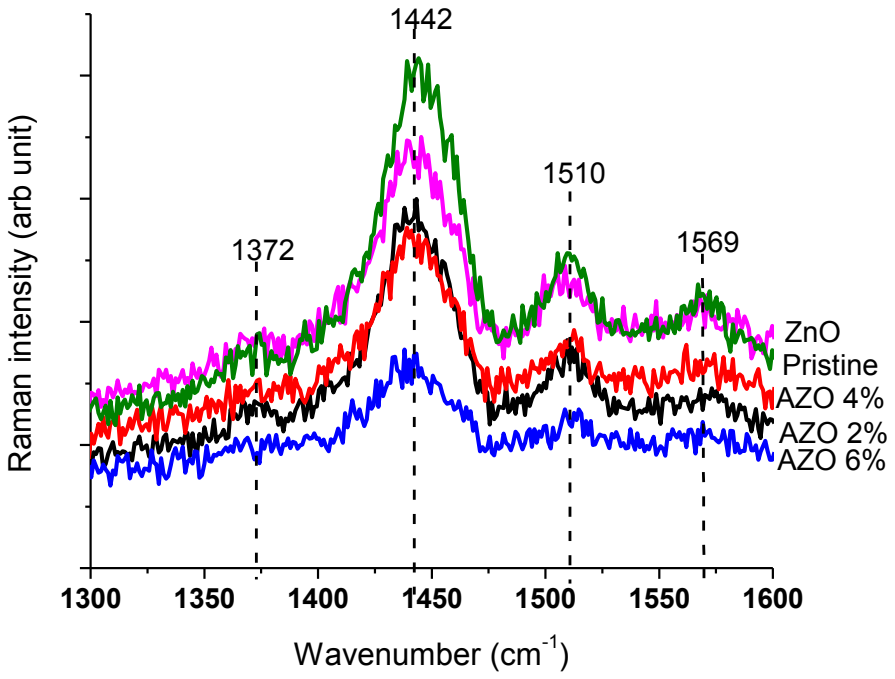

Figure 4.31 :Raman spectra of the pristine PEDOT:PSS and modified PEDOT:PSS with AZO in the range of 1300cm^{-1} to 1600cm^{-1}.

Figure 4.31 demonstrated the raman spectras of ZnO and AZO doped PEDOT:PSS in the range of 1300 cm^{-1} to 1600 cm^{-1}. At this range, the peaks at wavenumbers of 1372 cm^{-1}, 1442 cm^{-1}, 1510 cm^{-1} and 1569 cm^{-1} illustrate minor shifting of peaks with the doping of ZnO and AZO to PEDOT:PSS indicates that ZnO and AZO doping provides new arrangements in the chemical structure of PEDOT:PSS.

4.5 Current density – voltage (J-V) characterisations.

Overview.

In this work, it is essential to utilize the present modified PEDOT:PSS as buffer layer in organic solar cell device and obtain the current density-voltage (J-V) characteristics from all the devices. The various changes occur in the optical, electrical and morphology properties of the doped PEDOT:PSS with respect to its different doping material.

Hence, obtaining the J-V parameters of each device with glycerol, EG, ZnO and AZO doped PEDOT:PSS as the buffer layer, is a significant process in order to blend and conclude which is the optimum modified PEDOT:PSS that may contribute in enhancing the performance of organic solar cell. Open circuit voltage, V_{oc} is one of the most important parameters in the organic solar cell performance. Its value is strongly related to the contacts between the active layer with the electrodes which is usually referred as buffer layer in organic solar cell device (Cai et al., 2009). Hence the variation in V_{oc} is expected to occur with respect to the different in dopant PEDOT:PSS as buffer layer.

The J-V characteristics of organic solar cells with different buffer layer of glycerol, EG and AZO doped PEDOT:PSS under illumination of AM1.5 solar simulation (100 mW/cm^2) are obtained and presented in this chapter.

4.5.1 J – V characteristics of glycerol doped PEDOT:PSS.

The J-V plots of organic solar cell which consists of ITO/glycerol doped PEDOT:PSS/P3HT:PCBM/Al with different percentage of glycerol and undoped PEDOT:PSS (pristine) are shown in Figure 4.32. It can be seen that the photovoltaic performances of the devices using different concentration of glycerol are significantly improved relative to the pristine PEDOT:PSS as the buffer layer. The results of J-V characteristics are summarized in Table 4.11. The open circuit voltage, V_{oc}, current density, J_{sc}, fill factor, FF and the efficiency percentage, η of all devices were stated in Table 4.11.

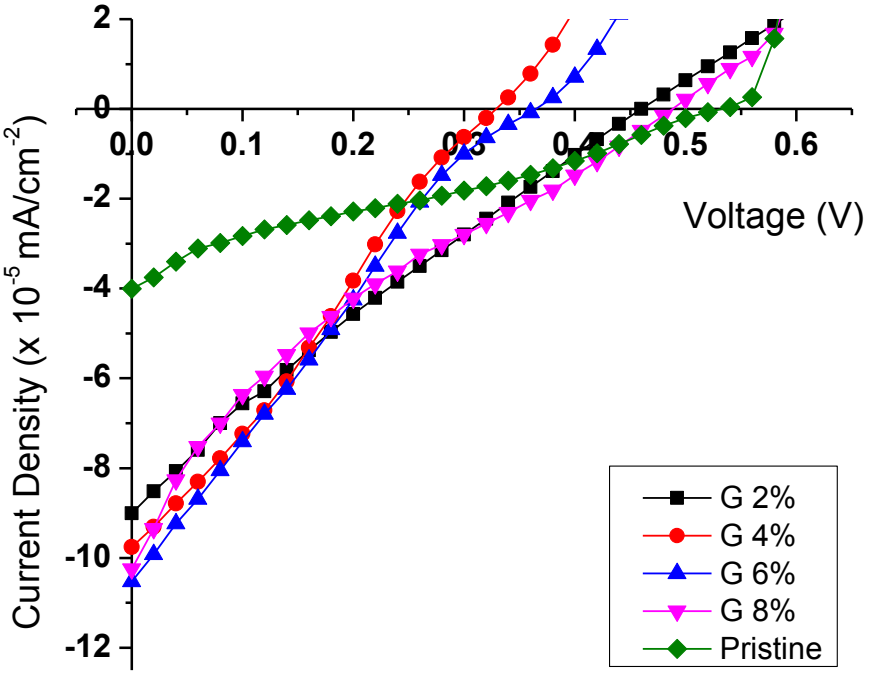

Figure 4.32 : J-V plots for glycerol modified PEDOT:PSS compared to pristine PEDOT:PSS.

Table 4.11 :J-V characteristics for glycerol modified PEDOT:PSS compared to pristine PEDOT:PSS.

% Doping	V_{oc}(V)	J_{sc}(x 10^{-5} mA cm^{-2})	FF (%)	η(x 10^{-3} %)
Pristine	0.54	4.0	24.67	5.3
2	0.46	9.0	22.45	9.3
4	0.33	9.8	26.74	8.6
6	0.36	10.6	23.67	9.0
8	0.49	9.7	17.66	8.4

From Table 4.11, it shown that the J_{sc} of the 2% doped PEDOT:PSS has been enhanced from 4.0 x 10^{-5} mAcm^{-2} to 9.0 x 10^{-5} mAcm^{-2}, compared to the undoped film. The small variations of J_{sc} in the range of 9.0 x 10^{-5} to 10.6 x 10^{-5} mA cm^{-2} may indicate minor improve charge transport of free charges results from a small formation of percolation pathways of the charge carriers (Beek et al., 2005).

Nevertheless, there is not much difference in J_{sc} photocurrents upon dopant amount; almost identical performance are obtained from these devices with variation of glycerol in PEDOT:PSS as the buffer layer (see Figure 4.33). For other photovoltaic parameters of the device, open circuit voltage, V_{oc} and fill factor show obvious variation with respect to the different glycerol concentration. The V_{oc} decreased drastically to 0.33 V with 4% glycerol doping and this trend is in good agreement with the work by S.Park et al which studied the PEDOT:PSS doped with sorbitol (Park et al., 2011). Park et al suggested that this behavior may be attributed to the development of shunts which is in well relation with the conducting pathways of the charge carriers from one layer to another layer in the device.

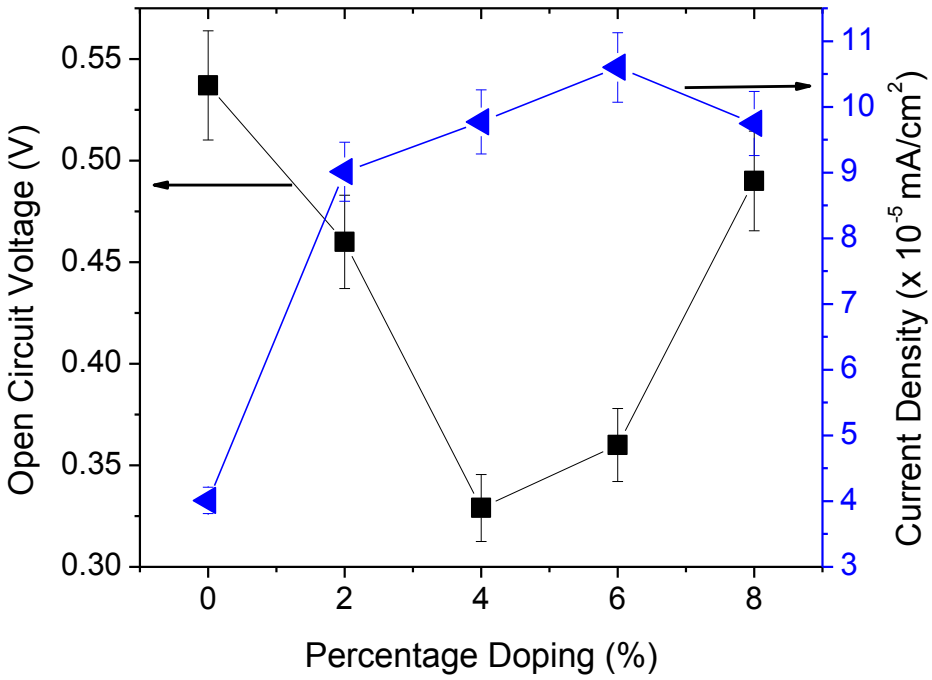

Figure 4.33 :The variation of V_{oc} and J_{sc} for glycerol modified PEDOT:PSS compared to pristine PEDOT:PSS.

The fill factor (FF) strongly related to the ability to prevent the recombination process between the diffused free charges at the interface of active layer and the electrode in the device. Figure 4.34 presents the effect of glycerol-doped PEDOT:PSS buffer layer on fill-factor, FF and power conversion efficiency, PCE of the photovoltaic devices. It is found that the glycerol doped PEDOT:PSS buffer layer contributes in altering the fill factor and the efficiency of the organic solar cell. At 4% glycerol content, the FF reaches the highest value, but further increase in glycerol concentration has caused a drastic drop of FF.

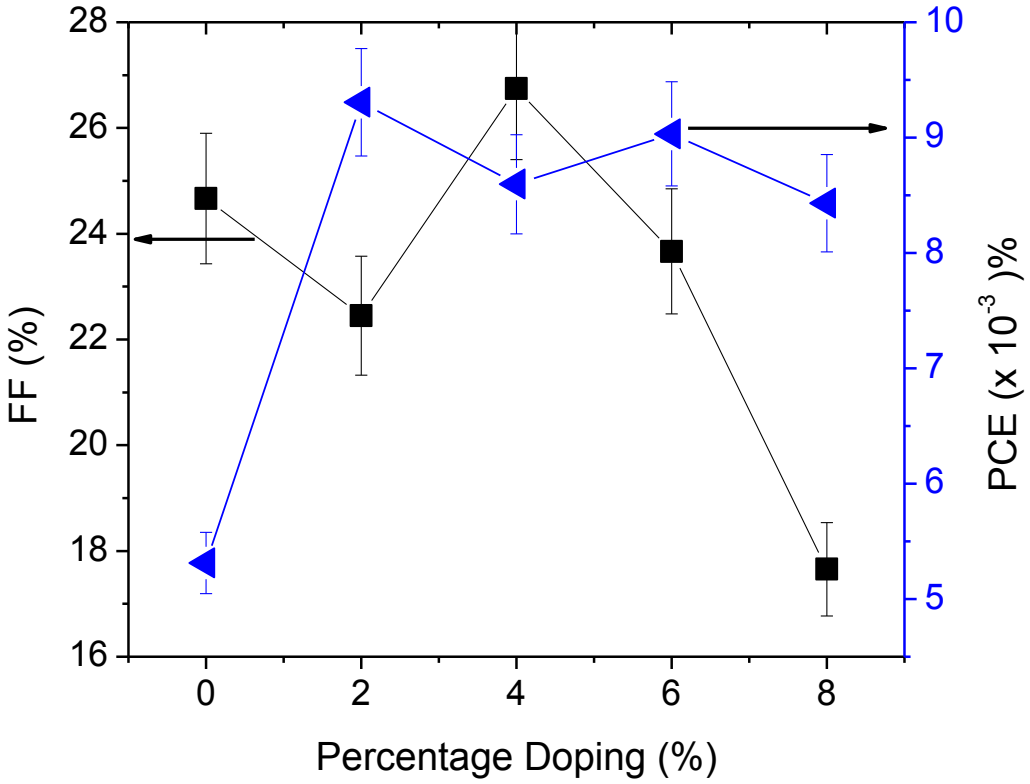

Figure 4.34 : The variation of fill-factor, FF and power conversion efficiency, PCE with respect to the glycerol doping.

The decrease in fill-factor with the increase in glycerol concentration may be due to the increase in the series resistance (R_s) in the device (Shrotriya et al., 2006). Nevertheless, the device efficiency reaches the maximum value at 9.31 x 10^{-3} % for device with 2 % glycerol doped PEDOT:PSS as the buffer layer. This result in agreement with the observation obtained in the conductivity measurement of the glycerol-PEDOT:PSS thin films (discussed in the previous section), in which 2% glycerol has produced the highest conductivity. Thus, based on this study only 2% of glycerol is needed incorporate the PEDOT:PSS in order to increase the performance of the organic solar cell.

4.5.2 J – V characteristics of EG doped PEDOT:PSS

The performance of organic solar cell device with EG doped PEDOT:PSS is presented by the J-V plot in Figure 4.35. Obvious changes in V_{oc} and J_{sc} have occurred upon the EG doping . The extracted V_{oc} and J_{sc}values (obtained from Figure 4.35) is presented in Figure 4.36. The plot shows that $V_{oc}$is reduced gradually while the J_{sc} shows unstable pattern with the increase amount of EG. It is suggested that the decrease in V_{oc} may due to the shunts which exist at the interlayer of the device structure. In addition, the increase in J_{sc} with addition of EG amount (such as at 6% EG) can be correlated to the rise of charges formation inferred from the photoluminescence quenching. In contrast, with the decrease in J_{sc}(at high content of EG, such as 8%) indicates the weaken in absorption of light by the anode and buffer layer side (Beek et al., 2005).

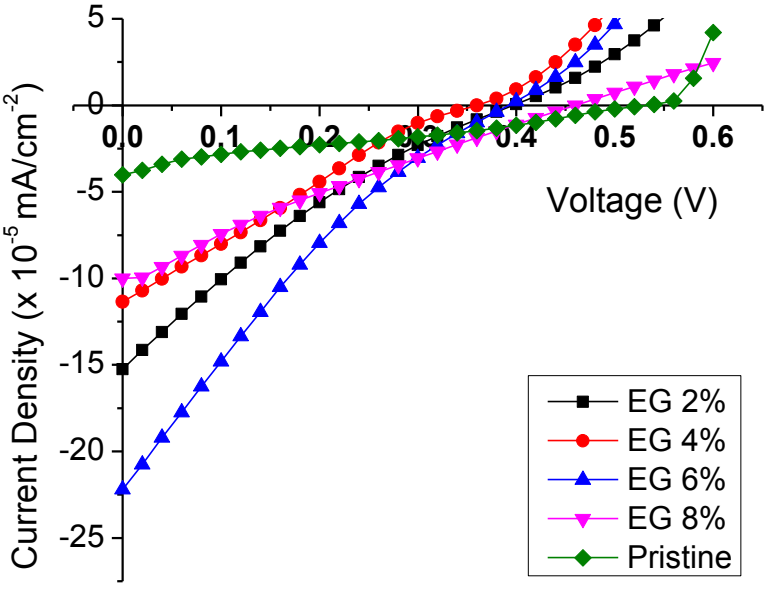

Figure 4.35: J-V plots for EG modified PEDOT:PSS compared to pristine PEDOT:PSS.

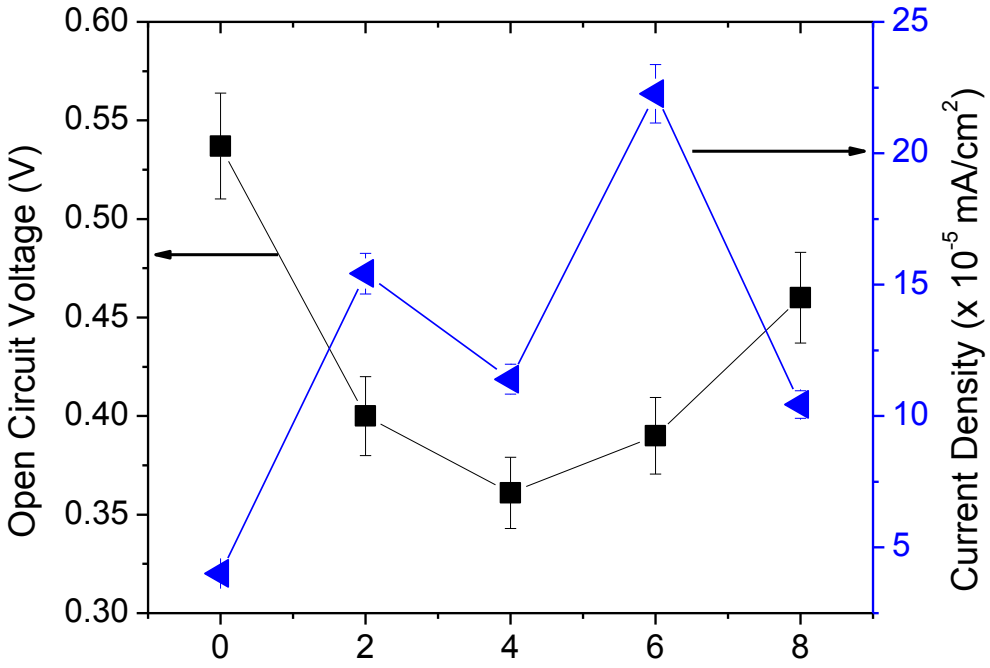

Figure 4.36 : The variation of V_{oc} and J_{sc} for EG modified PEDOT:PSS compared to pristine PEDOT:PSS.

The details of J-V parameters are listed in Table 4.12. In general, the enhancement occurred in the efficiency of doped PEDOT:PSS compared to the device with pristine PEDOT:PSS (Figure 4.37). As illustrated in Figure 4.37, the variation of fill factor seems to be insignificant with the additional content of EG doped PEDOT:PSS. Hence this indicates imbalance progress of the diffusion process to produce free charge carriers of electrons and holes. As a result, recombination of free charges may occur which reflect in the unstable trend of fill factor with the increased in EG content.

As indicated in Figure 4.37, there is no particular pattern in enhancing the performance of the organic solar cell by EG doping into PEDOT:PSS film as buffer layer. The highest efficiency PCE achieved is 17.0 x 10^{-3} % by using 6 % EG doped PEDOT:PSS. However, this amount of EG cannot be considered as the optimum amount to obtain the highest efficiency due to un-stable J_{sc} as well PCE results.

Table 4.12 : J-V characteristics for EG modified PEDOT:PSS compared to pristine PEDOT:PSS.

% Doping	V_{oc}(V)	J_{sc}(x 10^{-5} mA cm^{-2})	FF (%)	η(x 10^{-3} %)
Pristine	0.54	4.0	24.67	5.3
2	0.40	15.4	18.78	11.6
4	0.36	11.4	23.05	9.5
6	0.39	22.3	19.57	17.0
8	0.46	10.4	21.24	10.2

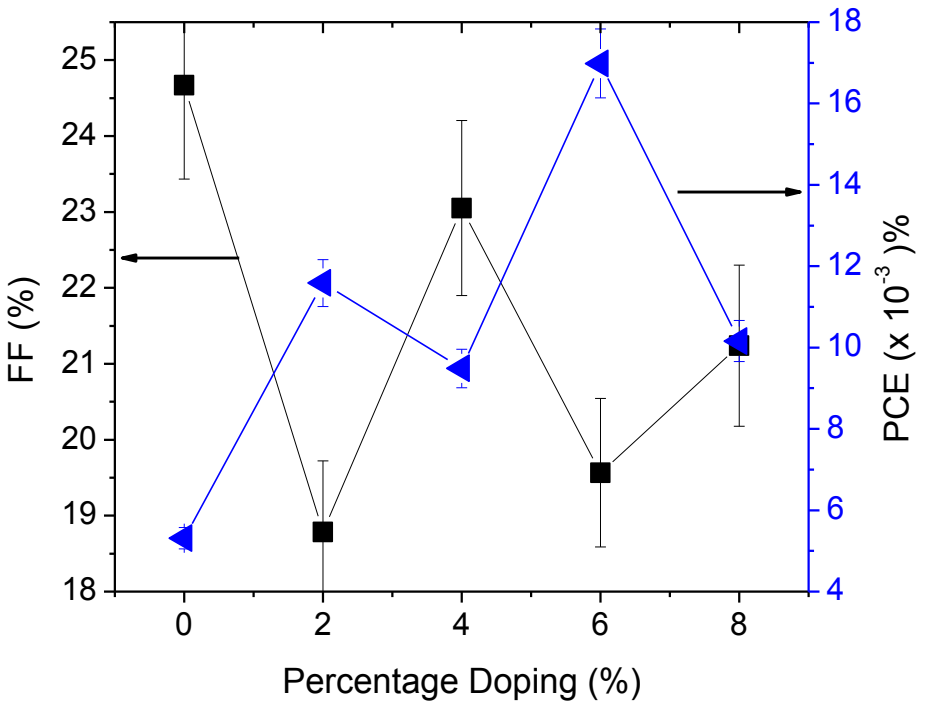

Figure 4.37 : The variation of FF and PCE for EG modified PEDOT:PSS compared to pristine PEDOT:PSS.

4.5.3 J – V characteristics of ZnO and AZO doped PEDOT:PSS.

Hybrid buffer layer of ZnO doped PEDOT:PSS and AZO doped PEDOT:PSS are used in organic solar cell and the measured J-V characteristics are presented in Figure 4.38. The list of electrical parameters obtained from the J-V characteristic plot are tabulated in Table 4.13. The V_{oc} values seems to be maintained at approximately 0.6 V for the pristine PEDOT:PSS, ZnO doped and (2% - 6%) AZO doped PEDOT:PSS as shown in Figure 4.39. This unaffected V_{oc} upon AZO doping amount reflects insignificant dopant in modifying the barrier height of the materials in organic solar cells. However, device produces the smallest V_{oc} value at 8% AZO indicating that large amount of AZO may act as impurity and impinge the mobility of the charges in the device.

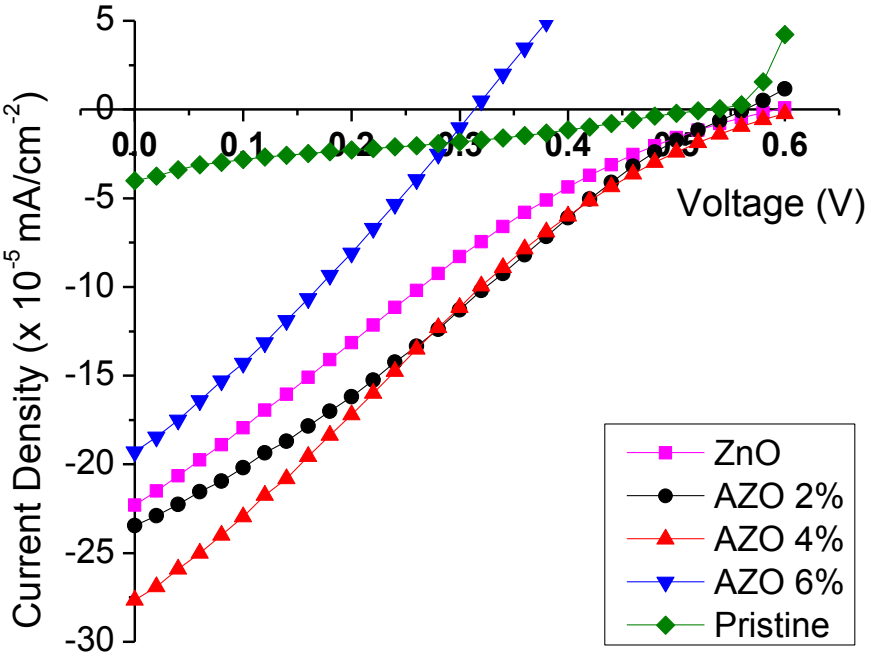

Figure 4.38: J-V plots for AZO modified PEDOT:PSS compared to pristine PEDOT:PSS.

Table 4.13 :J-V characteristics for AZO modified PEDOT:PSS compared to pristine PEDOT:PSS.

% Doping	$V_{oc\,(V)}$	J_{sc}(x 10^{-5} mA cm^{-2})	FF (%)	PCE (x 10^{-3} %)
Pristine	0.54	-4.0	24.67	5.3
ZnO	0.60	-22.3	20.23	27.0
2% AZO	0.57	-23.4	25.83	34.5
4% AZO	0.60	-27.7	21.47	35.6
6% AZO	0.31	-19.5	28.13	17.1

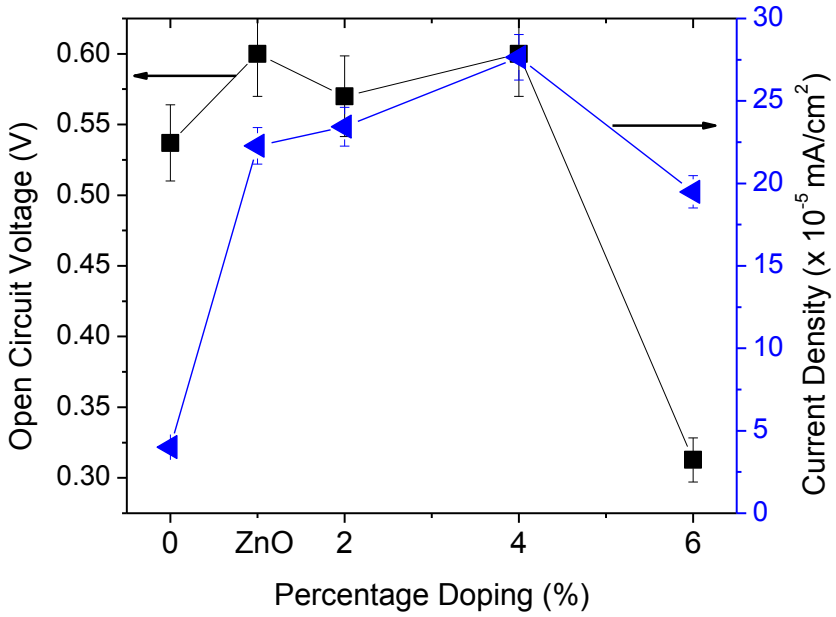

Figure 4.39: The variation of V_{oc} and J_{sc} for AZO modified PEDOT:PSS compared to pristine PEDOT:PSS.

On the other hand, the J_{sc} increased drastically with the introduction of ZnO and AZO in the buffer layer which is highly expected due to the n-type carriers content of these metal oxide, which increase the n-carriers concentration in the device thus allow more short

circuit current in the device. The existence of metal oxide in the buffer layer may improve the free charge transportation hence results in increase of the photocurrent in the device.

The plots of fill factor and power conversion efficiency PCE with respect to the ZnO and AZO doped PEDOT:PSS are presented in Figure 4.40. The plot of fill-factor demonstrates a very inconsistent value with respect to the variation of AZO amount in PEDOT:PSS. However, plot of efficiency can be taken as indication for device performance. It can be observed that the highest efficiency occur in the device with 4% AZO doped PEDOT:PSS. This result is actually in good agreement with the conductivity of the AZO-doped PEDOT:PSS films. Hence, the performance of organic photovoltaic device can be enhanced via AZO doping at only 4% concentration in PEDOT:PSS. However the further content of AZO (beyond 4% AZO) is likely to reduce the performance of the device, hence the best amount of approximately 4% of AZO doping to PEDOT:PSS may really contribute in increasing the efficiency of the organic solar cell.

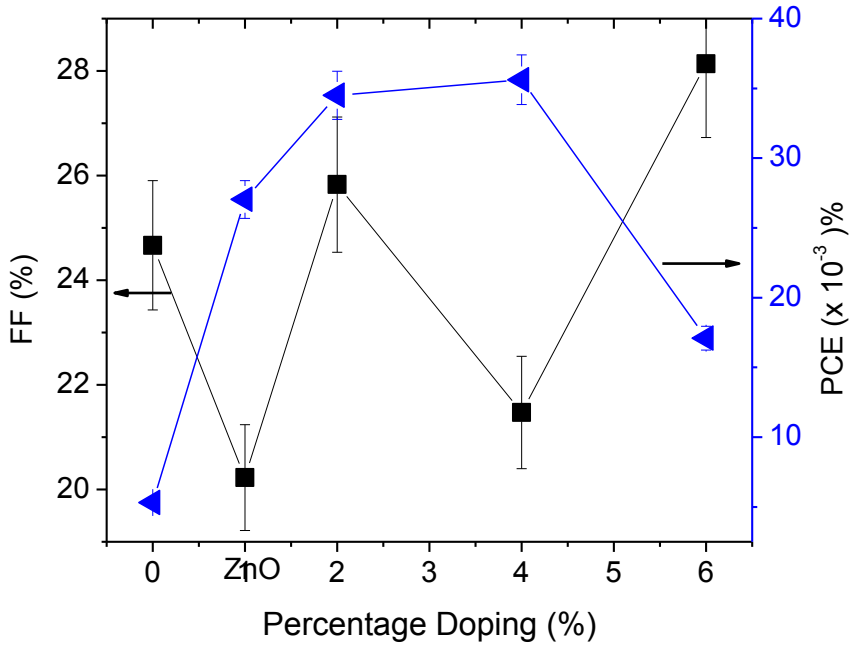

Figure 4.40 :The variation of FF and PCE for AZO modified PEDOT:PSS compared to pristine PEDOT:PSS.

4.5.4 Degradation in organic solar cell.

It is worthwhile to notice that in this work, the doped PEDOT:PSS has been successful in enhancing the efficiency of organic solar cell compared to the pristine PEDOT:PSS as the buffer layer. However, it is also significant to address the degradation in the device performance with certain amounts of doping materials to PEDOT:PSS. The fabricated device in this work were produced and observed in open atmosphere. Hence the reductions in their performance were expected in preliminary.

Organic electronic device showed high sensitivity to the humidity and also affected by the oxidation with the atmosphere (Rodriguez et al., 2011). Nevertheless, the exposure of the device to the surroundings also lead to the alteration to the surface which due to the swelling effect in PSS particles that reacted with the moisture in air which beneficial in improving the conductivity of PEDOT:PSS (Nardes et al., 2008). In addition, the degradation behavior in organic solar cell is highly depends on the internal stability attributable to the changes in several layers and interfaces of the device (Singh et al., 2014).Hence, although the fabricated organic solar cell with 2% glycerol, 6% EG and 4% AZO doped PEDOT:PSS as buffer layers showed good improvement in the device efficiency, the humidity by air exposure and the modifying in the interface layers in the device are the significant factors that may cause the degradation of the fabricated devices.

4.6 Summary.

In this chapter the results of optical, electrical, morphology and chemical structure properties were presented in details. In optical properties, all modified PEDOT:PSS thin films show great improvement with the doping treatment in their transmission spectra,

absorption coefficient and optical band gap. The conductivity of modified PEDOT:PSS were also enhanced compared to the pristine specifically in AZO doped PEDOT:PSS. Surface morphology varies according to the type and percentage of doping material show strong connection with optical and electrical properties of PEDOT:PSS. The effect of doping to PEDOT:PSS was also recognized by the shifting effect and intensity variations in Raman peaks which indicates that the doping treatment contribute in changing the arrangement of chemical structure in PEDOT:PSS. The modified PEDOT:PSS was then used as buffer layer in organic solar cell and the efficiency of the device was determined by measuring the current-voltage behavior with and without light. The efficiency show that all doped PEDOT:PSS as buffer layer offer good enhancement in improving the efficiency of organic solar cell where 4% AZO doped PEDOT:PSS as buffer layer exhibit the highest efficiency in the organic solar cell.

CHAPTER 5

RESULTS AND DISCUSSIONS OF THERMOELECTRIC EFFECT

Overview

This chapter describes the fabrication and characterization of thermoelectric effect based on the modified PEDOT:PSS. Apart of solar energy, the thermoelectric generator is one of other alternative methods in producing electrical power. The temperature gradient within the thin film is oneof the important factors in thermoelectric study. Hence an investigation on the modified PEDOT:PSS towards the temperature gradient across its thin film is crucial in this work.

The Seebeck coefficient and electrical conductivity can be expressed as their respective formulas concerning the carrier concentration by free carrier approximation. The increase in carrier concentration causes the proportional increase in electrical conductivity but the logarithmic decrease in Seebeck coefficient (Rowe, 1995).The effect on temperature difference is highly related to the thermoelectric effect which based on three factors; Seebeck coefficient (S), electrical (σ) and thermal (κ) conductivity. The Seebeck coefficient is the ratio of the voltage difference (ΔV) generates across the material when experienced a temperature difference (ΔT).

In order to obtain an accurate results on the performance of thermoelectric generator, a specific set- up equipment which consists of heat/exchanger/thermoelectric converter, the cold fluid loop, hot fluid loop, vacuum chamber, nitrogen gas, set of thermocouples and a data acquisition system are required (Niu et al., 2009).

The investigations are focused on the variation of current-voltage (I-V) characteristics with respect to the temperature difference across the modified PEDOT:PSS. It is well known that the electrical properties are temperature-dependent. Hence, with this measurements, it is expected that the effect of temperature difference across modified PEDOT:PSS may be appropriately addressed.Thus, the results obtained from the dependent of I-V on the temperature gradient may contribute in elaborating the thermoelectric effect.

5.1 The influence of thermal gradient on carrier concentration and output power.

In chapter 4, all modified PEDOT:PSS show changes to some extent, in their optical and electrical properties with different percentage of doping material. In this chapter, the current–voltage (I-V) plot of each modified PEDOT:PSS was measured with respect to the temperature difference across the PEDOT:PSS thin film. The fabrication of the thermoelectric device is described in Section 3.2.6 of Chapter 3.

The enhancement in electrical conductivity of materials depends on two major factors;(i) an increase in carrier concentration, n and (ii) the raise of the mobility of the charge carrier, μ (Du et al., 2011). In fact, the temperature gradient across the material can contribute in rising the material's conductivity because of the increasing number of thermally excited carriers, n (Yakuphanoglu, 2009). The addition in carrier number leads to the changes in the Seebeck coefficient which obtained from the ratio of the voltage drop (ΔV) when the material experienced changes in temperature (ΔT) (Liu et al., 2010).

This chapter elaborates the effect of temperature gradient of the modified PEDOT:PSS on their electrical properties. The temperature of all modified thin films were varied by means of hot water and cold water as described in section 3.2.6 of Chapter 3. Each doped PEDOT:PSS films was deposited onto a designed glass slide with aluminum as

their metal contact to the hot and cold region separately. Thus, the doped PEDOT:PSS thin films have experienced the temperature gradient from these two regions. Subsequently, the I-V plots of each modified PEDOT:PSS were extracted to study the effect of the open circuit voltage (V_{oc}) and short circuit current (I_{sc}) with respect to temperature gradient on the thin films. This effect occurs due to the fact that the changes in thermal may contribute in changing of energy ability of the electrons in the molecular structure, hence adjusting the energy level between HOMO and LUMO layer in organic materials. The variation of these energy level maybe indicated from the value of its open circuit voltage, V_{oc} (Pode,2011). The V_{oc} and I_{sc} is used to calculate the output power (P_o) produced by the respective doped PEDOT:PSS thin film by using equation 5.1 (Yakuphanoglu, 2009):

$$P_o = I_{sc}V_{oc} \qquad 5.1$$

5.1.1 Organic material - glycerol and ethylene glycol doped PEDOT:PSS.

Organic semiconducting materials are promising as thermoelectric materials mainly because of their large Seebeck coefficient and low thermal conductivity characteristics. However the real issue is that most of this class of material has low electrical conductivity.The electrical conductivity of organic semiconductor of conjugated polymers is strongly depend on several factors such as the morphology, microstructure and the number of counterions that balance the positive doping charge carried by the conjugated polymer chains (Crispin et al., 2003). Thus, the adjustment on these factors is essential in order to seek the optimized electrical conductivity of organic semiconducting materials to be applied in thermoelectric device.

The measurements of thermoelectric effect are presented here by focusing on the I-V characteristics. The variation of I-V curves of the doped PEDOT:PSS thin films was obtained with respect to the temperature difference across the films. Several I-V measurements were implemented for different amount of EG and glycerol dopants (2% to 8%). However, after many attempts in measuring this electrical property upon temperature gradient, only a few numbers of measurements have shown the relevant results. Most of I-V curves do not show any change upon variation in temperature gradient; in which the I-V curves are overlap with each other and cannot be distinguished, hence that curves were not presented here.

The best I-V plots in Figure 5.1(a-c) and Figure 5.2(a-b) show some variations with the changes in temperature difference produced by the pristine (undoped PEDOT:PSS), 2% and 4% of glycerol doped PEDOT:PSS, 4% and 6% of EG doped PEDOT:PSS thin films, respectively. In this study, only five samples are able to produce I-V results with a relevant trend. Nevertheless, it can be observed that there are very small changes of I-V curves, upon varying the temperature gradient, regardless of the dopant amount.

Subsequently, from these I-V plots, the output power of each organic doped PEDOT:PSS thin films were obtained from the V_{oc} and I_{sc} values. The variations of the calculated output power of these films, on the temperature gradient are presented in Figure 5.3(a-c) and Figure 5.4(d-e). The pristine PEDOT:PSS does not show any trend, in output power with the increasing of temperature gradient. For doped-PEDOT:PSS with 2% glycerol, the output power is stable at approximately 4.5 nanoWatts, for temperature gradient between 20 to 30^{o}C, but starts to drop when the temperature gradient reaches at 40 ^{o}C.

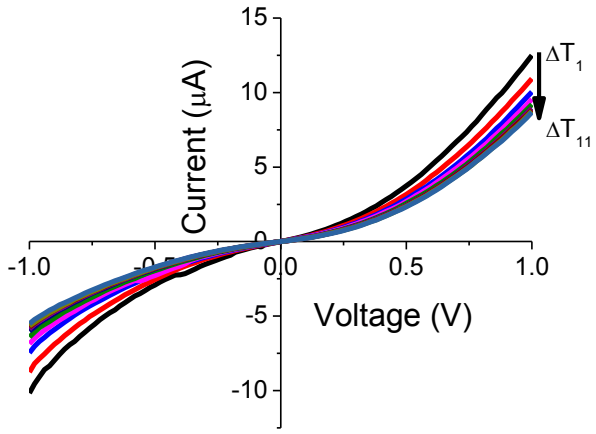

(a) pristine PEDOT:PSS

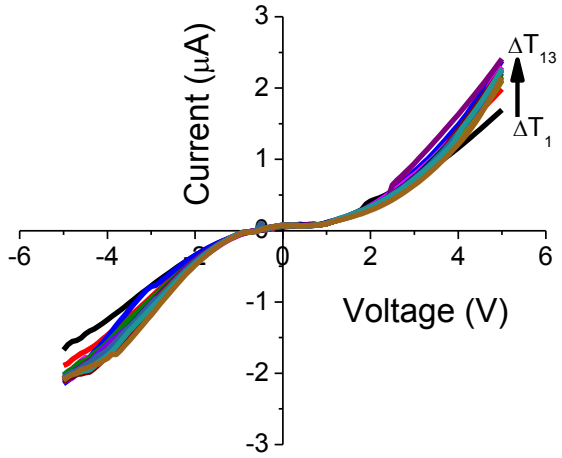

(b) 2% glycerol doped PEDOT:PSS

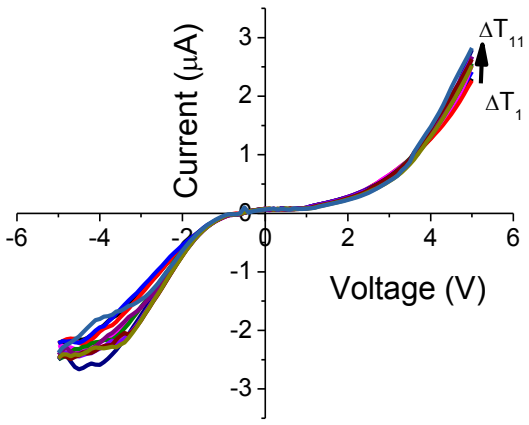

(c) 4% glycerol doped PEDOT:PSS

Figure 5.1 (a-c) : The variation in the current – voltage plots measured for pristine and glycerol doped PEDOT:PSS materials.

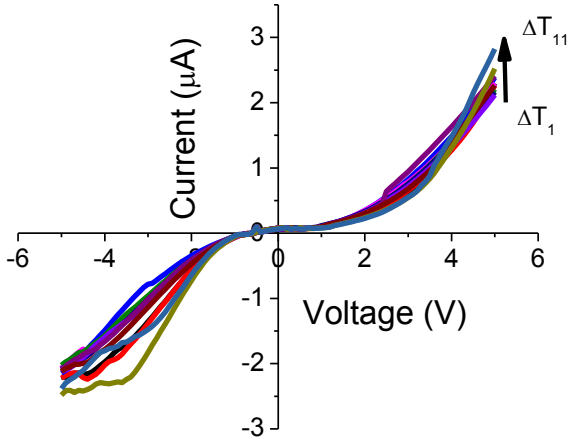

(a) 4% EG doped PEDOT:PSS

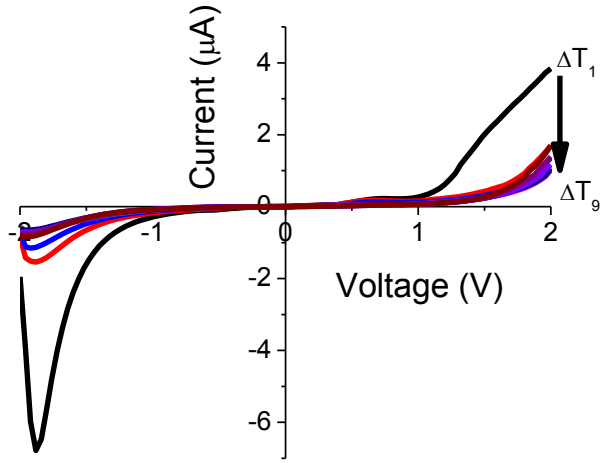

(b) 6% EG doped PEDOT:PSS

Figure 5.2 (a-b) : The variation in the current – voltage plots measured for EG doped PEDOT:PSS thin films.

For the film with 4% glycerol content in PEDOT:PSS, the output power gradually rise as the temperature difference increases from 20 ^{o}C to 30 ^{o}C, but become almost stable beyond temperature gradient of 30 ^{o}C. For the film with EG-doped, the output power can

increase with a small temperature gradient in the range of 15^{o}C to 25^{o}C. Nevertheless a larger temperature gradient has caused the output power falls. In addition, the result of output power is insignificant for the 6% EG doped-PEDOT:PSS film.

No proper results obtained for the I-V measurements of 6% and 8% of glycerol doped and 2% and 8% of EG doped PEDOT:PSS thin films. Hence there were no plots of output power versus temperature difference for these four thin films included in this report. As stated in section 2.4, the I-V measurement is a process to obtain current versus voltage or to observe the resistance characteristics in a device. It is mentioned in section 4.1 and 4,2 that the 6% to 8% of glycerol and EG doping show unsteady condition in terms of their optical and electrical properties. Hence, this condition also related to the changes in bonding structure in PEDOT:PSS with the doping treatment which provides obstacle to obtain appropriate result from the I-V measurement. Thus, this may lead to no significant results of output power in the respective range of glycerol and EG doping percentage to PEDOT:PSS.

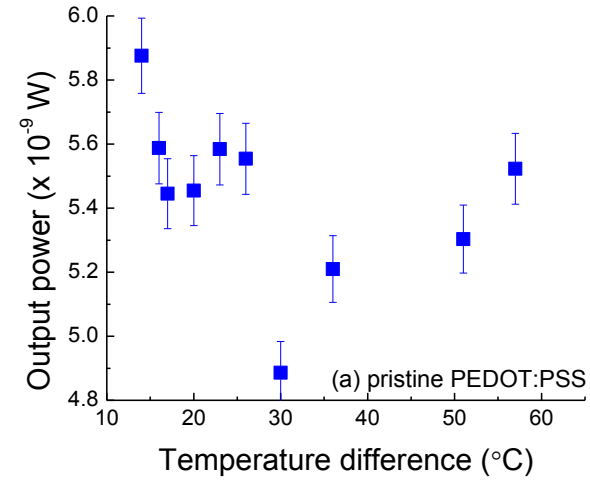

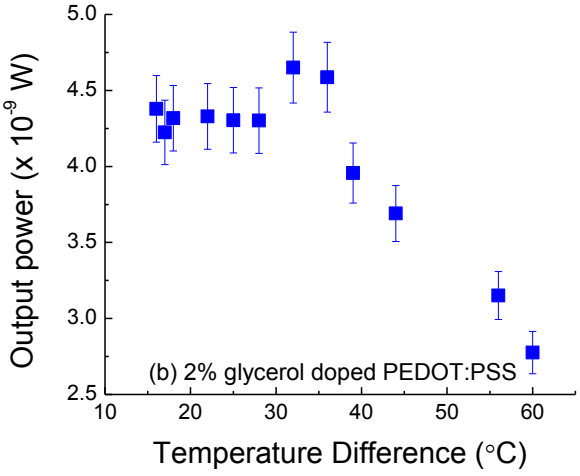

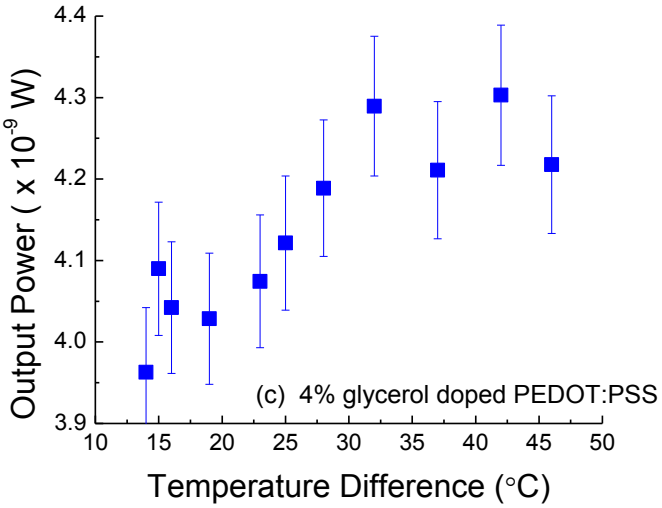

Figure 5.3 (a-c) : Output power (P_o) versus temperature difference (ΔT) produced by pristine and glycerol doped PEDOT:PSS.

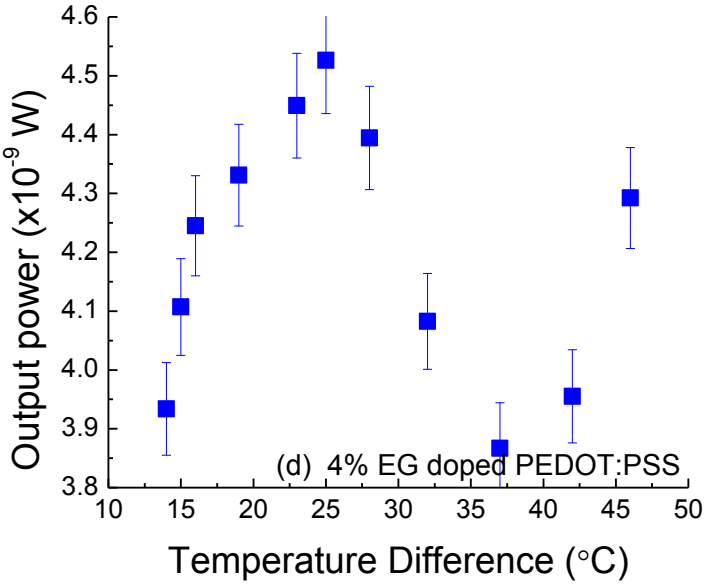

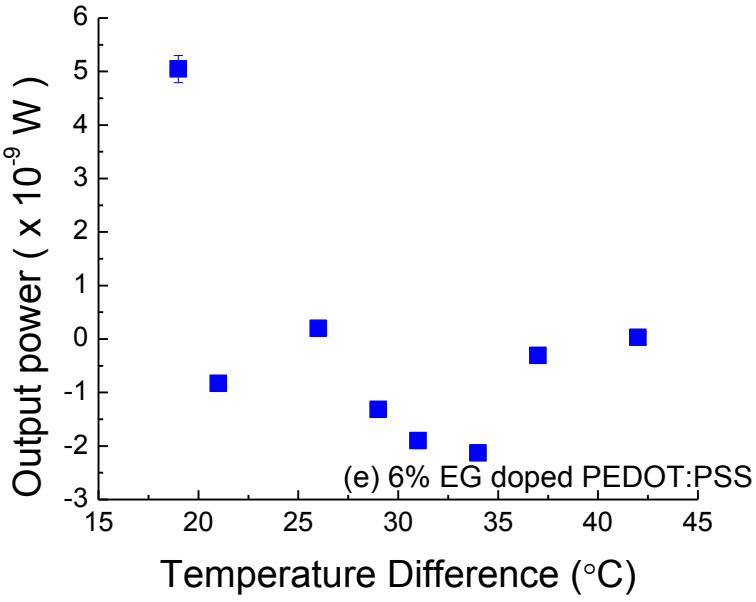

Figure 5.4 (d-e) : Output power (P_o) versus temperature difference (ΔT) produced by EG doped PEDOT:PSS.

5.1.2 Aluminum zinc oxide doped PEDOT:PSS

Metal oxides material is expected to offer benefits for high-temperature thermoelectric applications due to their high thermal stability and excellent oxidation resistance. The conventional solid-state reaction method of AZO has some drawbacks because of the incomplete mixing of the starting materials results in inhomogeneous materials. Hence the preparation of sol-gel which offers low cost, simple process and uniform mixture was used (Cai et al., 2003). Zinc oxide alone is a high potential TE candidate material because of its high carrier mobility and Seebeck coefficient (Ma et al., 2010).

Figure 5.5 (a-d) shows the I-V plots of AZO doped PEDOT:PSS measured according to the difference in temperature gradient. The I-V plot for each AZO doping PEDOT:PSS illustrated difference curve with variations in temperature gradient. These changes indicate that the electrical behavior is altered with the variation of temperature gradient across the thin film. All graphs show variations of I-V characteristics with respect to the temperature gradient from 15 K to 55 K. These differences provides output of values for open circuit voltage (V_{oc}) and short circuit current (I_{sc}) which influenced by the temperature gradient (ΔT). Output power (P_o) generated by each thermoelectric device was determined afterwards to evaluate the ability of these respective doped PEDOT:PSS according to the doping percentage of AZO. The plots of output power with respect to temperature gradient of each TE device are depicted in Figure 5.6.

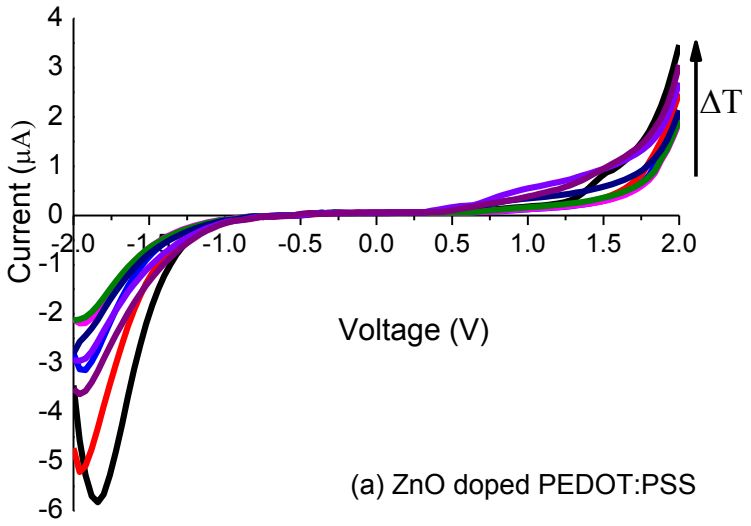

(a) ZnO doped PEDOT:PSS

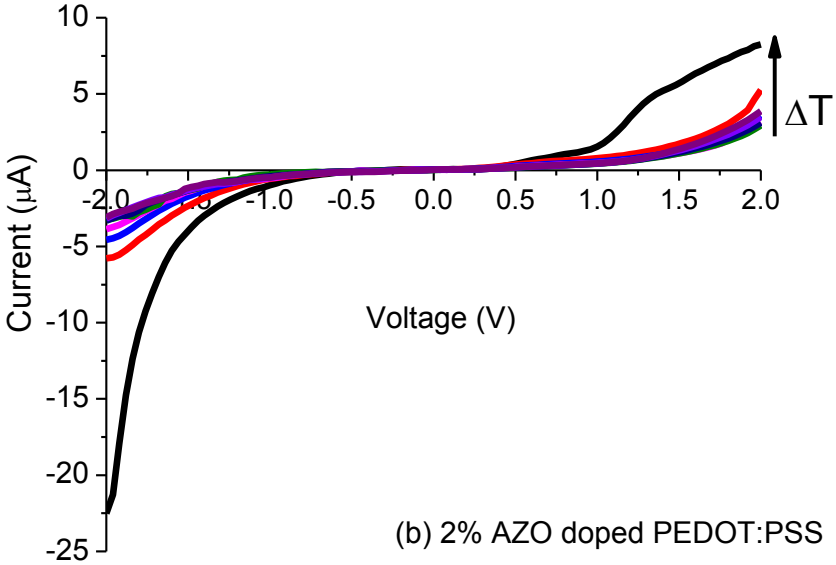

(b) 2% AZO doped PEDOT:PSS

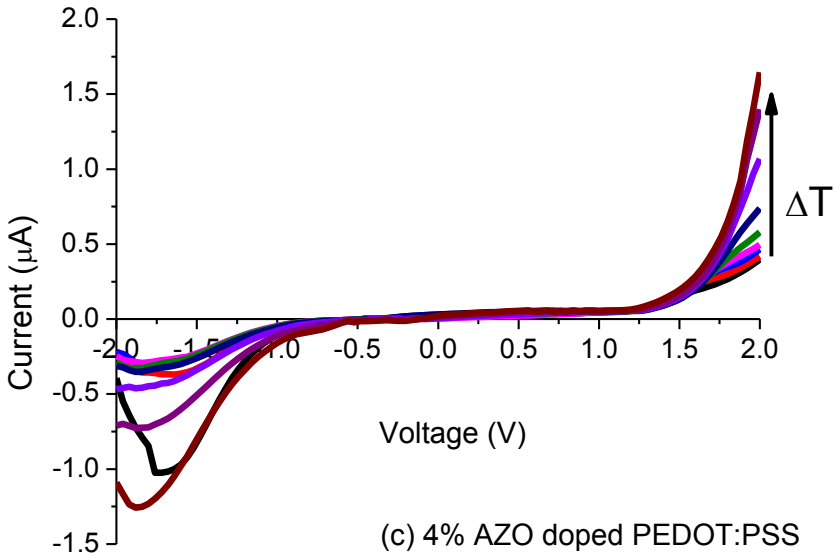

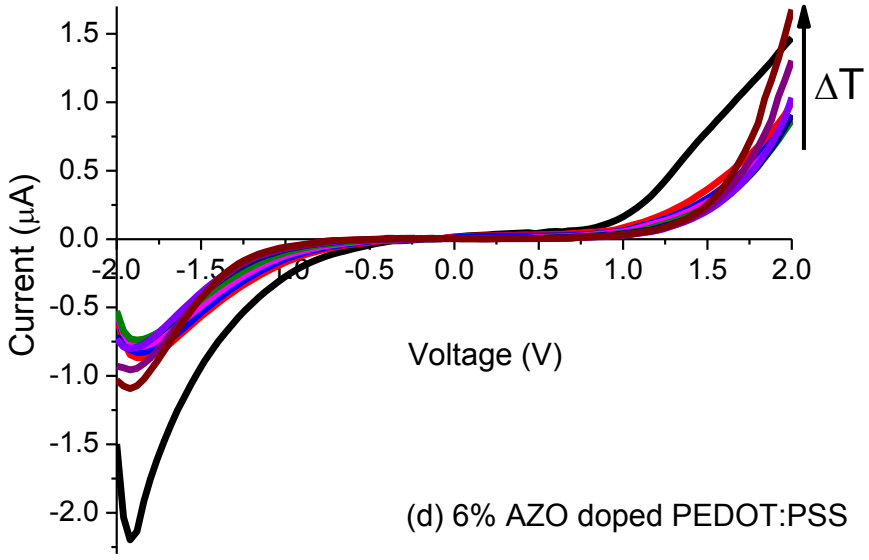

Figure 5.5(a-d) : Current – voltage plots of ZnO and AZO doped PEDOT:PSS

The trend of the graphs in Figure 5.6 illustrates that ZnO doped PEDOT:PSS shows opposite effect compared with AZO doped PEDOT:PSS. The increase in temperature gradient reduces the output power of ZnO doped PEDOT:PSS which is in contrast to the results obtained for the AZO doped PEDOT:PSS. The change in output power is highly influenced by the variation of V_{oc} while J_{sc} tends to be unstable with the temperature gradient. Hence, it is suggested that the temperature incline along the thin films of zinc oxide and AZO doped PEDOT:PSS contribute strongly in adjusting the HOMO and LUMO level of PEDOT:PSS material.

As shown in Section 4.1.3, that with ZnO and AZO doping, the E_g of PEDOT:PSS has been broaden from 2.80 eV in pristine to beyond 3.5 eV. The energy level difference between PEDOT:PSS (HOMO and LUMO) with ZnO and AZO (conduction band (CB) and valence band (VB)) forming a significant gap at the interface which attributed to the diode behavior in the TE module (Sharmaa et al., 2009).

These energy level alteration yield differences in the V_{oc} values of the respective thin films since V_{oc} values is indicated from the energy level diagram as the difference between the LUMO level of the first material with the HOMO level of the second material. In specific, the temperature gradient in these doped PEDOT:PSS contribute in restructuring their HOMO and LUMO energy level. As a result, the open circuit voltage, V_{oc} values of these doped PEDOT:PSS were varies accordingly (Pode, 2011).

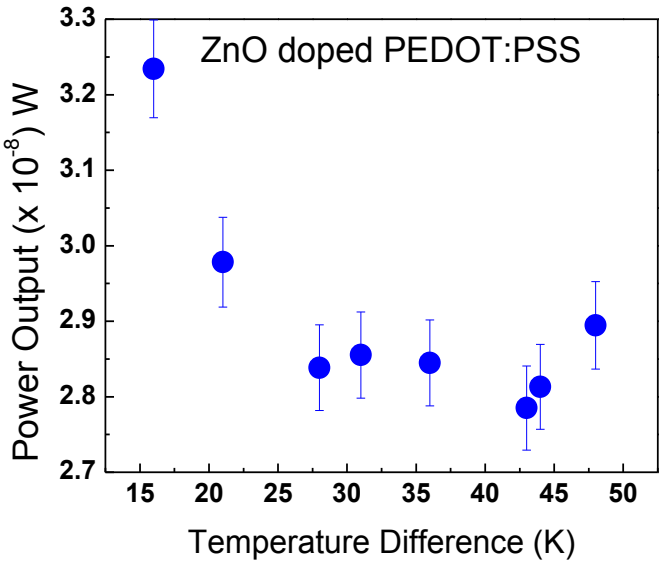
ZnO doped PEDOT:PSS
Power Output (x 10^{-8}) W
Temperature Difference (K)
3.3
3.2
3.1
3.0
2.9
2.8
2.7
15
20
25
30
35
40
45
50

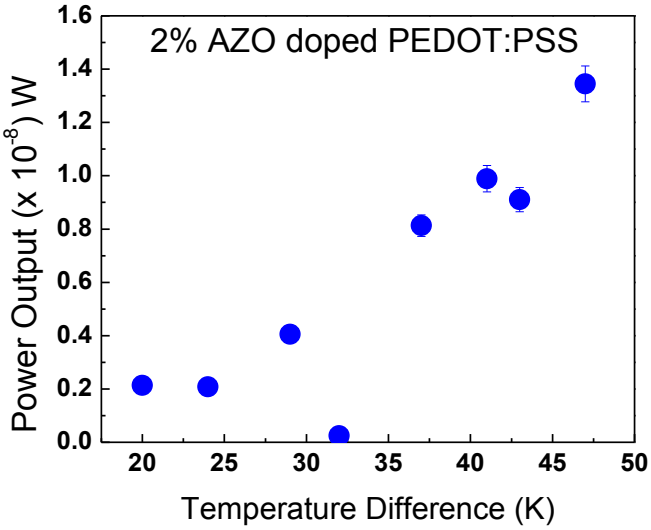
2% AZO doped PEDOT:PSS
Power Output (x 10^{-8}) W
Temperature Difference (K)
1.6
1.4
1.2
1.0
0.8
0.6
0.4
0.2
0.0
20
25
30
35
40
45
50

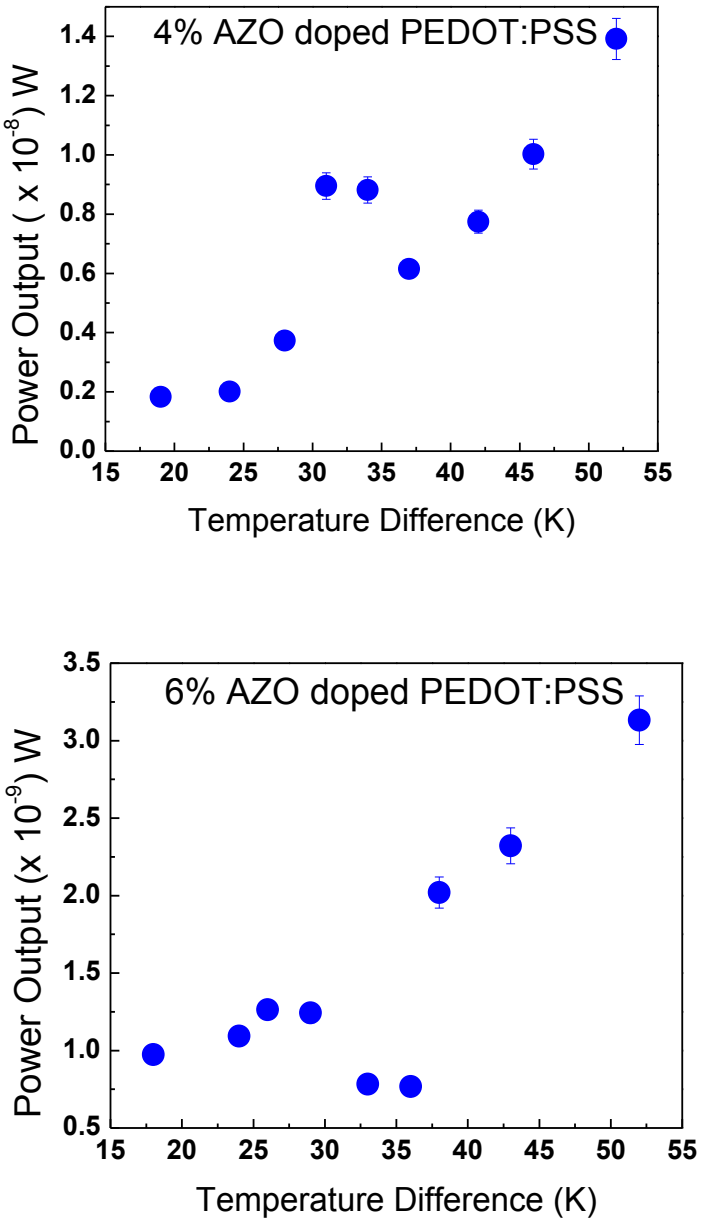

Figure 5.6: The power output generates from the I-V plots of different doped percentage of AZO versus the temperature gradient.

5.2 Studies on thermoelectric module of PEDOT:PSS and two organic materials, Alq_3 and PTCDA

Overview.

PEDOT:PSS PH1000 possesses the highest conductivity, to date is around 900 S/cm while its Seebeck coefficient is approximately 25 μV/K which make this conducting polymer the right candidate for p-type thermoelectric material. The Seebeck coefficient obtained from the PEDOT:PSS PH1000 used in this work is in good agreement with the range obtained by B.Zhang et al (Zhang et al., 2010). The desired factor for an efficient TE performance is based on its TE properties, thus the increased in conductivity and Seebeck coefficient of PEDOT:PSS PH1000 has encouraged us to use this material as an established p-type material in this work.

In contrast, investigations on the n-type organic material in TE device were claimed to be complex and less research has been done on this material (Zhang et al., 2010). The purpose of these further studies is to investigate the ability of two organic materials whether suitable to be one of the potential candidate as n-type organic thermoelectric materials. 3,4,9,10-Perylenetetracarboxylic dianhydride (PTCDA)and tris(8-hydroxyquinoline (Alq_3) are two organic materials which offered high potential in organic optoelectronic device application. Their interesting properties of high transparency, low cost and high electrical conductivity contribute strongly in upgrading the performance of organic optoelectronics device such as organic solar cell and organic light emitting diode. Thus, it seems noteworthy to study their thermoelectric properties for an application as organic n-type thermoelectric material.

The Seebeck coefficients of PTCDA and Alq_3 were determined and their electrical behavior were observed. Both materials were used as n-type thermoelectric material and merged with PEDOT:PSS PH1000 as p-type material in a simple basic built-in thermoelectric device/module as elaborated in chapter 3.0. The potential drops of this module were measured according to the temperature gradient variation and subsequently the Seebeck coefficient was determined. The Seebeck coefficient is the ratio of potential drop, ΔV with the temperature gradient, ΔT across the respective material as given by the following equation 5.2 (Liu et al., 2010):

$$S = \frac{\Delta V}{\Delta T} \qquad 5.2$$

5.2.1 Seebeck Coefficient and I-V Plots of Alq_3 as n-type and PEDOT:PSS as p-type thermoelectric materials

The calculated values of Seebeck coefficients (S) for PEDOT:PSS and Alq_3 used in this work are 25 μV/K and 2.8 μV/K respectively. The Seebeck coefficient value for Alq_3 suggested that this n-type material has produced a Seebeck effect with temperature difference. Thus, it has encouraged the pioneer work to further investigate on the application in TE device since it shows a good potential as a TE material.

However it is notable that the Seebeck coefficient of Alq_3 could be enhanced by several alternatives such as improving their electron injection, transport capability (Liang et al., 2008) and its electron mobility with the introduction of dopants consists of Bphen or C540 (Choy et al., 2006). Furthermore, the heating process of the aluminum contact can

also modify the structural properties of both p and n type materials (Rusu et al., 1998) and hence increasing the performance of the TE device.

The open circuit voltage, V_{oc} and temperature difference relation was plotted in Figure 5.5 based on the I-V measurement. The V_{oc} shows the linear region up to 35K of temperature gradient and seems to reach almost constant V_{oc} beyond that temperature gradient. Thus the range from 0K to 35K might so-called the effective temperature difference to diffuse the free charge carriers from hot to cold region. According to the work done by Xing Niu etal (Niu et al., 2009), the V_{oc} is directly related to the effective temperature difference between both junctions of the thermoelectric modules. Thus the decrease in changes rate of V_{oc} for temperature gradient beyond 35K might be due to the organic material properties which react inefficiently with the larger temperature difference more than 35K.

The relationship between V_{oc} and the temperature gradient is shown from equation 5.3 (Aydin et al., 2004) where *m* is the number of thermocouples, α is the relative Seebeck coefficient of the n- and p- type materials used in the respective device and ΔT_D is the temperature difference between cold and hot junctions of the TE device.

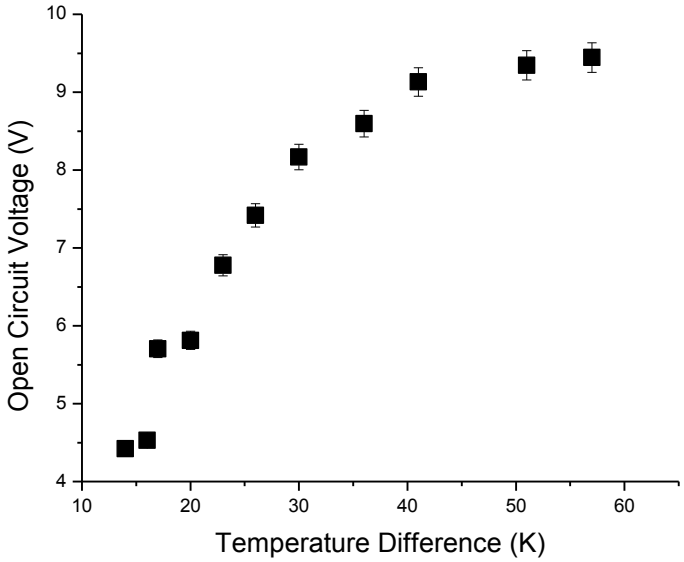

Figure 5.7: The variation of open circuit voltage (V_{oc}) with the temperature difference ΔT for thermoelectric device with Alq_3 and PEDOT:PSS.

$$V_{oc} = m\alpha\Delta T_D \qquad 5.3$$

In the present work, only one thermocouple was fabricated, thus *m* is equals to 1, hence from the plot on Fig. 5.7, the slope obtained from the plot at linear region represent the relative Seebeck coefficient of the device which is 0.127. By using the Seebeck coefficient value of PEDOT:PSS PH1000, the value of theoretical Seebeck coefficient for Alq_3 is approximately 3.2 μVK^{-1} which is in good agreement with the Seebeck coefficient of Alq_3 obtained from the experiment.

Figure 5.8 represents the plot of power output with respect to the variations of temperature difference. The module has generated an output electricity power in the range between 190 μW and 230 μW for the temperature gradient from 15K to 60K. It seems Alq_3 achieved a good agreement when associated with PEDOT:PSS and with the output power in micro scale indicates that Alq_3 could be utilized as a potential n-type material in TE device. The output power of this TE device is comparable with the one recently reported

by Bubnova etal. (Bubnova et al., 2011) using the organic conducting salt tetrathiafulvalene-tetracyanoquinodimethane (TTF-TCNQ) as an n-type material.

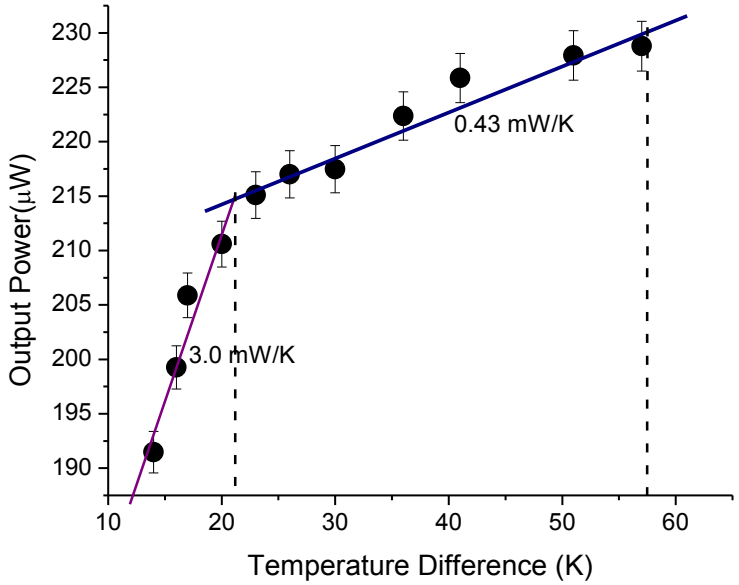

Figure 5.8: The plot of output power with the temperature difference.

The output power (P_o) of TE device is highly influenced by the temperature difference (ΔT_G) with the relationship shown in equation 5.4 (Aydin et al., 2004):

$$P_o = \frac{m^2\alpha^2}{4R_D}\Delta T_G^2 \qquad 5.4$$

The internal electrical resistance (R_D) of the studied TE device has been determined from equation 5.4 by finding the slopes at two difference regions as shown in the plot at Fig. 5.8. Thus, from this respective plot, the internal electrical resistance (R_D) of the TE device could be predicted as 0.1 Ω for the first region with the difference temperature below 22 K and approximately 0.4 Ω for the temperature difference beyond 22 K. The rose of R_D above 22 K shows a good agreement with the fact that the organic materials that have

been used are instable beyond certain temperature difference. Low thermal conductivity of an organic material that contributes to the flow of free charges in any electronic and optical device is based on certain temperature gradient (Farag et al., 2011). Hence, in this TE device, the temperature difference below 35 K could be an efficient value to promise a good charge transfer from the hot to the cold region.

In addition, the performance of the TE could be evaluated from the efficiency factor, ϕ which determined from equation 5.5 (Aydin et al., 2004) and from the slope attained from Fig. 5.8, the value is 2.71 $nWK^{-2}cm^{-2}$. The efficiency factor obtained from this work is about three orders of magnitude lower than the work by Glatz et al (Glatz & Muntwyler, 2006) on p-n poly-Si and p-n Bi_2Te_3indicating that the improvements of the thermoelectric properties are essential to produce an efficient device using this combination of p- and n- type organic materials (Aydin et al., 2004).

$$\emptyset = \frac{P_o}{A_D \Delta T^2} \qquad 5.5$$

5.2.2 The determination of Seebeck coefficients for thermoelectric device with high conductive PEDOT:PSS and PTCDA.

Referring to the research done on measuring the thermoelectric power of PTCDA films on Au contact with Pt films deposition for thermocouple measurement by Kushvaha et al (2011), PTCDA showed interesting values of Seebeck coefficient (Kushvaha et al., 2011), in the range of 342 μV/K to 372μV/K. Therefore, this suggested that the n-type material can be a good potential candidate as a TE material. However, a lower conductivity value of the PTCDA which obtained from the work by Sato et alwhich is only between 1.0 μS/cm to 1.0 S/cm shows an important issue that could be resolved by improving their electron injection and transport capability with the laser deposition and heat treatment(Sato

& Nishio, 2001) and also by introduction of alkali metal dopant to PTCDA material (Wuesten et al., 2006).

The I-V characteristic was measured under dark condition with the temperature dependent in the range of 60K to confirm the formation of free charge carriers in the device. The open circuit voltage and short circuit current gathered from the I-V characteristics show linear variation with the temperature difference and the graph of this relation is shown in Figure 5.9. This graph illustrates a good potential of PTCDA as the novel n-type material in TE device with the support of TE theory that the open circuit voltage is directly related to the effective temperature difference between both junctions of the thermoelectric modules (Niu et al., 2009).

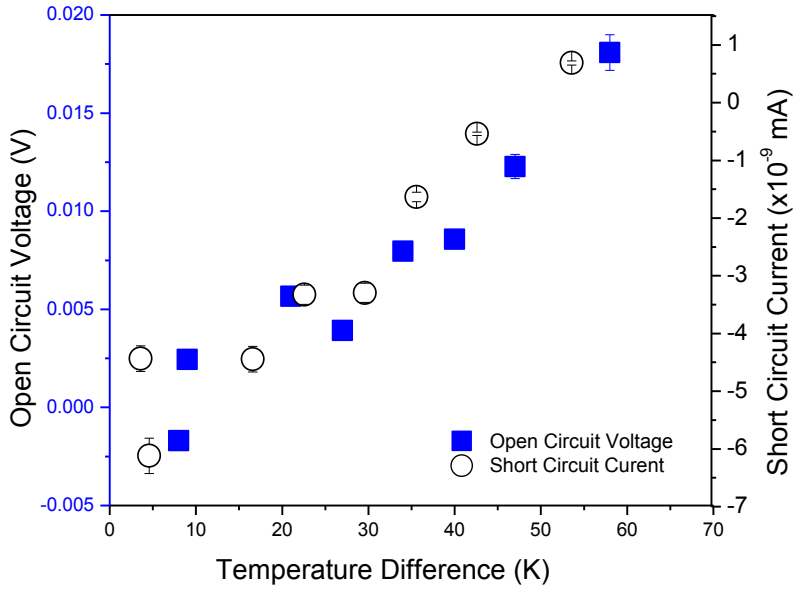

Figure 5.9: The influence of temperature difference to open circuit voltage and short circuit current of the TE device.

Consequently, the short circuit current, I_{sc} and open circuit voltage, V_{oc} for each temperature gradient were deducted and the output power that produced across the TE module was calculated. Figure 5.10 represents the plot of power output for the variations of

temperature difference. The module has generated an output electricity power in the range between 1 nW/cm^2 to 5 nW/cm^2 for the temperature gradient from 15K to 60K. Although both n- and p-type material in the TE device contributes to this nano scale output power, the major issue involved in exhibiting this result may be created by PTCDA since PEDOT:PSS PH1000 is the stable and establish p-type TE material.

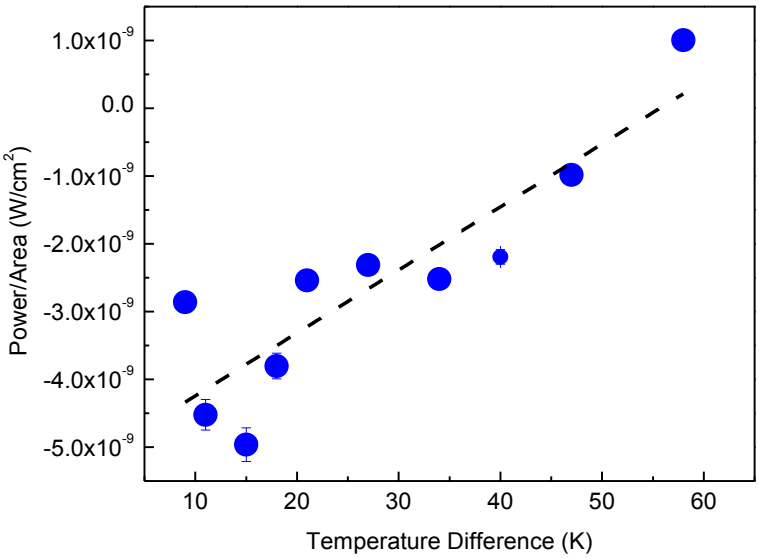

Figure 5.10: Output electric power generated by the TE module.

The charge transports in the ordered layers of PTCDA moves in two ways, parallel and perpendicular to the substrate. The electrons dominate in parallel direction while the perpendicular directions conquered by holes (Tengelin- Nilsson et al., 2000). The arrangement in the crystallinity ordered of perpendicular directions has increased the conductive contact, while the parallel directions of the charge transport has been limited by the distance between the adjacent molecules and the polar binding of the hydrogen and oxygen atoms (Stanculescu et al., 2008). Thus, due to these reasons, as a n-type material, the mobility of the electrons in PTCDA is slower compared to the holes and results in the poor charge injection in the TE device. From the graphs in Figure 5.9 and 5.10, the values

of α, R_D and ϕ for thermoelectric module with PTCDA as n-type material are also determined based on the equations explained in the previous section (5.2.1).

The slope of V_{oc} versus ΔT plot in Figure 5.9 is 33 mVK^{-1}. The m = 1 , thus this value is the relative Seebeck coefficient, α for this material. In addition, by using the same value of Seebeck coefficient for PH1000, 25μ VK^{-1}, the Seebeck coefficient value for PTCDA is found to be about 82.5 μVK^{-1}. From equation 5.4, the R_D value of this respective TE module is determined from plot in Figure 5.10. The R_D value estimated is about 1.2 kΩ, which is very high reflected by the small value of ϕ, about 1.45 $pWK^{-2}cm^{-2}$.

5.3 Summary

The current – voltage (I-V) plot for each modified PEDOT:PSS was measured with respect to the temperature difference across the PEDOT:PSS thin film. This chapter elaborates the effect of temperature difference to the electric properties. The variation of I-V curves for doped PEDOT:PSS thin film was obtained. According to their doping percentage, the I-V curves varies and the output power for each doped PEDOT:PSS was determined. It shows that with sufficient optimization, the modified PEDOT:PSS thin film specifically, AZO doped PEDOT:PSS own great potential as the candidate for thermoelectric material. Then, high conductive PEDOT:PSS PH1000 was paired with two organic material, Alq_3 and PTCDA in thermoelectric device and the thermoelectric behavior was observed by determining the Seebeck coefficient and the output power generates from the I-V plot. Other properties related to thermoelectric consists of efficiency factor and internal electrical resistance was also calculated from the I-V curves of the thermoelectric device.

CHAPTER 6

CONCLUSIONS AND FUTURE WORKS

Overview.

The history and background of organic solar cells and thermoelectric module have been elaborated accordingly, in the early part of this thesis. Next, the introducing of PEDOT:PSS material with its important function and disadvantages behavior in organic solar cell are addressed in order to provide a clearer perspective of the purpose of study in this work. The procedures including the synthesis of the samples, fabrication of organic solar cell and thermoelectric module, the measurement and characterization processes, the mathematical practices and significant parameter determinations are described in detail in the following chapter to deliver knowledge on this research. Later, the results obtained from the data processing are used in critical analysis in order to understand the behavior and variation occurs related to the parameters involve. Lastly, this chapter presents the conclusions which consist of the compilation of final view, comment on the analyzed results and also the suggestions for future directions based on this work.

The main intention of this research is to study the effect of different type of dopants (which is either organic or inorganic) on the physical properties of PEDOT:PSS thin films. The doped PEDOT:PSS thin films were successfully characterized in terms of their optical and electrical properties. The results and discussion of these thin films were presented in Chapter 4. The sharp and intense absorbance spectra were obtained with the presence of organic (glycerol and EG) and metal oxide (ZnO and AZO) as the doping materials to PEDOT:PSS thin films. It is observed that the hybrid of inorganic ZnO and AZO material

with PEDOT:PSS offers strong effect in modifying the optical properties of PEDOT:PSS thin films.

The absorbance spectra discovered a red-shifting peak from near ultraviolet (291 nm)in pristine and organic doping PEDOT:PSS to ultraviolet wavelength (351 nm) with inorganic material of ZnO and AZO doping to PEDOT:PSS. Furthermore, while widening the band gap, E_g, these dopants also strongly assisted in improving the absorption properties of PEDOT:PSS which is drastically increased to about one order of magnitude (1.1×10^5 cm^{-1}) compared to the pristine.

In order to apply the doped PEDOT:PSS thin films as buffer layer in organic solar cell, it is essential to improve the electrical properties as well. Hence, the further work has been focused on the electrical measurements of the doped PEDOT:PSS thin films. The dopant materials proved to be contribute in enhancing the electrical properties of PEDOT:PSS.

It is crucial to observe the changes of their surface morphology with respect to the different type of dopant material and different percentage amount of dopant material, in order to support the encouraging results obtained in the optical and electrical properties. Any changes occur in the organic thin film which affected their optical and electrical properties are significant with the alteration of the surface morphology of the thin film. The strong relation between the morphology and electrical properties can be visualized with the increase in their surface roughness. The short curved orientation in pristine PEDOT:PSS have been transformed to elongation and organized structure that produced a long stretched network of polymer chain with the existence of doping materials in PEDOT:PSS thin films.

In addition to the mentioned works, Raman spectra were measured to investigate the effect of doping on the chemical bonding of the PEDOT:PSS thin films. Almost all signature peaks of PEDOT:PSS appear with small shifting effect with respect to the several amount of doping percentage. In addition, obvious variations in the intensity of the Raman peaks were observed according to the different percentage of the doping materials of glycerol, EG and AZO concentrations as well which due to the presence of impurities, crack and defects in the doped PEDOT:PSS. The difference of Raman intensity revealed the alteration process occur in the PEDOT polymer chain with the presence of the doping material to PEDOT:PSS thin film. The modification occur consist of the conformational change which transformed the resonant structure of PEDOT:PSS from benzoid to quinoid structure.

Later, the doped PEDOT:PSS were utilized in organic solar cell as buffer layer. All devices produced diode behavior in the dark and under light illumination condition of the I-V characterization. The doped PEDOT:PSS thin film show improvement in the efficiency of the device, with 4% AZO doped PEDOT:PSS exhibit the highest efficiency which may suggested to be used as the hybrid inorganic/organic substance for organic solar cell application.

In Chapter 5, the doped PEDOT:PSS were employed in thermoelectric devices. The influence of different type of dopants on the thermoelectric paramaters was investigated. Interestingly, the I-V plots of all doped PEDOT:PSS thin films demonstrated a significant effect with the change in temperature gradient applied across the films. However upon the determination of output power, only several samples of doped PEDOT:PSS provided significant results. Many efforts were performed to obtain good readings from other devices were unsuccessful and they showed insignificant dependent with respect to the changes in

temperature gradient. In contrast, the ZnO doped and 2% to 6% AZO doped PEDOT:PSS produced a very attractive significant change with the variation of temperature gradient which were illustrated in their I-V plots. The temperature incline along the thin films of zinc oxide and AZO doped PEDOT:PSS contribute strongly in adjusting the HOMO and LUMO level of PEDOT:PSS which results in the V_{oc} alterations, hence allowed the formation of output power in the AZO doped PEDOT:PSS. Inspite the decreasing of output power with ZnO doped PEDOT:PSS at difference temperature gradient, AZO doped PEDOT:PSS exhibit totally the opposite result. It shows that the existence of aluminum provides a decent impact in improvement of zinc oxide and also as well as in PEDOT:PSS thin film. Although the results were not excellent, it is considered as encouraging improvement when compared to the pristine PEDOT:PSS thin film.

Finally, PEDOT:PSS of PH1000 high conductive solution was used as p-type material together with n-type organic materials of PTCDA and Alq_3 in the investigation of the output power generated in thermoelectric device. The Seebeck effect were observed by referring to their Seebeck values obtained which found to be 2.8 $\mu VK^{-1}$and 82.5 μVK^{-1} respectively, showed that these materials have good potential to be used as n-type material in thermoelectric device. The range of temperature gradient from 0^oC to 35^oC is suggested to be as the effective temperature difference to diffuse the free charge carriers of the studied materials from hot to cold region. The output power of the TE device produced is in micro scale for both thermoelectric devices using these two respective organic materials. The results obtained provide motivation in further studies on the effect of both organic materials in details, with proper procedures that related to thermoelectric properties.

6.1 Conclusions.

The results obtained in this work were concluded as the lists below:-

- All doped PEDOT:PSS exhibited higher transmittance spectra compared to the pristine PEDOT:PSS which achieved more than 90% of transmission of light after the doping process to PEDOT:PSS.
- The sharp and intense absorbance spectra revealed that these dopants strongly assisted in improving the absorption properties of PEDOT:PSS which is drastically increased to about one order of magnitude (1.1×10^5 cm^{-1}) compared to the pristine.
- The optical band gap, (E_g) is widen with the existence of the organic (glycerol and EG) and metal oxide (ZnO and AZO) as the doping materials to PEDOT:PSS thin films while 4% glycerol concentration contributes in enhancing the absorption properties up to 20×10^3 cm^{-1} compared to the pristine one, 11×10^3 cm^{-1}.
- The enhancement of the optical parameters in the modified PEDOT:PSS films has been achieved via this method.
- In electricalproperties aspect, sheet resistance values of all samples were reduced and in contrast increased their conductivity with the presence of all doping material in PEDOT:PSS. It was found that the 4% EG and 4% AZO doped PEDOT:PSS exhibited the maximum conductivity in micro range of approximately 3.5×10^{-6} S/cm.
- By using a simple method, the conductivity of the doped PEDOT:PSS has been improved and it is noteworthy that the conductivity can be enhanced to some extend without underwent a complex and expensive method.
- The AFM images revealed that the surface roughness of all doped PEDOT:PSS thin films are increased if compared to the pristine (rms roughness of 5.9nm), with 4%

of EG concentration exhibits the highest rms roughness of 23.6nm. The doped PEDOT:PSS show increment in surface roughness which related to the enhancement in the electrical conductivity in doped PEDOT:PSS thin films.

- Raman spectroscopy provides strong evidence that the doping of glycerol, EG and AZO to PEDOT:PSS offer significant effect to the molecular structure of PEDOT:PSS thin film where almost all Raman signature peaks appeared in the frequencies region of 1444 cm^{-1}, 1504 cm^{-1} and 1569 cm^{-1} and were slightly shifted with the presence of different doping material in PEDOT:PSS while obvious variation occur in the Raman intensity of all thin films which strongly reflected to the impurities and defects in PEDOT:PSS thin films.
- All doped PEDOT:PSS were successfully used as buffer layer in organic solar cell. The device performance of the doped PEDOT:PSS buffer layer exhibited a tremendous increment compared to the pristine PEDOT:PSS. The best performance achieved was the device with 4% AZO doped PEDOT:PSS, with an increase of about one factor of magnitude compared to the pristine buffer layer
- Small variations were observed in glycerol and EG doped PEDOT:PSS while further significant results obtained for ZnO and AZO doped PEDOT:PSS in the I-V plots of thermoelectric device which revealed that the thermoelectric output power was successfully generated with the temperature gradient effect across the TE device with the optimum temperature gradient in the range of 15^{o}C to 30^{o}C for organic doped PEDOT:PSS and 20^{o}C to 50^{o}C for ZnO and AZO doped PEDOT:PSS.
- The fabricated TE device of PEDOT:PSS PH1000 as p-type material and n-type organic materials of PTCDA and Alq_3 was successfully generates an output power

of electricity in the micro scale range between 190μW/cm^2 and 230 μW/cm^2 and between 1 nW/cm^{2}and 5 nW/cm^2 for Alq_3 and PTCDA, respectively.

6.2 Future works.

The used of PEDOT:PSS to date was not limited as buffer layer, instead several research works reported the successful of PEDOT:PSS as anode layer in optoelectronic devices. The results on the studied doped PEDOT:PSS could be further improved by other chemicals or heat treatment and other preparation technique. In addition, the work on synthesizing these doped PEDOT:PSS as anode material in optoelectronic is likely to be a good challenge since some other research works have established a specific and successful procedures in producing PEDOT:PSS layer as anode component in organic solar cell. Hence, maybe by using this specific and conventional methodology, further investigation on these doped PEDOT:PSS as anode layer in organic solar cell or other optoelectronic devices is possible in future.

On the other hand, if the issue on the availability of equipment involved the measurements of thermoelectric properties could be overcome, the further research on the studied n-type organic materials could be implemented in details and may results in providing new knowledge in thermoelectric technology in future.

REFERENCES

Aernouts, T., Vanlaeke, P., Geens, W., Poortmans, J., Heremans, P., Borghs, S., . . . Leenders, L. (2004). Printable anodes for flexible organic solar cell modules. *Thin Solid Films, 451–452*(0), 22-25.

Aydin, M. E., Akkiliç, K., & Kiliçoğlu, T. (2004). Relationship between barrier heights and ideality factors of H-terminated Pb/p-Si contacts with and without the interfacial oxide layer. *Applied Surface Science, 225*(1-4), 318-323.

Beek, W. J. E., Wienk, M. M., Kemerink, M., Yang, X., & Janssen, R. A. J. (2005). Hybrid Zinc Oxide Conjugated Polymer Bulk Heterojunction Solar Cells. *Journal Physics Chemistry, 109*, 9505-9516.

Bell, L. E. (2008). Cooling, heating, Generating Power and Recovering Waste Heat with Thermoelectric Systems. *Science, 321*, 1457.

Benanti, T. L., & Venkataraman, D. (2006). Organic solar cells: An overview focusing on active layer morphology. *Photosynthesis Research, 87*, 73-81.

Blair, A., & D.Venkataraman. (2011). Timeline of organic-based solar cells.

Brown, T. M., Kim, J. S., Friend, R. H., Cacialli, F., Daik, R., & Feast, W. J. (1999). Built-in field electro absorption spectroscopy of polymer light-emitting diodes incorporating doped poly(3,4-ethylenedioxythiophene) hole injection layer. *Appl.Phys.Lett, 75*, 1679-1681.

Bubnova, O., Khan, Z. U., Malti, A., Braun, S., Fahlman, M., Berggren, M., & Crispin, X. (2011). Optimization of the thermoelectric figure of merit in the conducting polymer poly(3,4-ethylenedioxythiophene). *Nat Mater, 10*(6), 429-433.

Cai, W., Gong, X., & Cao, Y. (2009). Polymer solar cells: Recent development and possible routes for improvement in the performance. *Solar Energy Materials & Solar Cells, 94*(2), 114-127.

Chen, Y., Kang, K. S., Han, K. J., Yoo, K. H., & Kim, J. (2009). Enhanced optical and electrical properties of PEDOT: PSS films by the addition of MWCNT-sorbitol. *Synthetic Metals, 159*, 1701-1704.

Choy, W. C. H., K.N.Hui, H.H.Fong, Y.J.Liang, & P.C.Chui. (2006). Improving the efficiency of organic light emitting devices by using co-host electron transport layer. *Thin Solid Films, 509*(1-2), 193-196.

Colomban, P., & Slodczyk, A. (2009). Raman Intensity: An Important Tool in the Study of Nanomaterials and Nanostructures. *Acta Physica Polonica A, 116*(1), 1-12.

Cook, J. H., Al-Attar, H. A., & Monkman, A. P. (2014). Effect of PEDOT:PSS resistivity and work function on PLED performance. *Organic Electronics, 15*, 245-250.

Crispin, X., Marciniak, S., Osikowicz, W., Zotti, G., Denier van der Gon, A. W., Louwet, F., . . . Saklaneck, W. (2003). Conductivity, morphology, interfacial chemistry and stability of poly(3,4-ethylene dioxythiophene)-poly(styrene sulfonate):A photoelectron spectroscopy study. *Journal of Polymer Science and Polymer Physics, B41*, 2561-2583.

Cruz-Cruz, I., Reyes-Reyes, M., Aguilar-Frutis, M. A., Rodriguez, A. G., & Lopez-Sandoval, R. (2010). Study of the effect of DMSO concentration on the thickness of the PSS insulating barrier in PEDOT:PSS thin films. *Synthetic Metals, 160*, 1501-1506.

D.M.Rowe. (1995). *Handbook of Thermoelectrics*. USA: CRC Press.

Dahou, F. Z., Cattin, L., Garnier, J., Querfelli, J., Morsli, M., Louarn, G., . . . C.Bernede, J. (2010). Influence of anode roughness and buffer layer nature on organic solar cells performance. *Thin Solid Films, 518*, 6117-6122.

Dimitriev, O. P., Grinko, D. A., Noskov, Y. V., Ogurtsov, N. A., & Pud, A. A. (2009). PEDOT:PSS films—Effect of organic solvent additives and annealing on the film conductivity. *Synthetic Metals, 159*(21–22), 2237-2239.

Du, Y., S.Z.Shen, K.Cai, & Casey, P. S. (2011). Research progress on polymer–inorganic thermoelectric nanocomposite materials. *Progress in Polymer Science*.

Elmoazzen, H. Y., Poovadan, A., K.Law, G., Elliot, J. A. W., McGann, L. E., & Jomha, N. M. (2007). Dimethyl sulfoxide toxicity kinetics in intact articular cartilage. *Cell Tissue Banking, 8*, 125-133.

Farag, A. A. M., G.Osiris, W., & S.Yahia, I. (2011). Photovoltaic performance analysis of organic device based on PTCDA/n-Si heterojunction. *Synthetic Metals, 161*(17–18), 1805-1812.

Feng-Xing, J., Jing-Kun, X., Bao-Yang, L., Yu, X., Rong-Jin, H., & Lai-Feng, L. (2008). Thermoelectric Performance of Poly(3,4-ethylenedioxythiophene):Poly(styrenesulfonate). *Chinese Phys. Lett., 25*, 2202-2205.

Fournier, C., Bamiduro, O., Mustafa, H., Mundle, R., R B Konda, Williams, F., & Pradhan, A. K. (2008). Effects of substrate temperature on the optical and electrical properties of Al:ZnO films. *Semiconductor Science And Technology, 23*.

Gasiorowski, J., R.Menon, K.Hingerl, M.Dachev, & N.S.Sariciftci. (2013). Surface morphology, optical properties and conductivity changes of poly(3,4-ethylenedioxythiophene):poly(styrenesulfonate) by using additives. *Thin Solid Films, 536*, 211-215.

Glatthaar, M., Niggemann, M., Zimmermann, B., Lewer, P., Riede, M., Hinsch, A., & Luther, J. (2005). Organic solar cells using inverted layer sequence. *Thin Solid Films, 491*(1–2), 298-300. doi: 10.1016/j.tsf.2005.06.006

Glatz, W., & Muntwyler, C. H. S. (2006). Optimization and fabrication of thick flexible polymer based micro thermoelectric generator. *Sensors and Actuators A, 132*, 337-345.

Godoy, A., L.Cattin, L.Toumi, F.R.Dı´az, M.A.delValle, G.M.Soto, . . . J.C.Bernede. (2010). Effects of the buffer layer inserted between the transparent conductive oxide anode and the organic electron donor. *Solar Energy Materials & Solar Cells, 94*, 648–654.

Gong, X., M.Tong, Y.Xia, W.Cai, J.S.Moon, Y.Cao, . . . A.J.Heeger. (2009). High-detectivity polymer photodetectors with spectral response from 300 nm to 1450 nm. *Science, 325*, 1665-1667.

Gou, X., Xiao, H., & Yang, S. (2010). Modeling, experimental study and optimization on low-temperaturewaste heat thermoelectric generator system. *Applied Energy, 87*, 3131–3136.

Gregg, B. A., & Hann, M. C. (2003). Comparing organic to inorganic photovoltaic cells: theory, experiment and simulation. *Journal of Applied Physics, 93*(6), 3605-3614.

Halls, J. J. M., Cornil, J., Santos, D. A. d., Hwang, D.-H., Holmes, A. B., Bredas, J. L., & Friend, R. H. (1999). Excited-State Energy- and Charge-Transfer at Polymer/Polymer Interfaces. *Synthetic Metals, 101*, 105-106.

Han, Y.-K., Chang, M.-Y., Huang, W.-Y., Pan, H.-Y., Ho, K.-S., Hsieh, T.-H., & Panb, S.-Y. (2011). Improved Performance of Polymer Solar Cells FeaturingOne-Dimensional PEDOT Nanorods in a Modified Buffer Layer. *Journal of The Electrochemical Society, 158*(3), 88-93.

Hau, S. K., Yip, H.-L., Zou, J., & Jen, A. K.-Y. (2009). Indium tin oxide-free semi-transparent inverted polymer solar cells using conducting polymer as both bottom and top electrodes. *Organic Electronics, 10*(7), 1401-1407.

Heo, S. W., Baek, K. H., Lee, T. H., Lee, J. Y., & Moon, D. K. (2013). Enhanced performance in inverted polymer solar cells via solution process: Morphology controlling of PEDOT:PSS as anode buffer layer by adding surfactants. *Organic Electronics, 14*, 1629-1635.

Hochbaum, A. I. (2007). Enhanced Thermoelectric Performance of Rough Silicon Nanowires. *Nature, 451*, 163.

Huang, C.-J., Chen, K.-L., Tsao, Y.-J., Chou, D.-W., Chen, W.-R., & Meen, T.-H. (2013). Study of solvent-doped PEDOT: PSS layer on small molecule organic solar cells. *Synthetic Metals, 164*, 38-41.

Huang, J., P.F.Miller, Mello, J. C. d., Mello, A. J. d., & D.D.C.Bradley. (2003). Influence of thermal treatment on the conductivity and morphology of PEDOT/PSS films. *Synthetic Metals, 139*(3), 569-572.

Huang, T.-S., Huang, C.-Y., Su, Y.-K., Fang, J.-S., Rao, M. V. M., Guo, T.-F., & Wen, T.-C. (2008). High-Efficiency Polymer Photovoltaic Devices With Glycerol-Modified Buffer Layer. *IEEE Photonics Technology Letters 20*, 1935-1937.

Johnev, B., Vogel, M., Fostiropoulos, K., Mertesacker, B., Rusu, M., Lux-Steiner, M. C., & Weidinger, a. (2005). Monolayer passivation of the transparent electrode in organic solar cells. *Thin Solid Films, 488*, 270.

Jönsson, S. K. M., Birgerson, J., Crispin, X., Greczynski, G., Osikowicz, W., Denier van der Gon, A. W., . . . Fahlman, M. (2003). The effects of solvents on the morphology and sheet resistance in poly(3,4-ethylenedioxythiophene)–polystyrenesulfonic acid (PEDOT–PSS) films. *Synthetic Metals, 139*(1), 1-10.

Ju, X., Feng, W., Kittichungchit, V., Hori, T., Moritou, H., Fujii, A., & Ozaki, M. (2009). Study on the bulk junction type organic solar cells with double zinc oxide layer. *Thin Solid Films, 518*(2), 786-790.

K.F.Cai, E.Muller, C.Drasar, & A.Mrotzek. (2003). Preparation and thermoelectric properties of Al-dopes ZnO ceramics. *Materials Science and Engineering B, 104*, 45-48.

Karabulut, M., Ertap, H., Mammadov, H., Ugurlu, G., & Ozturk, M. K. (2014). Properties of PbS thin films grown on glass and layered GaSe crystal substrates by chemical bath deposition. *Turkish Journal of Physics, 38*, 104 - 110.

Karagiannidis, P. G., Kalfagiannis, N., Georgiou, D., Laskarakis, A., Hastas, N. A., Pitsalidisa, C., & Logothetidis, S. (2012). Effects of buffer layer properties and annealing process on bulk heterojunction morphology and organic solar cell performance. *Journal of Materials Chemistry, 22*, 14624-14632.

Kietzke, T. (2007). Review Article: Recent Advances in Organic Solar Cells. *Advances in OptoElectronics, 2007*.

Kim, G.-H., Song, H.-K., & Kim, J. Y. (2011). The effect of introducing a buffer layer to polymer solar cells on cell efficiency. *Solar Energy Materials & Solar Cells, 95*, 1119–1122.

Kim, J. Y., J.H.Jung, D.E.Lee, & J.Joo. (2002). Enhancement of electrical conductivity of poly(3,4-ethylenedioxythiophene)/poly(4-styrenesulfonate) by a change of solvents. *Synthetic Metals, 126*, 311-316.

Kumar, B. R., & Rao, T. S. (2012). *Effect of Aluminum concentration on structural and optical properties of DC reactive magnetron sputtered Zinc Aluminum Oxide thin films for transparent electrode applications*. Paper presented at the International Symposium on Vacuum Science & Technology and its Application for AcceleratorsJournal of Physics: Conference Series.

Kuo, S.-Y., Chen, W.-C., Lai, F.-I., Cheng, C.-P., Kuo, H.-C., Wang, S.-C., & Hsieh, W.-F. (2006). Effects of doping concentration and annealing temperature on properties of highly-oriented Al-doped ZnO films. *Journal of Crystal Growth, 287*, 78-84.

Kushvaha, S. S., Hofbauer, W., Loke, Y. C., Samarendra, P. S., & O'Shea, S. J. (2011). Thermoelectric measurements using different tips in atomic force microscopy`. *Journal Of Applied Physics 109*.

Laskarakis, A., Karagiannidis, P. G., Geogiou, D., Nikolaidou, D. M., & Logothetidis, S. (2013). Optical investigation of the effect of solvent and thermal annealing on the optoelectronic properties of Poly(3,4-ethylenedioxythiophene): polystrenesulfonate) films. *Thin Solid Films, 541*, 102-106.

Lee, K. E., Wang, M., Kim, E. J., & Hahn, S. H. (2009). Structural, electrical and optical properties of sol-gel AZO thin films. *Current Applied Physics, 9*, 683-687.

Lee, M.-W., M.-Y.Lee, J.-C.Choi, J.-S.Park, & C.-K.Song. (2010). Fine patterning of glycerol-doped PEDOT:PSS on hydrophobic PVP dielectric with ink jet for source and drain electrode of OTFTs. *Organic Electronics, 11*(5), 854-859.

Liang, C.-J., Wang, Y., & Yi, L.-X. (2008). Organic Light Emitting Diodes Using Doped Alq3 as the Hole-transport Layer. *China Physics Letters, 25*(5), 1832-1835.

Lin, C.-F., W.-F.Su, C.-I.Wu, & -C.Cheng, I. (2012). *Organic, Inorganic, and Hybrid Solar Cells*: Wiley.

Liu, C., Lu, B., Yan, J., Xu, J., Yue, R., Zhu, Z., . . . Chen, P. (2010). Highly conducting free-standing poly(3,4-ethylenedioxythiophene)/ poly(styrenesulfonate) films with improved thermoelectric performances. *Synthetic Metals, 160*, 2481-2485.

Ma, N., Li, J.-F., Zhang, B. P., Lin, Y. H., Ren, L. R., & Chen, G. F. (2010). Microstructure and thermoelectric properties of Zn1-xAlxO ceramics fabricated by spark plasma sintering. *Journal of Physics and Chemistry of Solids, 71*, 1344-1349.

Mamat, M. H., Sahdan, M. Z., Khusaimi, Z., Ahmed, A. Z., Abdullah, S., & Rusop, M. (2010). Influence of doping concentrations on the aluminum doped zinc oxide thin films properties for ultraviolet photoconductive sensor applications. *Optical Materials, 32*, 696–699.

Manounia, A. E., Manjónb, F. J., Mollarb, M., B.Maríb, Gómezc, R., Lópezd, M. C., & Ramos-Barradod, J. R. (2006). Effect of aluminium doping on zinc oxide thin films grown by spray pyrolysis. *Superlattices and Microstructures, 39*, 185-192.

Mauger, S. A., Chang, L., Rochester, C. W., & Moulé, A. J. (2012). Directional dependence of electron blocking in PEDOT:PSS. *Organic Electronics, 13*, 2747–2756.

Mermazadeh, R., Panahi, F., & Shim, Y.-B. (2012). *Low temperature carbon monoxide sensor based on Co(salen) doped PEDOT:PSS*. Paper presented at the IMCS 2012- The 14th International Meeting on Chemical Sensors, Nuremberg, Germany.

Meyers, A., & Weck, M. (2004). Solution and Solid-State Characterization of Alq3-Functionalized Polymers. *Chemical Materials, 16*(7), 1183-1188.

Muhammad, F. F., Hapip, A. I. A., & Sulaiman, K. (2010). Study of optoelectronic energy bands and molecular energy levels of tris(8-hydroxyquinolinate) gallium and aluminum organometallic materials from their spectroscopic and electrochemical analysis. *Journal of Organometallic Chemistry, 695*, 2526-2531.

Muhammad, F. F., & Sulaiman, K. (2011). Tuning the Optical Band Gap of DH6T by Alq3 Dopant. *Sains Malaysiana, 40*(1), 17-20.

Na, S.-I., Kim, S.-S., Jo, J., & Kim, D.-Y. (2008). Efficient and Flexible ITO-Free Organic Solar Cells Using Highly Conductive Polymer Anodes. *Advanced Materials, 20*, 4061-4067.

Nardes, A. M., Kemerink, M., Kok, M. M. d., Maturova, E. V., & Janssen, R. A. J. (2008). Conductivity, work function, and environmental stability of PEDOT:PSS thin films treated with sorbitol. *Organic Electronics, 9*(5), 727-734.

Nguyen, T. P., & Vos, S. A. d. (2004). An investigation into the effect of chemical and thermal treatments on the structural changes of poly(3,4-ethylenedioxythiophene)/ polystyrenesulfonate and consequences on its use on indium tin oxide substrates. *Applied Surface Science, 221*(1-4), 330-339.

Nicoara, N., E.Román, J.M.Gómez-Rodríguez, J.A.Martín-Gago, & J.Méndez. (2006). Scanning tunneling and photoemission spectroscopies at the PTCDA/Au interface. *Organic Electronics, 7*(5), 287-294.

Niu, X., Yu, J., & Wang, S. (2009). Experimental study on low-temperature waste heat thermoelectric generator. *Journal of Power Sources, 188*, 621-626.

Nyberg, T. (2004). An alternative method to build organic photodiodes. *Synthetic Metals, 140*(2–3), 281-286.

Ouyang, J., Chu, C.-W., Chen, F.-C., Xu, Q., & Yang, Y. (2005). High conductivity Poly(3,4-ethylenedioxythiophene):Poly(styrenesulfonate) Film and Its Application in Polymer Optoelectronic Devices. *Advanced Functional Materials, 15*(2), 203-208.

Ouyang, J., Xu, Q., Chu, C.-W., Yang, Y., Li, G., & Shinar, J. (2004). On the mechanism of conductivity enhancement in poly(3.4-ethylenedioxythiophene):poly(styrene sulfonate) film through solvent treatment. *Polymer, 45*, 8443-8450.

Park, J., Lee, A., Yim, Y., & Han, E. (2011). Electrical and thermal properties of PEDOT:PSS films doped with carbon nanotubes. *Synthetic Metals, 161*, 523–527.

Park, S., Tark, S. J., & Kim, D. (2011). Effect of sorbitol doping in PEDOT:PSS on the electrical performance of organic photovoltaic devices. *Current Applied Physics, 11*(6), 1299-1301.

Pathak, C. S., Singh, J. P., & Singh, R. (2015). Effect of dimethyl sulfoxide on the electrical properties of PEDOT:PSS/n-Si heterojunction diodes. *Current Applied Physics, 15*(4), 528-534.

Pearton, S. J., Norton, D. P., Ip, K., Heo, Y. W., & T.Steiner. (2004). Recent advances in processing of ZnO. *Journal of Vacuum, Science and Technology B, 22*, 932-948.

Pejova, B. (2014). Optical absorption of semiconductor quantum dot solids. *Semiconductor Science and Technology, 29*, 045007.

Peumans, P., & Forrest, S. R. (2004). Organic photosensitive devices. Google Patents.

Po, R., Carbonera, C., Bernardia, A., & Camaioni, N. (2011). The role of buffer layers in polymer solar cells *Energy Environment Science, 4*, 285-310.

Pode, R. (2011). On the problem of open circuit voltage in metal phthalocyanine/C60 organic solar cells. *Advanced Materials Letters, 2(1)*, 3-11.

Qingfeng Dong, & Yinhua Zhou. (2010). All-spin-coating vacuum-free processed semi-transparent inverted polymer solar cells with PEDOT:PSS anode and PAH-D interfacial layer. *Organic Electronics, 11*, 1327-1331.

Ravindran, R., Juliet, S., Gopalan, A. K. K., Kavalimakkil, A. K., Ramankutty, S. A., Nair, S. N., . . . Ghosh, S. (2011). Toxicity of DMSO, Triton X 100 and Tween 20 against Rhipicephalus (Boophilus) annulatus. *J Parasit Dis, 35*, 237–239.

Robinson, J. W. (1975). *Atomic absorption spectroscopy*. New York, (NY): Marcel Dekker.

Rodriguez, A. B., Voigt, M. M., Martin, S. J., Whittle, T. J., Dalgliesh, R. M., Thompson, R. L., . . . Geoghegan, M. (2011). Structure of films of poly(3,4-ethylene dioxythiophene)-poly(styrene sulfonate) crosslinked with glycerol. *Journal of Materials Chemistry, 21*, 19324.

Rusu, M., Stanciub, A., Bulacovschib, V., Rusu, G. G., Bucescu, M., & Rusu, G. I. (1998). Temperature dependence of the electrical conductivity and Seebeck coefficient of new poly(ester-syloxane)urethane elastomers in thin films. *Thin Solid Films, 326*, 256–262.

Sato, H., & Nishio, S. (2001). Polymer laser photochemistry, ablation, reconstruction, and polymerization. *Journal of Photochemistry and Photobiology C: Photochemistry Reviews, 2*(2), 139-152.

Schaarschmidt, A., Farah, A. A., Aby, A., & Helmy, A. S. (2009). Influence of Nonadiabatic Annealing on the Morphology and Molecular Structure of PEDOT-PSS Films. *The Journal Of Physical Chemistry B, 113*, 9352-9355.

Semaltianos, N. G., Logothetidis, S., Hastasa, N., Perrieb, W., Romanib, S., & S.Potterb. (2010). *Chemistry and Physics Letters, 484*, 283-289.

Sharmaa, B. K., Khare, N., & Ahmad, S. (2009). A ZnO/PEDOT:PSS based inorganic/organic hetrojunction. *Solid State Communications, 149*, 771-774.

Shrotriya, V., Li, G., Yao, Y., Chu, C.-W., & Yang, Y. (2006). Transition metal oxides as the buffer layer for polymer photovoltaic cells. *Applied Physics Letters, 88*, 073508 -073501.

Singh, V., Arora, S., Arora, M., Sharma, V., & Tandon, R. P. (2014). Characterization of doped PEDOT: PSS and its influence on the performance and degradation of organic solar cells. *Semiconductor Science and Technology, 29*.

Sirringhaus, H., Kawase, H. T., Friend, R. H., Shimoda, T., Inbasekaran, M., Wu, W., & Woo, E. P. (2000). High-resolution inkjet printing of all-polymer transistor circuits. *Science, 290*, 2123-2126.

Skotheim, T. A., L.Elsenbaumer, R., & R.Reynolds, J. (1998). *Handbook of Conducting Polymers*: M.Dekker.

Spanggaard, H., & Krebs, F. C. (2004). A brief history of the development of organic and polymeric photovoltaics. *Solar energy materials and solar cells, 83*(2-3), 125-146.

Stanculescu, A., Stanculescu, F., Socol, M., & Grigorescu, O. (2008). Electrical transport in crystalline perylene derivatives films for electronic devices. *Solid Statte Sciences, 10*(12), 1762-1767.

Tamburri, E., Guglielmotti, V., Orlanducci, S., & Terranova, M. L. (2011). Structure and I2/I− redox catalytic behaviour of PEDOT–PSS films electropolymerized in aqueous medium: Implications for convenient counter electrodes in DSSC. *Inorganica Chimica Acta, 377*(1), 170-176.

Tang, G., Liu, H., & Zhang, W. (2013). The Variation of Optical Band Gap for ZnO:In Films Prepared by Sol-Gel Technique. *Advances in Materials Science and Engineering, 2013*.

Teguh, J. S., Sum, T. C., & Yeow, E. K. L. (2014). Effect of charge accumulation on the stability of PEDOT:PSS during device operation. *Chemical Physics Letters, 607*, 52-56.

Tekin, E., Gans, B.-J. d., & Schubert, U. S. (2004). Ink-jet printing of polymers – from single dots to thin film libraries. *Journals of Materials Chemistry, 14*, 2627-2632.

Tengelin-Nilsson, M., L.Ilver, & J.Kanski. (2000). Photoemission and low-energy electron diffraction studies of 3,4,9,10-perylene tetracarboxylic dianhydride layers on Si(111):H. *Surface Science, 464*(2-3), 265-271.

Topsoe, H. (1968). *Haldor Topsoe Semiconductor Division* (2nd Revised ed.): Vedbeek

Tritt, M., & A.Subramanian, M. (2006). Thermoelectric Materials, Phenomena, and Applications: A Bird's Eye View. *MRS Bulletin, 31*, 188-229.

Tsai, H.-W., Pei, Z., Chen, C.-C., Cheng, S.-J., Hsieh, W.-S., Li, P.-W., & Chanc, Y.-J. (2011). Anode engineering for photocurrent enhancement in a polymer solar cell and applied on plastic substrate. *Solar Energy Materials & Solar Cells, 95*(2), 611-617.

Tsai, K.-H., Shiu, S.-C., & Lin, C.-F. (2008). Improving the conductivity of hole injection layer by heating PEDOT:PSS. *Proceeding of SPIE, 7052*.

Tsai, T.-C., Chang, H.-C., Chen, C.-H., & Whang, W.-T. (2011). Widely variable Seebeck coefficient and enhanced thermoelectric power of PEDOT:PSS films by blending thermal decomposable ammonium formate. *Organic Electronics, 12*, 2159-2164.

Tseng, Y.-K., Gao, G.-J., & Chien, S.-C. (2010). Synthesis of c-axis preferred orientation ZnO:Al transparent conductive thin films using a novel solvent method. *Thin Solid Films, 518*, 6259-6263.

Vining, C. B. (2009). An Inconvenient Truth About Thermoelectrics. *Nature Materials 8*, 83.

Wang, J., Meng, L., Qi, Y., Li, M., Shi, G., & Liu, M. (2009). The Al doping contents dependence on the crystal growth and energy band structure in Al:ZnO thin films. *Journal of Crystal Growth, 311*, 2305-2308.

Wichiansee, W., & Sirivat, A. (2009). Electrorheological properties of poly(dimethylsiloxane) and poly(3,4-ethylenedioxy thiophene)/poly(stylene sulfonic acid)/ethylene glycol blends. *Materials Science and Engineering: C, 29*(1), 78-84. doi: 10.1016/j.msec.2008.05.018

Williams, R. (1960). Becquerel Photovoltaic Effect In Binary Compounds. *The Journal of Chemical Physics, 32*(5), 1505-1514.

Wuesten, J., Ziegler, C., & Ertl, T. (2006). Electron transport in pristine and alkali metal doped perylene-3,4,9,10-tetracarboxylicdianhydride (PTCDA) thin films. *Phys. Rev. B, 74*.

Xia, Y., & Ouyang, J. (2011). PEDOT:PSS films with significantly enhanced conductivities induced by preferential salvation with cosolvents and their application in polymer photovoltaic cells. *Journal of Material Chemistry, 21*, 4927-4936.

Xia, Y., Sun, K., & Ouyang, J. (2012). Highly conductive poly (3,4-ethylenedioxythiophene) : poly(styrene sulfonate)films treated with an amphiphilic compound as the transparent electrode of polymer solar cells. *Energy & Environmental Science, 5*, 5325.

Xiong, Z., & Liu, C. (2012). Optimization of inkjet printed PEDOT:PSS thin films through annealing processes. *Organic Electronics, 13*, 1532-1540.

Yakuphanoglu, F. (2009). Electrical conductivity, Seebeck coefficient and optical properties of SnO_2 film deposited on ITO by dip coating. *Journal of Alloys and Compounds, 470*, 55-59.

Yan, H., Chen, Z., Zheng, Y., Newman, C., Quinn, J. R., Dötz, F., . . . Facchetti, A. (2009). A high-mobility electron-transporting polymer for printed transistors. *Nature, 457*, 679-686.

Yan, H., & Okuzaki, H. (2009). Effect of solvent on PEDOT/PSS nanometer-scaled thin films:XPS and STEM/AFM studies. *Synthetic Metals, 159*, 2225-2228.

Yin, B., Liu, Q., Yang, L., Wu, X., Liu, Z., Hua, Y., . . . Chen, Y. (2010). Buffer layer of PEDOT:PSS/Graphene Composit for Polymer Solar Cells. *Journal of Nanoscience and Nanotechnology, 10*, 1934-1938.

Yoo, D., Son, W., Kim, S., Lee, J. J., Lee, S. H., Choi, H. H., & Kim, J. H. (2014). Gradual thickness-dependent enhancement of the thermoelectric properties of PEDOT:PSS nanofilms. *RSC Advances, 4*(103), 58924-58929.

Yusli, M. N., Yun, T. W., & Sulaiman, K. (2009). Solvent effect on the thin film formation of polymeric solar cells. *Materials Letters, 63*, 2691–2694.

Zahn, D. R. T., G.N.Gavrila, & M.Gorgoi. (2006). The transport gap of organic semiconductors studied using the combination of direct and inverse photoemission. *Chemical Physics, 325*(1), 99-112.

Zarrinkhameh, M., Zendehnam, A., Hosseini, S. M., Robatmili, N., & Arabzadegan, M. (2014). Effect of oxidation and annealing temperature on optical and structural properties of SnO_2. *Bulletin Material Sciences, 37*, 533-539.

Zhang, B., Sun, J., Katz, H. E., Fang, F., & Opila, R. L. (2010). Promising Thermoelectric Properties of Commercial PEDOT:PSS Materials and Their Bi_2Te_3 Powder Composites. *Applied Materials and Interfaces, 2*(No.11), 3170-3178.

Zhang, W., Bi, X., Zhao, X., Zhao, Z., Zhu, J., Dai, S., . . . Yang, S. (2014). Isopropanol-treated PEDOT:PSS as electron transport layer in polymer solar cells. *Organic Electronics 15*(12), 3445–3451.

LIST OF PUBLICATIONS AND PAPERS PRESENTED

Published paper (ISI cited):-

1. Rahman, Z.A., K. Sulaiman, et al. (2012). PEDOT:PSS Thin film as Transparent Electrode in ITO-Free Organic Solar Cell. *Advanced Materials Research*, **501**, 252-256.

2. Rahman, Z.A., Rusop, M., Ahmad, Shuhaimi, A., Sulaiman, K. (2012). Electronic Properties and Electrical Characteristics of Modified PEDOT:PSS as a Buffer Layer in Organic Solar Cell. *IEEE, ICEDSA 2012*, 198-202. DOI: 10.1109/ICEDSA.2012.6507796

3. Rahman, Z.A., K. Sulaiman, et al. (2013). The Seebeck Effect of 3,4,9,10-Perylenetetracarboxylic dianhydride (PTCDA) as a Novel N-type Material in a Thermoelectric Device. *Advanced Materials Research*, **667**, 165-171.

4. Sulaiman, K., Ahmad, Z., Fakir, M.S., Wahab, F.A., Abdullah, S.M., Rahman, Z.A.(2013). Organic Semiconductors: Applications in Solar Photovoltaic and Sensor Devices. *Materials Science Forum*, **737**, 126-132.

5. Zafar, Q., Ahmad, Z., Sulaiman,K., Hamzah,A.S., Rahman, Z.A. (2014). A MEHPPV/VOPcPhO composite based diode as a photodetector. *Sensors and Actuators A: Physical*, 206, 138-143.

Conference paper presented:-

1. Rahman, Z. A., K. Sulaiman, et al. (2012). Electronic Properties and Electrical Characteristics of Modified PEDOT:PSS as a Buffer Layer in Organic Solar Cell. 3rd IEEE International Conference on Electronics Design, Systems and Applications (ICEDSA). Kuala Lumpur, MALAYSIA IEEE**:** 198-202.

Presentation in conference:-

1. ICMAT 2011 – The International Conference on Materials for Advanced Technologies - 26 June to 1 July, 2011 in Singapore – POSTER PRESENTATION.

2. Conference on NANOTECHNOLOGY APPLICATIONS IN ENERGY & ENVIRONMENT 2012 (NAEE2012) 20 -21 September 2012, Bandung Institute of Technology, Indonesia – POSTER PRESENTATION

3. IEEE International Conference on Electronics Design, Systems and Applications (ICEDSA). Kuala Lumpur,MALAYSIA, 2012 – ORAL PRESENTATION

4. Physics Colloqium, Department of Physics, University Malaya, 2013 – ORAL PRESENTATION.